1991

Synthesis and characterization of reduced ternary molybdenum oxides and soluble copper(II) alkoxide complexes

Sheng-Chang Chen
Iowa State University

Order Number 9126184

Synthesis and characterization of reduced ternary molybdenum oxides and soluble copper(II) alkoxide complexes

Chen, Sheng-Chang, Ph.D.

Iowa State University, 1991

U·M·I
300 N. Zeeb Rd.
Ann Arbor, MI 48106

Synthesis and characterization of reduced ternary molybdenum oxides and soluble copper(II) alkoxide complexes

by

Sheng-Chang Chen

A Dissertation Submitted to the

Graduate Faculty in Partial Fulfillment of the

Requirements for the Degree of

DOCTOR OF PHILOSOPHY

Department: Chemistry
Major : Inorganic Chemistry

Approved:

Signature was redacted for privacy.

In Charge of Major Work

Signature was redacted for privacy.

For the Major Department

Signature was redacted for privacy.

For the Graduate College

Iowa State University
Ames, Iowa

1991

TABLE OF CONTENTS

LIST OF TABLES

LIST OF FIGURES

GENERAL INTRODUCTION

There has been remarkable progress in the chemistry of reduced ternary or quaternary molybdenum oxides containing infinite chains of trans-edge-shared Mo_4O_6 octahedral cluster units since the discovery of the milestone compound $NaMo_4O_6$[1] by Torardi in 1979. Six different crystallographic structure types have been identified as belonging to this class of compounds. Type I, $M_xMo_4O_6$ (M = Na, In, Pb, Sn, Ba)[1,2], is characterized by $[Mo_4O_6]$ infinite octahedral cluster chains extended along the tetragonal c-axis.[1] These chains are then coupled through Mo-O-Mo interchain linkages to weave a square pattern and form channels parallel to c-axis in which the ternary metal ions are located.

Type II, $^tA^oA_{1-x-y}{}^oB_x{}^oMo_yMo_4O_7$ (A = Fe, Zn; B = Al, Sc, Tl),[3] where the superscripts t and o refer to tetrahedral and octahedral sites, respectively, are orthorhombic with the infinite cluster chains extending along the b-axis. The repeat unit along the chains is doubled compared to that in compounds of type I. A consequence of this doubling is that the octahedral cluster units are tilted slightly about the edge-shared Mo-Mo bonds to give an alternating long-short pattern of apex-apex Mo-Mo distances along the chain. Infinite chains are interlinked in the ab plane through unique O atoms having square planar geometry and forming bonds to two Mo (waist) atoms of each adjacent chain. In the c direction the infinite chains of one layer are shifted by 1/2 c with respect to the layers above and below and the layers are coupled through Mo-O-A and Mo-O-B interlayer linkages.

Only one compound has been found that belongs to the structure type III, $Mn_{1.5}Mo_8O_{11}$.[4] In this monoclinic structure, the infinite chains composed of highly distorted $Mo_4O_{5.5}$ octahedral repeat units run parallel to the c-axis. The odd stoichiometry is introduced by the unique coupling of adjacent chains through three oxygen atoms with different coordination geometries around them: trigonal planar, square planar, and sawhorse.

Structure type IV is represented by $Ca_{5.45}Mo_{18}O_{32}$.[5] This monoclinic compound is unique in having three kinds of infinite chains, each of which run parallel to the b-axis. These three kinds of chains are indicated by the formula $Ca_{5.45}(MoO_3)_2(Mo_2O_{3.5})_4(Mo_4O_6)_2$ with repeat units (MoO_3) consisting of single Mo atom chains like those found in the rutile structure, repeat units ($Mo_2O_{3.5}$) composed of trans-edge-shared rhomboidal clusters like those found in $NaMo_2O_4$,[5] and repeat units (Mo_4O_6) like those in $NaMo_4O_6$.[1]

Compounds of type V are $LiMo_8O_{10}$ and $ZnMo_8O_{10}$.[6] The outstanding feature of this structure type is that the infinite octahedral cluster chains run in two orthogonal directions, parallel to the a and b tetragonal axes.

Structure type VI, $M_4Mo_4O_{11}$ (M = Nd, Sm, Eu, Gd, Tb, Dy, Ho, Er, Tm, Yb, and Lu),[7] are orthorhombic with the infinite cluster chains extending along the c-axis. The most prominent structural feature of this structure type is that the molybdenum oxide cluster chains are "diluted" within the ternary metal oxide lattice. Consequently, there are no direct Mo-O-Mo interchain linkages.

In comparison to the large number of compounds containing infinite chains of trans-edge-shared Mo_4O_6 octahedral cluster units, examples of compounds containing discrete oligomeric cluster units are rather scarce. In 1986, $In_{11}Mo_{40}O_{62}$[8] was the first compound reported having finite chains of octahedral cluster units; in this case units with both four and five trans-edge-shared Mo_6 octahedra were observed. A compound containing a discrete Mo_6 octahedron is realized in the structure of $BaMo_6O_{10}$.[9] The compound $Tl_{0.6}Sn_{0.6}Mo_7O_{11}$[10] containing a chain fragment of three trans-edge-shared Mo_6 octahedra has been more recently discovered by Simon and coworkers. An x-ray powder investigation of $LaMo_5O_8$[11] indicated that the structure was composed of trans-edge-shared Mo_{10} bioctahedral units. Recently, with a slightly different electron balance, the compound $PbMo_5O_8$[10] was reported to be isostructural with $LaMo_5O_8$.

All the examples of oligomeric cluster units thus far reported, where the fragments of the Mo_4O_6 infinite chain (n = 1 to 5 condensed octahedra) have been identified as building blocks, show an identical coupling of the clusters and can be described by the general formula $Mo_{4n+2}O_{6n+2}O_{4/2}$, where n is the number of Mo_6 octahedra trans-edge-fused together. However, the physical properties of these compounds having oligomeric cluster units were not reported and thus required further study.

In order to better understand the chemistry of highly reduced ternary molybdenum oxides, this research emphasized the preparation of compounds containing oligomeric cluster units and compounds containing potassium (up to now only $K_2Mo_8O_{16}$[12] is known) as the counterion. As a result of it, compounds containing units of three trans-

edge-shared Mo_6 octahedra (n = 3), $K_3Mo_{14}O_{22}$ (Section 1), and units of two trans-edge-shared Mo_6 octahedra (n = 2), $Ba_2Mo_{10}O_{16}$ (Section 2) were discovered. In attempts to prepare $K_2Sr_2Mo_{18}O_{28}$ (n = 4) in the temperature range between 1250 and 1280 ^oC, the compound $Sr_{0.62}Mo_4O_6$ (Section 3) was discovered. Compound KMo_4O_6 prepared at much higher temperature of 1430 ^oC is also reported in Section 3.

Alkoxides of copper(II) are of interest as molecular precursors to solid state materials such as the high-Tc superconducting copper oxide complexes. Unfortunately, the chemistry of copper(II) alkoxides has not been well-developed. Most of these compounds have been found to be insoluble and polymeric, with essentially unknown structures.[13] Structural information has been derived in most cases from studies of spectroscopic and physical properties. As a consequence of this insoluble, polymeric nature of copper(II) alkoxides, efforts in the preparation of high-Tc superconductors from solutions of alkoxide precursors were hampered by a lack of soluble copper(II) alkoxides.[14-17] There is thus a need to prepare new copper(II) alkoxide derivatives which are soluble in a range of organic solvents and which can be definitively structurally characterized. With such soluble alkoxides in hand it might then be possible to apply sol-gel technology[18] to the preparation of the complex copper oxide high-Tc superconducting compounds.

In 1989, McMullen et al. structurally characterized a soluble monomeric copper(II) siloxide complex, $Cu[OSi(OCMe_3)_3]_2(py)_2$(1) but its use as a precursor to high-Tc superconducting copper oxides has not been tested.[19] In the same year, Horowitz et al. reported the preparation of two soluble copper(II) alkoxides, $Cu(OCH_2CH_2NEt_2)_2$(2)

and $Cu(OCH_2CH_2OBu)_2$(3), and their use in the solution route to high-Tc superconductors.[20] About the same time, Goel et al. also reported the preparation of a soluble copper(II) alkoxide, $[Cu(OCH_2CH_2OCH_2CH_2OMe)_2]_n$(4) where $n \geq 5$, and its use in the hydrolytic synthesis of $YBa_2Cu_3O_{7-x}$.[21] However, the structure of 2, 3, and 4 were undetermined. Two volatile monomeric copper(II) alkoxides, $Cu[OCHMeCH_2NMe_2]_2$(5) and $Cu[OCH_2CH_2NMeCH_2CH_2NMe_2]_2$(6), have been more recently structurally characterized by Buhro and coworkers.[22]

The insoluble, polymeric structures of conventional copper(II) alkoxides are due to extensive alkoxide bridging.[23] The tendencies for bridging may be decreased and solubilities increased by using chelating alkoxide ligands.[24] Sections 4 and 5 present the synthesis and characterization of four new copper(II) alkoxide complexes containing the bidentate chelating alkoxide ligand, hep, the anion of 2-(2-hydroxyethyl)pyridine. Section 6 reports some partially characterized reduced molybdenum oxides and a novel copper(II) alkoxide complex.

Explanation of Dissertation Format

This dissertation consists of six sections, the first five sections are formatted for publication in a technical journal and the last section details the incomplete work on several compounds. While the references cited in the general introduction may be found at the end of the dissertation, each section contains an independent listing of references cited in that section.

SECTION 1. SYNTHESIS, STRUCTURE, AND PHYSICAL PROPERTIES OF $K_3Mo_{14}O_{22}$ - AN OXIDE CONTAINING Mo_{14} EDGE-SHARED TRIOCTAHEDRAL CLUSTERS

INTRODUCTION

Synthesis of new reduced ternary molybdenum oxides has been an active research area in this laboratory for the past decade. Since the discovery of the first reduced ternary molybdenum oxide, $NaMo_4O_6$,[1] in 1979, a series of compounds analogous to $NaMo_4O_6$ have been prepared in this laboratory, where the counterions are K,[2] In,[3] Pb,[3] Sn,[4] Sr,[2] and Ba.[5] The structure of $NaMo_4O_6$ contains infinite chains of Mo_6 octahedra trans-edge-fused together and can be described by the general formula $Mo_{4n+2}O_{6n+2}O_{4/2}$ with $n = \infty$, where n is the number of Mo_6 octahedra trans-edge fused together.

Compounds containing discrete oligomeric cluster units cut from these chains have been prepared, but so far only a few members are known. The oligomeric segments can be represented by the formula $Mo_{4n+2}O_{6n+4}$. The first member containing Mo_6 octahedral clusters (n = 1) is realized only in the structure of $BaMo_6O_{10}$.[8] Compounds containing the discrete Mo_{10} trans-edge-shared bioctahedral cluster (n = 2) are known for $LaMo_5O_8$[7] and $PbMo_5O_8$[8] ($M_2Mo_{10}O_{16}$ with M = La or Pb). $Tl_{1.6}Sn_{1.2}Mo_{14}O_{22}$[8] is the only compound known that contains the discrete oligomeric cluster unit with n = 3. The clusters $Mo_{18}O_{28}^{7-}$ and $Mo_{22}O_{34}^{8-}$ with n = 4 and 5, respectively, were discovered together in the structure of $In_{11}Mo_{40}O_{62}$.[9] By means of Extended Hückel calculations the metal-metal bonding in the reduced ternary molybdenum oxides containing either the infinite chains[10] or the discrete oligomeric clusters[11] of Mo_6 octahedra has been studied in detailed by Hoffmann et al. This section describes the

synthesis, structure, and physical properties of $K_3Mo_{14}O_{22}$, an oxide that contains the discrete oligomeric cluster unit with n = 3.

EXPERIMENTAL

Materials and Methods

The reduced nature of these molybdenum oxides requires that precautions be taken during preparation. In general it was necessary that all reactants be dried to minimize the amount of adventitious water in the reactions. Reactions were carried out in sealed molybdenum, nickel, or fused-silica tubes to ensure that the correct stoichiometry was maintained. Reactants were mixed together and thoroughly ground to obtain a homogeneous mixture before being pressed into pellets. In cases where optimum crystal growth was desired, the reactants were left as the mixed powders, which increased the size of crystals that were grown.

Molybdenum powder (99.99%) was used as obtained from Aldrich Chemical Company. Prior to use, the powder was dried at 120° C under dynamic vacuum for 24 hrs and stored in a desiccator. MoO_3 (Fisher Certified A.C.S.) was fired at 550°C for 12 hrs and stored in a desiccator. Potassium molybdate was prepared by the reaction of KOH (Fisher Certified A.C.S.) with a stoichiometric quantity of MoO_3 in deionized water. The molybdate solution was filtered, its volume reduced by heating, and the precipitate collected on a glass frit. The product was then dried at 120° C for 10 hrs and stored in a dry box. Molybdenum tubing was obtained from Thermo-Electron Corp. (99.97%) and MoO_2 powder from Alfa Products (99.0%).

Physical Measurements

The magnetic susceptibility measurements were carried out on a powdered sample with a SQUID magnetosusceptometer. The magnetic field strength was set at 30 KG. The experimental data were corrected for the diamagnetic contribution from quartz tube in which a powdered sample of $K_3Mo_{14}O_{22}$ was held. X-band ESR spectra were recorded on powdered samples with a Bruker ER200-SRC instrument equipped with an Oxford Instruments ESR 900 flow-through cryostat and a DTC-2 digital temperature controller. A Hewlett-Packard 5342 Å microwave frequency counter was used to accurately measure the frequency of the spectrometer. A nominal frequency of 9.767 GHz and a modulation frequency of 100 KHz was used.

Electrical resistivity measurements were carried out on a pressed pellet sintered in an evacuated fused quartz ampoule at 1200^0 C for one day. The measurement is based on the Van der Pauw four-probe method for electrical conductivity measurement.[12] The method entails passage of a constant current through the sample using two contacts while measuring the concurrent potential drop with the remaining two leads. The sample was prepared by attaching four platinum wires, which served as the voltage and current leads, to the pellet with Epo-Tech silver epoxy. The voltage drops across the sample were recorded as a function of temperature. The temperature readings were provided by platinum and carbon glass resistance thermometers. The voltage across a standard calibrated resistor was measured periodically to insure a constant current throughout the experiment.

Synthesis and Analysis

This crystalline compound was first discovered in a multiphase product obtained from a reaction of stoichiometric amounts of MoO_3, Mo, and a two-fold excess of K_2MoO_4 for the target compound $KMo_{11}O_{17}$. The reactants were ground together in a dry box, sealed in an electron-beam welded, evacuated molybdenum tube (3 cm long x 0.8 cm inner diameter), and fired under Ar(g) at 1430°C for 4 days. The outer surface of the Mo-tube was oxidized to MoO_2 but the inner surface was still shiny and remained as Mo. The reaction mixture was washed with water to remove the unreacted K_2MoO_4. Crystals observed in the product mixture were found to have needle (to be discussed in Section 3), hexagonal pyramidal, and truncated pyramidal morphologies.

A Guinier powder diffraction pattern of the bulk product indicated the presence of "$K_{2+x}Mo_{12}O_{19}$," a phase previously investigated and formulated by Charlie Torardi[13] and Lorraine Aleandri.[14] Weak lines due to Mo were also observed in the powder pattern. Preliminary film work on several crystals indicated that they were either twins or polycrystals. An x-ray single crystal diffraction data set was collected on a crystal (0.08 x 0.04 x 0.01 mm) cut off from a hexagonal pyramidal crystal. The data were collected with a Rigaku AFC6R diffractometer at 22°C. The unit cell was indexed as monoclinic with the space group $P2_1/a$ (#14) and the lattice parameters a = 9.916 Å, b = 9.325 Å, c = 10.439 Å, and β = 103.96°. Because of overall weak intensities and the consequently limited data set, it was not possible to refine the crystal structure.

Good quality crystals of this compound were later prepared by reacting a mixture of K_2MoO_4, MoO_2, and Mo in a mole ratio of 3:11:8 (i.e. aiming at $K_3Mo_{11}O_{17}$) in a

molybdenum tube which, in turn, was sealed in a quartz tube and fired at 1250°C for 8 days. The resulting product was washed with water to remove unreacted K_2MoO_4. A Guinier powder pattern of the bulk product was identical to the previous preparations. X-ray single crystal data collection and structure solution were thus performed on a crystal selected from this reaction product. Subsequently, a single-phase sample of $K_3Mo_{14}O_{22}$ was prepared by heating a pressed pellet containing stoichiometric amounts of MoO_3, Mo, and a two-fold excess of K_2MoO_4 in a quartz tube at 1200°C for 8 days. The excess K_2MoO_4 was removed by washing thoroughly with H_2O. The excess K_2MoO_4 here was used as a molten salt medium to facilitate the formation of $K_3Mo_{14}O_{22}$.

X-ray Powder Diffraction Data

An Enraf Nonius Delft triple focusing Guinier x-ray powder diffraction camera was used with Cu $K\alpha_1$ radiation (λ = 1.54056 Å) to obtain d-spacings. National Bureau of Standards silicon powder was mixed with the sample as an internal standard. The observed versus calculated d-spacings are listed in Table 1.1. The diffraction pattern could be indexed based on cell dimensions determined from the single crystal diffraction data. The cell parameters computed by a least-squares method using 31 strongest diffraction lines are a = 9.930(3) Å, b = 9.323(5) Å, c = 10.444(5) Å, and β = 103.93(4)°. As shown in Table 1.1, the relatively poor precision of cell parameters is presumably due to some very weak diffraction lines, such as (1 2 0) and (-1 2 1), that are barely seen on the Guinier powder pattern and can not be read precisely.

Table 1.1. X-ray powder diffraction data for $K_3Mo_{14}O_{22}$

d-spacings (Å) observed	d-spacings (Å) calculated[b]	Intensities[a]	h k l
6.70(1)	6.697	s	1 1 0
6.077(9)	6.075	w	-1 1 0
5.211(6)	5.199	vw	1 1 1
4.414(4)	4.412	vw	-1 1 2
4.207(4)	4.196	vw	1 2 0
4.036(4)	4.029	vw	-1 2 1
3.426(3)	3.430	w	0 2 2
3.108(2)	3.108	m	0 3 0, -3 1 1
3.039(2)	3.038	w	-2 2 2
2.963(2)	2.969	s	2 1 2
2.899(2)	2.898	vw	-1 3 1
2.832(2)	2.830	vw	1 1 3
2.781(2)	2.784	vw	1 3 1
2.693(2)	2.691	ms	-3 2 1
2.505(1)	2.505	m	1 2 3
2.482(1)	2.479	m	-4 0 1
2.413(1)	2.411	s	2 1 3
2.399(1)	2.396	m	-4 1 1
2.335(1)	2.333	m	-4 1 2
2.277(1)	2.277	w	-1 2 4
2.262(1)	2.261	vw	-3 3 1
2.224(1)	2.223	m	4 0 1
2.205(1)	2.206	w	-2 2 4
2.192(1)	2.189	w	-4 2 1
2.078(1)	2.074	vw	1 2 4
2.044(1)	2.043	w	-3 2 4
1.948(1)	1.946	s	2 3 3, -2 3 4
1.941(1)	1.938	s	-4 3 1
1.909(1)	1.905	w	3 2 3
1.833(1)	1.834	w	1 4 3
1.826(1)	1.823	w	-5 2 1

[a]Intensities: s = strong, ms = medium strong, m = medium, w = weak, and vw = very weak

[b]Refined monoclinic cell parameters a = 9.930(3) Å, b = 9.323(5) Å, c = 10.444(5) Å, and $\beta = 103.93(4)^{o}$

X-ray Single Crystal Data Collection

A black trigonal prismatic crystal of $K_3Mo_{14}O_{22}$ having approximate dimensions of 0.06 x 0.06 x 0.08 mm was mounted on a glass fiber. Data were collected with a Rigaku AFC6R diffractometer at room temperature up to $2\theta = 50^{o}$ by using graphite-monochromated Mo Kα radiation and a 12 KW rotating anode generator. A scan mode of ω-2θ was used. Lattice parameters and orientation matrix for data collection were measured from 15 carefully centered reflections with $13^{o} < 2\theta < 17^{o}$. The lattice was found to belong to the monoclinic system with cell dimensions: a = 9.916(2) Å, b = 9.325(2) Å, c = 10.439(2) Å, $\beta = 103.96(1)^{o}$, and V = 936.7(5) $Å^3$. Three standard reflections which were measured after every 150 reflections showed no apparent variation in intensity during the data collection. The linear absorption coefficient number for Mo Kα is 96.0 cm^{-1}. An empirical absorption correction was applied, based upon azimuthal scans of several reflections with transmission factors in the range from 0.873 to 1.000. The intensity data were corrected for Lorentz and polarization effects. A correction for secondary extinction was also applied and gave a coefficient of 2.946(1) x 10^{-6}. Of the 1878 reflections which were collected in the quadrant (h, k, $\pm$l), 1771 were unique ($R_{int} = 0.003$) and 1060 were considered as observed ($I > 3\sigma(I)$).

Structure Solution and Refinement

The space group $P2_1/a$ (#14) was chosen based on the systematic absences of h0l: $h \neq 2n$ and 0k0: $k \neq 2n$. The structure was solved by direct methods (MULTAN)[15] and refined on $|F|$ by full matrix least-square techniques in the TEXSAN[16] package of programs. Three oxygen atoms (O4, O10, and O11) could not be refined anisotropically and the least square refinement scale factor was fixed at 0.4007; all other atoms were refined anisotropically to give R = 0.052 and Rw = 0.068. A θ-dependent numerical correction for absorption was then applied and the structure was refined in CHES.CAT[17,18] programs. The subsequent structure was refined anisotropically to R = 0.034 and Rw = 0.0412. At this stage, the temperature factors of the oxygen atoms were highly anisotropic. When a correction for secondary extinction was applied, the temperature factors for oxygen atoms improved and the refinement converged to give R = 0.0314 and Rw = 0.0369 with a secondary extinction coefficient of $2.946(1) \times 10^{-6}$. The final electron density difference map was flat with a highest peak of 2.0 $e^-/Å^3$ near Mo3.

Details of the data collection and refinement of $K_3Mo_{14}O_{22}$ are given in Table 1.2. Final positional parameters are listed in Table 1.3 and corresponding selected bond distances and angles (based on the single crystal lattice parameters) are given in Table 1.4 and 1.5, respectively. The anisotropic thermal parameters of atoms are listed in Table 1.6. Observed and calculated structure factors are available as supplementary materials.

Table 1.2. X-ray crystallographic data for $K_3Mo_{14}O_{22}$

formula	$K_3Mo_{14}O_{22}$
formula weight	1812.46
crystal system	monoclinic
space group	$P2_1/a$ (#14)
a, Å	9.916(2)
b, Å	9.325(2)
c, Å	10.439(2)
β, deg	103.96(1)
V, $Å^3$	936.7(5)
Z	2
calcd density, g/cm^3	6.425
F000	1634
crystal size, mm	0.06 x 0.06 x 0.08
μ(Mo Kα), cm^{-1}	95.966
diffractometer	Rigaku AFC6R
λ, Å, graphite-monochromated	0.71069
T, ^oC	23
2θ, deg	0-50
scan mode	ω-2θ
No. reflections collected	1771
No. observations ($I > 3\sigma(I)$)	1060
No. variables	176
goodness of fit indicator[a]	1.62
max. shift in final cycle	0.005
largest peak in final diff. map, $e/Å^3$	2.0
transmission coefficient	0.87-1.00
R[b], Rw[c]	0.031, 0.037

[a] Quality-of-fit = $[\Sigma\omega(|Fo| - |Fc|)^2/(N_{obs} - N_{parameters})]^{1/2}$

[b] $R = \Sigma||Fo| - |Fc||/\Sigma|Fo|$

[c] $Rw = [\Sigma\omega(|Fo| - |Fc|)^2/\Sigma\omega|Fo|^2]^{1/2}$; $\omega = 1/\sigma^2(|Fo|)$

Table 1.3. Atomic coordinates (x 10^4) for $K_3Mo_{14}O_{22}$

ATOM	X	Y	Z	(10^3) U_{eq}[a]
Mo1	1227.(1)	3885.(1)	1400.(1)	12.
Mo2	9146.(1)	3774.(1)	2748.(1)	13.
Mo3	2282.(1)	6263.(1)	2876.(1)	13.
Mo4	8473.(1)	3706.(1)	144.(1)	13.
Mo5	1906.(1)	3843.(1)	4104.(1)	13.
Mo6	474.(1)	3814.(1)	8647.(1)	13.
Mo7	9754.(1)	3719.(1)	5934.(1)	13.
K1	0.0(0)	0.0(0)	0.0(0)	21.
K2	667.(3)	119.(4)	3136.(3)	21.
O1	3254.(12)	7596.(12)	9945.(9)	19.
O2	4017.(10)	7559.(11)	2812.(8)	14.
O3	3143.(12)	2555.(10)	5722.(8)	16.
O4	1340.(10)	5049.(11)	5630.(8)	12.
O5	2235.(10)	5011.(11)	8571.(8)	13.
O6	7154.(10)	4799.(10)	8580.(9)	13.
O7	3864.(13)	2511.(10)	8593.(10)	15.
O8	6527.(10)	4899.(11)	5753.(9)	15.
O9	9694.(11)	7323.(11)	5627.(9)	14.
O10	2536.(11)	7580.(10)	7128.(8)	12.
O11	9694.(12)	2373.(10)	1502.(9)	12.

[a]The complete temperature factor is $\exp(-8\pi^2 U_{eq} \sin^2\theta/\lambda^2)$, where $U_{eq} = 1/3 \Sigma_{ij} U_{ij} a_i^* a_j^* a_i \cdot a_j$ in units of $Å^2$

Table 1.4. Selected bond distances (Å) for $K_3Mo_{14}O_{22}$

Mo1-Mo2'	2.765(2)	Mo1-Mo3	2.758(2)
Mo1-Mo4'	2.735(2)	Mo1-Mo4	2.822(20
Mo1-Mo5	2.739(2)	Mo1-Mo6'	2.722(2)
Mo1-Mo6	2.791(2)	Mo2-Mo4	2.639(2)
Mo2-Mo5'	2.761(2)	Mo2-Mo6	2.754(2)
Mo2-Mo7	2.797(2)	Mo2-Mo7(Inter)	3.234(2)
Mo3-Mo4	3.060(2)	Mo3-Mo5	2.666(2)
Mo3-Mo6'	2.811(2)	Mo3-Mo7'	2.613(2)
Mo4-Mo6	2.720(2)	Mo4-Mo6'	2.808(2)
Mo5-Mo7(Inter)	3.191(2)	Mo5-Mo7'	2.801(2)
Mo6-Mo7	2.750(2)	Mo7-Mo7'(Inter)	3.194(2)
Mo1-O1	2.01(1)	Mo1-O6	2.02(1)
Mo1-O10	2.11(1)	Mo1-O11	2.10(1)
Mo2-O4	2.17(1)	Mo2-O5	2.04(1)
Mo2-O9	2.07(1)	Mo2-O10	2.12(1)
Mo2-O11	2.01(1)	Mo3-O2	2.12(1)
Mo3-O3	2.02(1)	Mo3-O6	2.00(1)
Mo3-O7	2.04(1)	Mo3-O8	1.95(1)
Mo4-O1	2.08(1)	Mo4-O5	2.04(1)
Mo4-O6	2.09(1)	Mo4-O7	2.09(1)
Mo4-O11	2.05(1)	Mo5-O3	2.19(1)
Mo5-O4	2.13(1)	Mo5-O8	1.92(1)
Mo5-O9	2.00(1)	Mo5-O10	1.92(1)
Mo6-O1	2.04(1)	Mo6-O2	2.08(1)
Mo6-O5	2.09(1)	Mo6-O7	2.01(1)
Mo7-O2	1.90(1)	Mo7-O3	1.97(1)
Mo7-O4	2.09(1)	Mo7-O4(Inter)	2.08(1)
Mo7-O9	2.08(1)	K1•••K2	3.181(3)
K1-O1	2.97(1)	K1-O5	2.79(1)
K1-O6	2.89(1)	K1-O7	2.83(1)
K1-O11	2.771(9)	K2-O2	2.96(1)
K2-O3	2.80(1)	K2-O4	2.94(1)
K2-O5	3.05(1)	K2-O6	2.95(1)
K2-O7	3.13(1)	K2-O8	2.71(1)
K2-O8'	2.858(9)	K2-O9	2.78(1)
K2-O10	2.96(1)	K2-O11	2.73(1)

Table 1.5. Selected bond angles (deg.) for $K_3Mo_{14}O_{22}$

Mo2'-Mo1-Mo3	88.56(5)	Mo2'-Mo1-Mo4'	57.34(4)
Mo2'-Mo1-Mo4	121.00(5)	Mo2'-Mo1-Mo5	60.22(4)
Mo2'-Mo1-Mo6	118.43(5)	Mo2'-Mo1-Mo6'	60.24(4)
Mo3-Mo1-Mo4'	121.15(6)	Mo3-Mo1-Mo4	66.50(4)
Mo3-Mo1-Mo5	58.01(4)	Mo3-Mo1-Mo6	124.45(6)
Mo3-Mo1-Mo6'	61.72(4)	Mo4'-Mo1-Mo4	90.31(5)
Mo4'-Mo1-Mo5	117.51(5)	Mo4'-Mo1-Mo6	61.08(4)
Mo4'-Mo1-Mo6'	59.79(4)	Mo4-Mo1-Mo5	124.51(6)
Mo4-Mo1-Mo6	57.96(4)	Mo4-Mo1-Mo6'	60.85(4)
Mo5-Mo1-Mo6	177.47(6)	Mo5-Mo1-Mo6'	91.54(5)
Mo6-Mo1-Mo6'	89.41(5)	Mo1'-Mo2-Mo4'	60.74(4)
Mo1'-Mo2-Mo5'	59.42(4)	Mo1'-Mo2-Mo6	59.10(4)
Mo1'-Mo2-Mo7	88.20(5)	Mo4-Mo2-Mo5'	120.12(5)
Mo4-Mo2-Mo6	60.53(4)	Mo4-Mo2-Mo7	119.91(6)
Mo5'-Mo2-Mo6	90.39(5)	Mo5'-Mo2-Mo7	60.51(4)
Mo6-Mo2-Mo7	59.33(4)	Mo1-Mo3-Mo4	57.74(4)
Mo1-Mo3-Mo5	60.64(4)	Mo1-Mo3-Mo6'	58.50(4)
Mo1-Mo3-Mo7'	92.18(5)	Mo4-Mo3-Mo5	118.38(5)
Mo4-Mo3-Mo6'	56.97(4)	Mo4-Mo3-Mo7'	117.70(5)
Mo5-Mo3-Mo6'	91.17(5)	Mo5-Mo3-Mo7'	64.08(5)
Mo6'-Mo3-Mo7'	60.79(4)	Mo1'-Mo4-Mo1	89.69(5)
Mo1'-Mo4-Mo2	61.91(4)	Mo1'-Mo4-Mo3	117.47(5)
Mo1'-Mo4-Mo6'	60.45(4)	Mo1'-Mo4-Mo6	59.87(4)
Mo1-Mo4-Mo2	122.28(6)	Mo1-Mo4-Mo3	55.76(4)
Mo1-Mo4-Mo6'	57.82(4)	Mo1-Mo4-Mo6	60.45(4)
Mo2-Mo4-Mo3	178.04(7)	Mo2-Mo4-Mo6'	122.36(5)
Mo2-Mo4-Mo6	61.83(5)	Mo3-Mo4-Mo6'	57.05(4)
Mo3-Mo4-Mo6	116.21(5)	Mo6-Mo4-Mo6'	89.10(5)
Mo1-Mo5-Mo2'	60.36(4)	Mo1-Mo5-Mo3	61.35(4)
Mo1-Mo5-Mo7'	88.65(5)	Mo2'-Mo5-Mo3	90.55(5)
Mo2'-Mo5-Mo7'	60.37(4)	Mo3-Mo5-Mo7'	57.04(4)

Table 1.5. (continued)

Mo1-Mo6-Mo1'	90.59(5)	Mo1-Mo6-Mo2	119.22(6)
Mo1-Mo6-Mo3'	124.41(5)	Mo1-Mo6-Mo4'	58.47(4)
Mo1-Mo6-Mo4	61.58(4)	Mo1-Mo6-Mo7	179.35(6)
Mo1'-Mo6-Mo2	60.66(4)	Mo1'-Mo6-Mo3'	59.78(4)
Mo1'-Mo6-Mo4'	61.33(4)	Mo1'-Mo6-Mo4	60.34(5)
Mo1'-Mo6-Mo7	90.06(5)	Mo2-Mo6-Mo3'	87.73(5)
Mo2-Mo6-Mo4'	121.90(6)	Mo2-Mo6-Mo4	57.64(4)
Mo2-Mo6-Mo7	61.08(4)	Mo3'-Mo6-Mo4'	65.98(4)
Mo3'-Mo6-Mo4	119.77(6)	Mo3'-Mo6-Mo7	56.04(4)
Mo4'-Mo6-Mo4	90.90(5)	Mo4'-Mo6-Mo7	121.96(5)
Mo4-Mo6-Mo7	118.73(6)	Mo2-Mo7-Mo3'	90.88(5)
Mo2-Mo7-Mo5'	59.12(4)	Mo2-Mo7-Mo6	59.53(4)
Mo3'-Mo7-Mo5'	58.88(4)	Mo3'-Mo7-Mo6	63.17(4)
Mo6'-Mo7-Mo6	89.67(5)	Mo1-O1-Mo6	87.3(4)
Mo6-O2-Mo7	87.5(4)	Mo3-O3-Mo7'	82.1(4)
Mo2-O4-Mo7	82.2(3)	Mo5-O4-Mo7'	83.5(3)
Mo2-O5-Mo4	80.6(4)	Mo2-O5-Mo6	83.7(4)
Mo4-O5-Mo6	82.3(4)	Mo3-O6-Mo4	96.6(4)
Mo1-O1-Mo4	131.7(5)(inter)[a]	Mo1-O6-Mo3	86.7(4)
Mo6-O1-Mo4	135.8(5)(inter)	Mo1-O6-Mo4	86.7(4)
Mo6-O2-Mo3	133.5(5)(inter)	Mo3-O7-Mo4	95.7(4)
Mo7-O2-Mo3	134.1(5)(inter)	Mo3-O7-Mo6'	88.0(4)
Mo3-O3-Mo5'	135.3(6)(inter)	Mo4-O7-Mo6'	86.5(4)
Mo7'-O3-Mo5'	135.1(5)(inter)	Mo3-O8-Mo5	87.0(4)
Mo2-O4-Mo7'	99.3(4)(inter)	Mo2-O9-Mo5'	85.4(4)
Mo2-O4-Mo5	177.1(5)(inter)	Mo1-O10-Mo5	85.6(4)
Mo5-O4-Mo7	98.3(4)(inter)	Mo5-O10-Mo2	139.8(5)
Mo7-O4-Mo7'	100.3(4)(inter)	Mo2-O11-Mo4	81.2(4)
Mo2-O9-Mo7'	102.2(4)(inter)	Mo1'-O11-Mo2	84.7(4)
Mo5'-O9-Mo7'	102.9(4)(inter)	Mo1'-O11-Mo4	82.6(4)
Mo1-O10-Mo2	128.9(4)(inter)		

[a]Intercluster angle

Table 1.6. Anisotropic temperature factors ($Å^2 \times 10^3$) for $K_3Mo_{14}O_{22}$[a]

ATOM	U11	U22	U33	U12	U13	U23
Mo1	11.5(6)	10.5(6)	15.3(5)	0.5(6)	2.5(4)	0.2(5)
Mo2	11.3(6)	11.6(6)	14.9(6)	-1.2(5)	2.5(4)	0.2(5)
Mo3	11.9(6)	11.6(6)	15.9(6)	-0.9(5)	2.9(4)	-0.6(5)
Mo4	11.0(6)	12.2(6)	15.6(6)	-0.3(5)	2.4(4)	0.9(5)
Mo5	12.2(6)	11.7(7)	15.7(5)	-0.4(6)	2.0(4)	0.4(5)
Mo6	12.4(6)	11.8(6)	15.3(5)	0.6(5)	3.2(4)	0.2(5)
Mo7	12.5(5)	10.6(6)	15.1(5)	0.2(5)	2.4(4)	-0.1(5)
K1	24.(2)	17.(2)	21.(2)	-1.(2)	4.(2)	-5.(2)
K2	21.(2)	20.(2)	23.(2)	0.(1)	3.(1)	2.(1)
O1	24.(7)	22.(6)	11.(4)	0.(5)	6.(5)	4.(4)
O2	6.(6)	13.(6)	22.(5)	-5.(4)	-2.(4)	2.(4)
O3	18.(6)	18.(6)	11.(5)	-5.(4)	1.(4)	-1.(4)
O4	11.(5)	8.(5)	16.(4)	1.(4)	2.(4)	0.(4)
O5	13.(5)	17.(5)	10.(4)	3.(4)	6.(4)	-1.(4)
O6	10.(5)	7.(5)	21.(5)	5.(4)	5.(4)	6.(4)
O7	17.(6)	8.(4)	20.(4)	0.(4)	1.(4)	3.(4)
O8	12.(5)	16.(5)	19.(5)	-2.(4)	1.(4)	-2.(4)
O9	14.(6)	10.(5)	19.(5)	1.(4)	5.(4)	-1.(4)
O10	13.(6)	9.(5)	16.(4)	2.(4)	2.(4)	1.(4)
O11	11.(5)	8.(5)	18.(4)	3.(4)	-4.(4)	3.(4)

[a]The form of the anisotropic displacement parameter is $\exp[-2\pi^2\{h^2a^2\ U(1,1) + k^2b^2\ U(2,2) + l^2c^2\ U(3,3) + 2hkab\ U(1,2) + 2hlac\ U(1,3) + 2klbc\ U(2,3)\}]$, where a, b, and c are reciprocal lattice constants

RESULTS AND DISCUSSION

Description of Structure

Fig. 1.1 is an ORTEP drawing of a Mo_{14} trans-edge-shared trioctahedral cluster unit in $K_3Mo_{14}O_{22}$ showing the complete coordination by oxygen to give $Mo_{14}O_{34}$. The cluster is centrosymmetrical and has a very interesting pairing between apical Mo atoms. The apical Mo atoms of the same octahedron are moved in an opposite direction along the chain axis to give an alternating long-short pattern of the Mo-Mo distances. This results also in short bonds on top when the corresponding bonds on bottom are long. This alternating pairing is different from the simple pairing observed in the discrete oligomeric cluster units of n = 4 and 5 in $In_{11}Mo_{40}O_{62}$, where the apical Mo atoms of the same octahedron are shifted in the same direction along the chain axis and give the bond alternations between apical Mo atoms reminiscent of the C-C bond alternations in butadiene and 1,4-pentadienyl anion, respectively. Fig. 1.2(a) and (b) illustrate the simple pairing of apical Mo atoms in the latter compound. The Mo5-Mo1-Mo6 bond angle of 177.47(6)^o and Mo1-Mo6-Mo7 of 179.35(6)^o indicate that Mo atoms in the basal planes of the octahedra are in the same plane. The apical Mo atoms in $K_3Mo_{14}O_{22}$ are simply shifted to each other without any tilting of the octahedra around the shared edges, as opposed to the structure of $Sc_{0.75}Zn_{1.25}Mo_4O_7$[19] shown in Fig. 1.2(c), where the octahedra are tilted around the shared edges to give alternating apical Mo-Mo bond lengths along the infinite chain. This preference for an alternating pairing of the apical molybdenum atoms over a tilting of the Mo_6 octahedra showed by

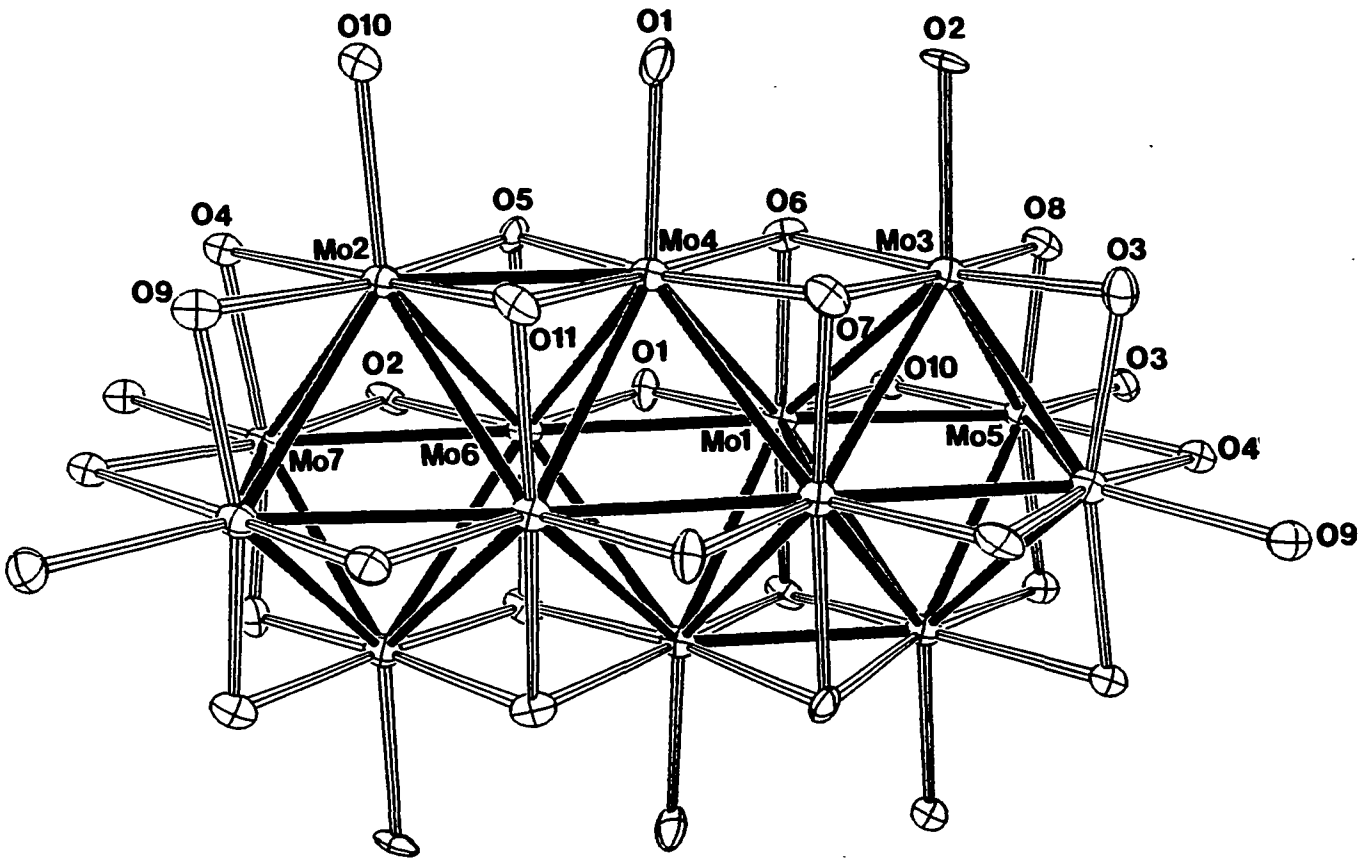

Fig. 1.1. ORTEP drawing (50 % thermal ellipsoids) of a trans-edge-shared trioctahedral cluster in $K_3Mo_{14}O_{22}$ showing the complete coordination by oxygen to form the $Mo_{14}O_{34}$ unit. Solid lines represent Mo-Mo bonds and open lines represent Mo-O bonds.

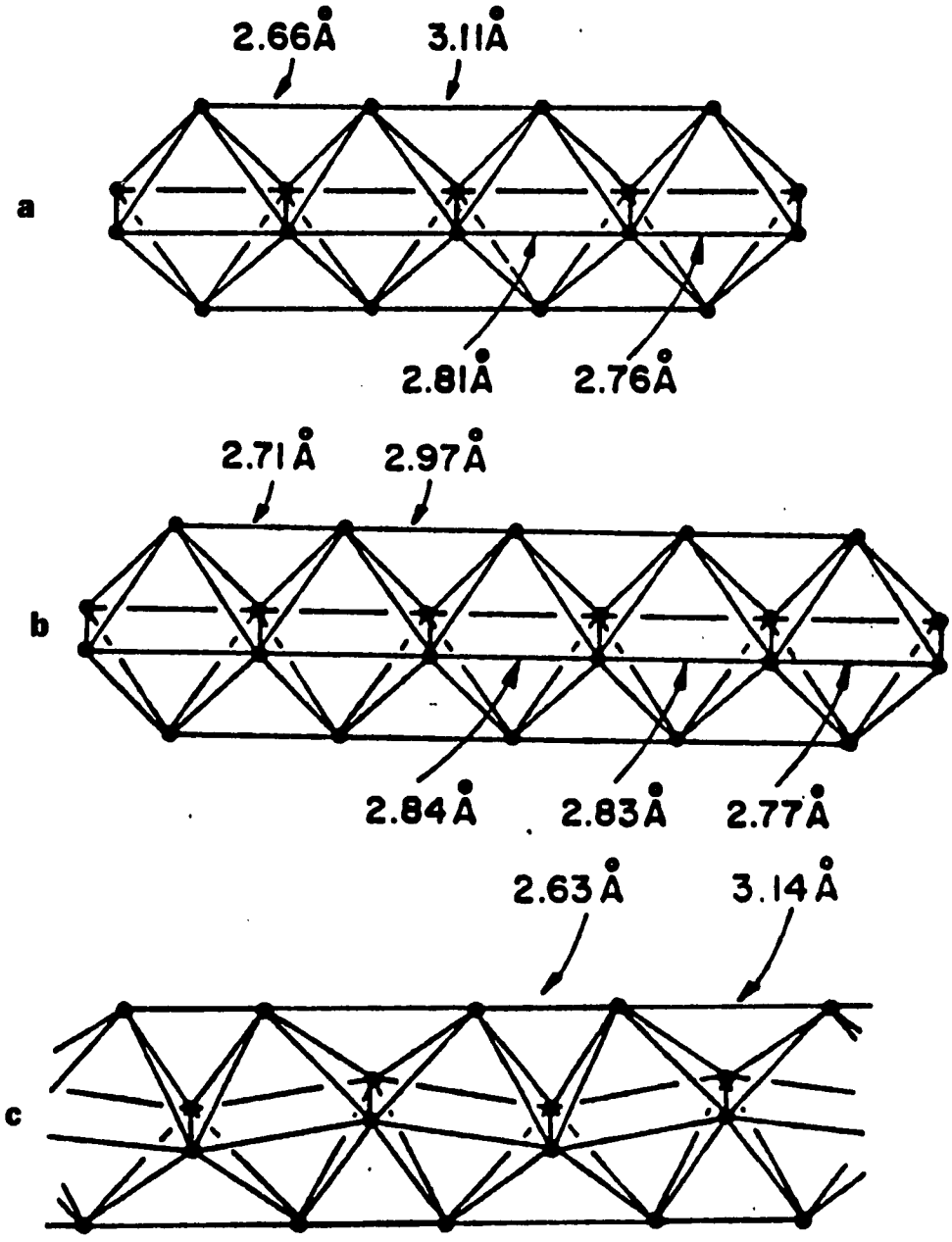

Fig. 1.2. Alternating apex-apex Mo-Mo bond lengths in (a) $Mo_{18}O_{28}^{7-}$, (b) $Mo_{22}O_{34}^{8-}$, and (c) $Sc_{0.75}Zn_{1.25}Mo_4O_7$. The structures shown in (a) and (b) occur in the compound $In_{11}Mo_{40}O_{62}$.

$Mo_{14}O_{22}^{3-}$ is also suggested by Extended Hückel calculations of the total energy changes for the idealized $Mo_{14}O_{22}^{3-}$ cluster.[20] The total energy difference between alternating pairing and tilting distortions of the $Mo_{14}O_{22}^{3-}$ cluster with a shorter apical Mo-Mo distance of 2.65 Å is 0.14 e.v..

Distances between Mo atoms located in the basal planes of the octahedra also show an alternating pattern along the chain axis. The Mo pairs at the ends are separated by 2.750(2) Å (Mo6-Mo7) and 2.739(2) Å (Mo1-Mo5), whereas the inner Mo pairs (Mo1-Mo6 and Mo1'-Mo6') have a bond distance of 2.791(2) Å. The bond distance between Mo atoms in the shared edges of the octahedra (or edges perpendicular to the chain axis) shows a similar alternating pattern, longer on the ends and shorter in the middle of the molecule. Similar bond length alternations between Mo atoms in the basal plane and between shared edges of the octahedra were observed in the discrete $Mo_{18}O_{28}^{7-}$ and $Mo_{22}O_{34}^{8-}$ cluster units of $In_{11}Mo_{40}O_{62}$.

All of the Mo atoms in $K_3Mo_{14}O_{22}$ are bonded to five O atoms, except Mo1, Mo1', Mo6 and Mo6', which are coordinated to four O atoms. The Mo-O bond distances in $K_3Mo_{14}O_{22}$ range from 1.90 to 2.19 Å (average 2.05 Å). The shortest Mo-O bond is between Mo7 and O2, and the longest one is between Mo5 and O3. These unusually short and long distances do not seem to be correlated in any particular way with the structural distortion of the $Mo_{14}O_{22}^{3-}$ cluster, the intercluster connection, or the coordination number around the O atoms. The relatively long distances (ave. 2.12 Å) of Mo-O4 bonds, as compared to the average Mo-O distance of 2.05 Å, most likely arise from the higher coordination number (CN = 4) around O4 atoms due to the intercluster

connections. A similar reason may explain the rather short bond distances (ave. 1.935 Å) of Mo-O8, namely that the O8 atoms are only 2-coordinated.

The intra-cluster Mo-Mo distances in the Mo_{14} cluster unit lie between 2.613 and 3.060 Å (average 2.764 Å). It is surprising that the shortest intra-cluster Mo-Mo distance in $K_3Mo_{14}O_{22}$ is the outer edge Mo3-Mo7', whereas the shortest intra-cluster Mo-Mo distance in $BaM_8O_8^{21}$ is the apical Mo-Mo distance. This unusually short bond distance between apex and waist Mo atoms may be a result of the structural distortion leading to the alternating pairing between the apical Mo atoms. The average bond distances of Mo-O and Mo-Mo in $K_3Mo_{14}O_{22}$ do not differ significantly from those in $BaMo_8O_{10}$ (ave. Mo-O = 2.05 Å; ave. Mo-Mo = 2.759 Å), $BaMo_5O_8$ (ave. Mo-O = 2.06 Å; ave. Mo-Mo = 2.752 Å), $PbMo_5O_8$ (ave. Mo-O = 2.06 Å; ave. Mo-Mo = 2.752 Å), $Tl_{0.8}Sn_{0.6}Mo_7O_{11}$ (ave. Mo-O = 2.06 Å; Ave. Mo-Mo = 2.78 Å), and $In_{11}Mo_{40}O_{62}$ (ave. Mo-O = 2.07 Å; ave. Mo-Mo = 2.79 Å).

Perspective views of the structure of $K_3Mo_{14}O_{22}$ perpendicular to the c-axis and along the b-axis showing the intercluster connections are provided in Figs. 1.3 and 1.4, respectively. The oxygen atoms O5, O6, O7, O8 and O11 are edge-bridging only within the cluster unit (O^i). O1, O2, O3, O9, and O10 are either edge-bridging between Mo atoms or terminal to Mo atoms and coordinate neighboring clusters at either terminal or edge-sharing positions (O^{i-a} or O^{a-i}). O4 atoms are edge-sharing between two neighboring cluster units (O^{i-i}). Therefore, both inter-and intra-cluster sharing of O atoms can be described by the connectivity formula $K^{3+}[Mo_{14}(O_{10}{}^iO_{4/2}{}^{i-i}O_{10/2}{}^{i-a})O_{10/2}{}^{a-i}]^{3-}$. Of special note is the peculiar teeter-toter geometry around O4 which is bonded to four Mo atoms between cluster units with

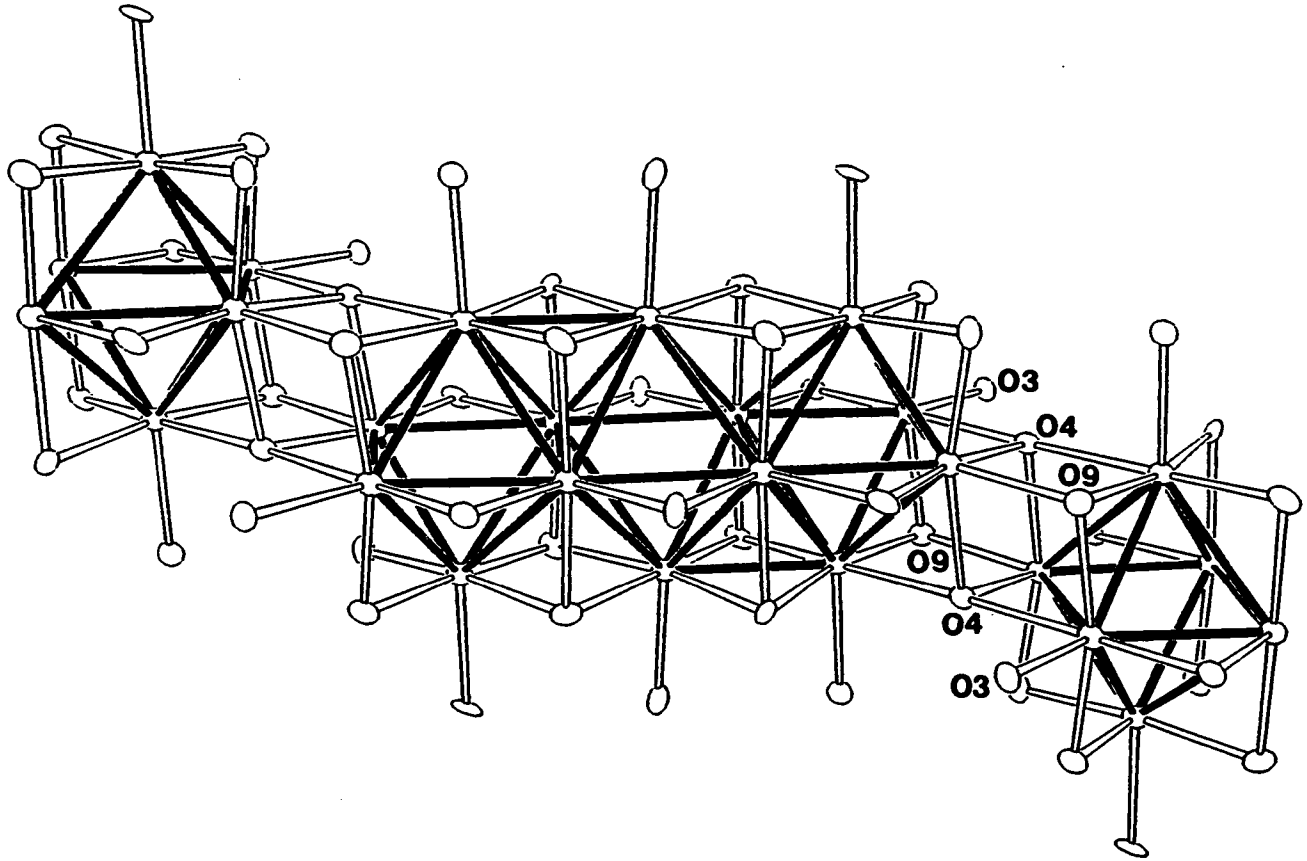

Fig. 1.3. ORTEP drawing (50 % thermal ellipsoids) of a perspective view of the $K_3Mo_{14}O_{22}$ structure showing the intercluster connections along the c-axis. Solid lines are Mo-Mo bonds and open lines are Mo-O bonds.

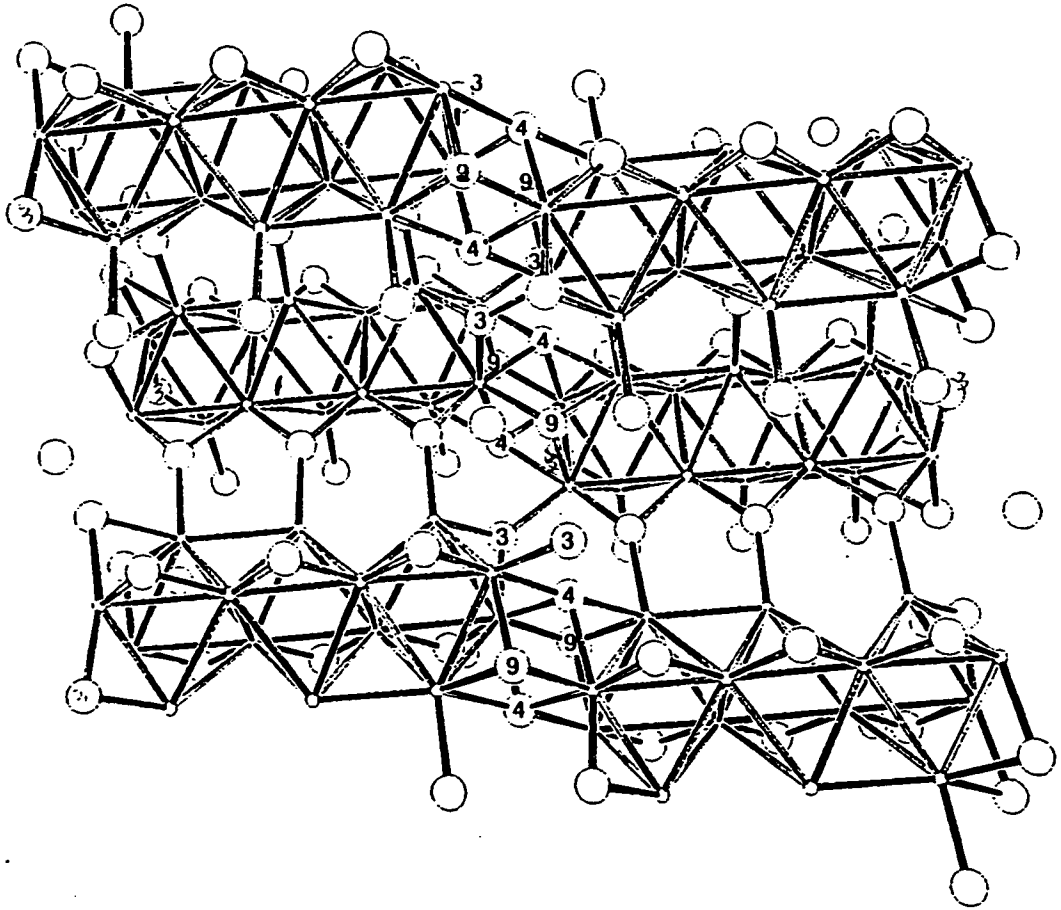

Fig. 1.4. A perspective view of the structure of $K_3Mo_{14}O_{22}$ along the b-axis showing the intercluster connections. For clarity the inner oxygens O5, O6, O7, O8, and O11 are not shown here.

respect to Mo-O bonding. O8 is only two coordinated and the rest of the O atoms are three coordinated. A similar fashion of intercluster connection along the chain axis is also observed in the structure of $Y_6I_{10}Ru$,[22] in which Ru atoms are encapsulated at centers of the $Y_6(I_4^iI_{4/2}^{i-i}I_{4/2}^{i-a})I_{4/2}^{a-i}$ clusters, and the edge-bridging positions in the octahedron are occupied by I atoms. The shortest inter-cluster Mo-Mo distances of 3.191(2) Å (Mo5-Mo7), 3.194(2) Å (Mo7-Mo7), and 3.234(2) Å (Mo2-Mo7) are much longer than corresponding distances in $BaMo_6O_{10}$ and $BaMo_5O_8$. This suggests that the Mo_{14} cluster units in this compound should behave more or less as isolated units with very weak metal-metal coupling, as illustrated in Fig. 1.5.

The coordination around the K atoms is shown in Fig. 1.6, where it is seen that K1 is surrounded by 10 oxygen atoms (at distances of 2.77(9) to 2.97(1) Å) and K2 by 11 oxygen atoms (at 2.658(9) to 2.96(1) Å.) Oxygen atoms O5, O6, O7, and O11 are in bridging positions between K1 and K2 atoms. The K-O distances are a little shorter than the calculated K-O distances (2.97 and 3.02 Å) based on crystal radii for K^+ (1.59 Å, CN = 10; 1.64 Å, CN = 12) and O^{2-} (1.38 Å, CN = 4)[23] and accordingly the K^+ ions are tightly bonded to the oxygen atoms and do not exhibit large thermal parameters. Fig. 1.7 is an ORTEP drawing (50% thermal ellipsoids) of the unit cell of $K_3Mo_{14}O_{22}$ as viewed down the c-axis showing the cross-linking of clusters. Four trans-edge-shared trioctahedral cluster units are coupled through Mo-O-Mo inter-cluster linkage to form channels where the K^+ ions are located. This inter-cluster linking arrangement is quite similar to that found in the infinite chain compounds, e.g. $NaMo_4O_6$.[1]

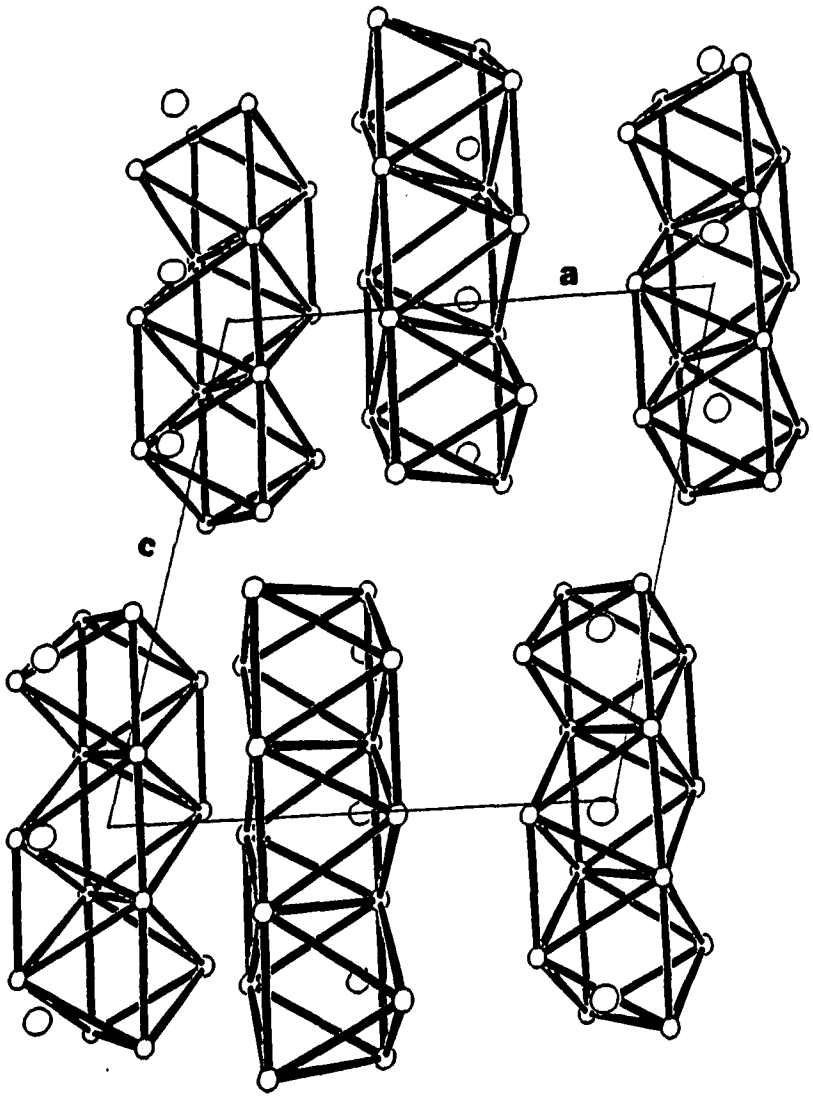

Fig. 1.5. ORTEP drawing (50 % thermal ellipsoids) of a perspective view of the condensed cluster units and K atoms in $K_3Mo_{14}O_{22}$ along [010]; Mo atoms are small ellipsoids, K atoms are large ellipsoids. Clusters are centered at (0, 1/2, 0) and (1/2, 0, 0).

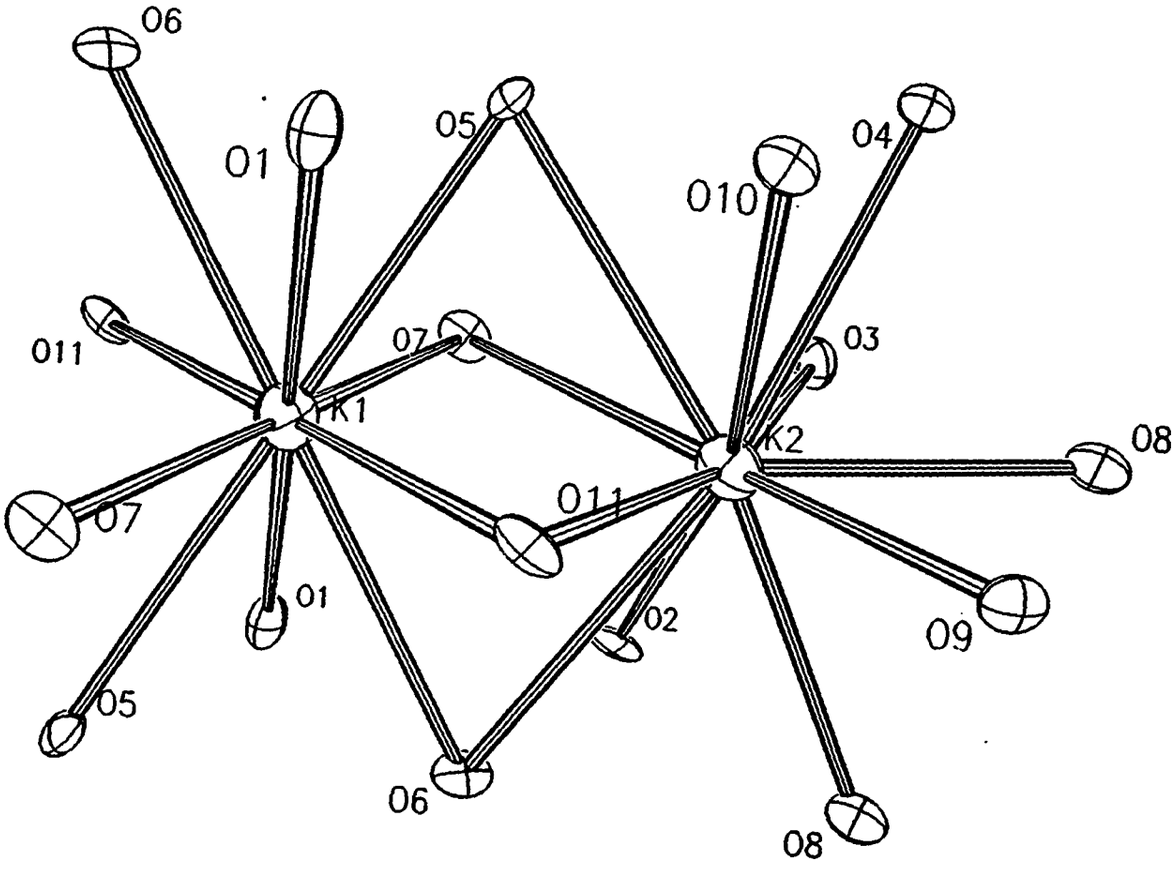

Fig. 1.6. Coordination environments about the K atoms in $K_3Mo_{14}O_{22}$.

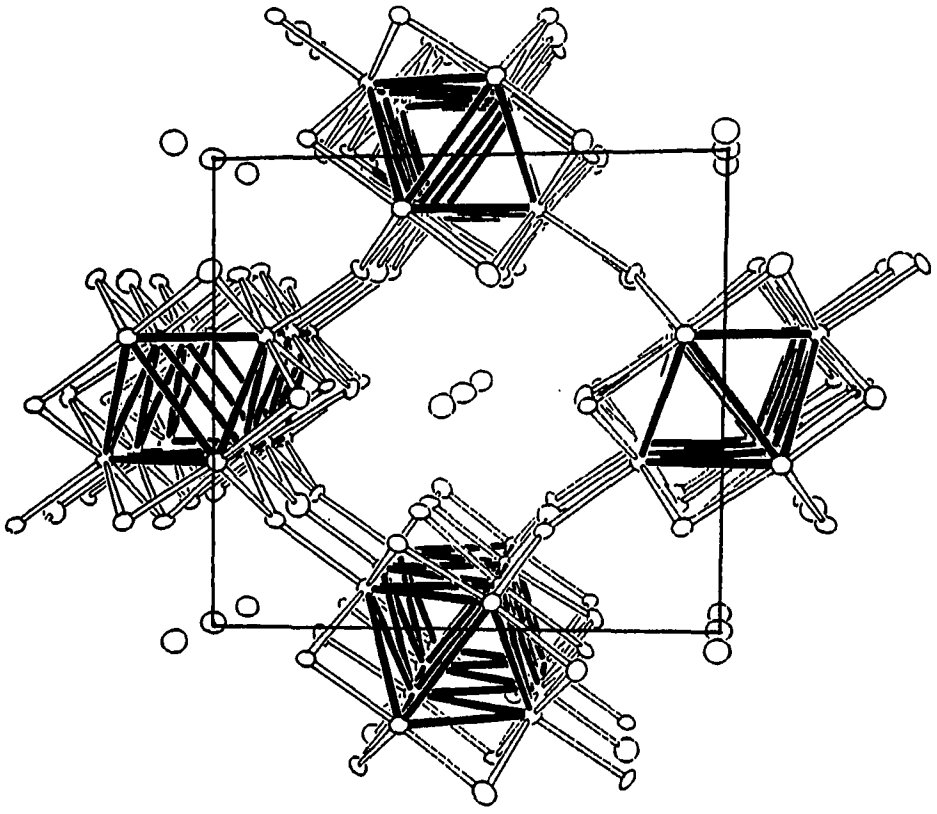

Fig. 1.7. ORTEP drawing (50 % thermal ellipsoids) of the unit cell of $K_3Mo_{14}O_{22}$ as viewed down the c-axis showing the cross-linking of clusters by Mo-O-Mo bridge bonding and the pockets formed for the K atoms (shown as unconnected ellipsoids). Mo-Mo bondings are represented by solid lines and Mo-O bondings by open lines.

Bond Length-Bond Order Relationships

The application of bond length-bond order relationships has provided interesting insights into the structure and bonding of the reduced molybdenum oxides synthesized in this research laboratory.[24] The bond order of the metal-metal bonds is determined by use of Pauling's bond order equation[25] eq. 1,

$$d(n) = d(1) - 0.61 \log n, \quad (1)$$

where d(n) and d(1) are the bond distances for bonds with orders of n and 1, respectively, and n is the bond order. The distance used for d(1) is 2.614 Å, based on calculation of distances to the nearest neighbors and the next nearest neighbors in bcc molybdenum metal.[24] Bond strengths(s) of Mo-O bonds are calculated from the empirical relation (eq.2) developed by Brown and Wu[26] and used by Bart and Ragaini.[27]

$$s(Mo\text{-}O) = [d(Mo\text{-}O)/1.882]^{-6.0} \quad (2)$$

where s is the bond length in valence units (v.u.) and d(Mo-O) is the observed Mo-O bond distance (Å). Since s(Mo-O) is given in v.u. the sum of all Mo-O bond orders about a given Mo atom shall give the valence of that atom. The numerical values of these calculations are tabulated in Table 1.7.

Table 1.7. Bond length - bond order relationships for $K_3Mo_{14}O_{22}$

Atom	d(Mo-Mo)		n	d(Mo-O)		s
Mo1	2.765(2)		0.560(4)	2.01(1)		0.67(2)
	2.758(2)		0.576(4)	2.02(1)		0.65(2)
	2.735(2)		0.628(4)	2.10(1)		0.52(2)
	2.822(2)		0.450(4)	2.11(1)		0.50(2)
	2.739(2)		0.619(4)		Σs	2.34(8)
	2.722(2)		0.660(4)			
	2.791(2)		0.507(4)			
		Σn	4.00(3)			
Mo2	2.765(2)		0.560(4)	2.17(1)		0.43(1)
	2.639(2)		0.908(8)	2.04(1)		0.62(2)
	2.761(2)		0.569(4)	2.07(1)		0.57(2)
	2.754(2)		0.584(4)	2.12(1)		0.49(2)
	2.797(2)		0.496(4)	2.01(1)		0.67(2)
		Σn	3.12(2)		Σs	2.78(9)
Mo3	2.758(2)		0.576(4)	2.12(1)		0.49(2)
	3.060(2)		0.180(2)	2.02(1)		0.65(2)
	2.666(2)		0.819(6)	2.00(1)		0.69(2)
	2.811(2)		0.470(4)	2.04(1)		0.62(2)
	2.613(2)		1.00(1)	1.95(1)		0.81(2)
		Σn	3.05(3)		Σs	3.3(1)
Mo4	2.735(2)		0.628(4)	2.08(1)		0.55(2)
	2.822(2)		0.450(4)	2.04(1)		0.62(2)
	2.639(2)		0.908(8)	2.09(1)		0.53(2)
	3.060(2)		0.180(2)	2.09(1)		0.53(2)
	2.720(2)		0.666(4)	2.05(1)		0.60(2)
	2.808(2)		0.475(4)		Σs	2.8(1)
		Σn	3.31(3)			

Table 1.7. (continued)

Atom	d(Mo-Mo)		n	d(Mo-O)		s
Mo5	2.739(2)		0.619(4)	2.19(1)		0.40(1)
	2.761(2)		0.569(4)	2.13(1)		0.48(1)
	2.666(2)		0.819(4)	1.92(1)		0.89(2)
	2.801(2)		0.488(4)	2.00(1)		0.69(2)
		Σn	2.50(2)	1.92(1)		0.89(2)
					Σs	3.35(8)
Mo6	2.722(2)		0.660(4)	2.04(1)		0.62(2)
	2.791(2)		0.507(4)	2.08(1)		0.55(2)
	2.754(2)		0.584(4)	2.09(1)		0.53(2)
	2.811(2)		0.470(4)	2.01(1)		0.67(2)
	2.720(2)		0.666(4)		Σs	2.37(8)
	2.808(2)		0.475(4)			
	2.750(2)		0.594(4)			
		Σn	3.96(3)			
Mo7	2.797(2)		0.496(4)	1.90(1)		0.94(3)
	2.613(2)		1.00(1)	1.97(1)		0.76(2)
	2.801(2)		0.488(4)	2.09(1)		0.53(2)
	2.750(2)		0.594(4)	2.08(1)		0.55(2)
		Σn	2.58(2)	2.08(1)		0.55(2)
					Σs	3.3(1)

Metal-Metal MCE(Σn) = 2 Σ(Σn) = 45.0(4) e^-

Total valence of Mo_{14} unit = 2 Σ(Σs) = 42(1) v.u.

MCE(Σs) = 6 e^- x 14 - 42(1) = 42(1) e^-

The number of metal-centered electrons (MCE) per $Mo_{14}O_{22}^{3-}$ cluster unit may be estimated from the sum of the metal-metal bond orders and results in MCE(Σn) = 45.0(4) e^-. The total valence of the $Mo_{14}O_{22}^{3-}$ cluster unit is 42(1) v.u., obtained by summing the individual valences of the Mo atoms in the $Mo_{14}O_{22}^{3-}$ cluster unit. The number of electrons utilized for metal-metal bonding is then calculated by subtraction of 42(1) from 84, the maximum number of valence electrons for fourteen molybdenum atoms. The resulting MCE(Σs) of 42(1) e^- is consistent with the MCE(f) of 43 e^-, derived from the formula and the expected valences of K and O in $K_3Mo_{14}O_{22}$. The unusually high total Mo-Mo bond order derived from MCE(Σn) is about two electrons more than those derived from MCE(Σs) and MCE(f).

While it is possible that the Mo-Mo bonding is unusually strong in this compound, the high total bond order given by Σn may also arise from the selection of a value for d(1)(Mo-Mo) which is slightly too large. The value used in these calculations, d(1) = 2.614 Å, has been found as most suitable for the infinite chain compounds like $NaMo_4O_6$. In discrete cluster compounds this value may be somewhat too long because the average coordination number of the Mo atoms is lower. Further indication that the total Mo-Mo bond orders about each Mo are slightly too high is provided by the total valence electron count obtained from the sum $N(e) = \Sigma n + \Sigma s$, which should be equal to 6.00 for Mo. In $K_3Mo_{14}O_{22}$ an average value of 6.1(1) for N(e) was found.

Magnetic Properties

Molar magnetic susceptibility data of $K_3Mo_{14}O_{22}$ collected on a powdered sample over the temperature range of 5-400 K are given in Fig. 1.8. The dotted line drawn through the data is derived from the best least squares fitting to the Curie-Weiss law. The small hump at 50 K results from the antiferromagnetic transition in crystalline O_2, a trace amount of which was condensed on the sample and very difficult to be removed completely. The calculated effective moment of 0.54 μ_B is too low for one unpaired electron per cluster unit as calculated from the formula of $K_3Mo_{14}O_{22}$ and can not be explained by the spin-orbital coupling effects because of the low symmetry (Ci) in the $Mo_{14}O_{22}^{3-}$ cluster unit. And yet this value of 0.54 μ_B is reproducible for samples from different preparations. Investigation of ESR spectra at room temperature resulted in the observation of a signal from an unpaired electron with g = 1.912. Based upon this value a moment of 1.66 μ_B is calculated for one mole. The observed moment of 0.54 μ_B indicates that it arises from an impurity in the sample or that unpaired electrons reside on only a small fraction of the cluster units. The latter could occur if either some divalent ion M^{2+} or some vacancies occur on the K^+ sites of the structure. The g value of 1.912 calculated from the ESR signal indicates that the unpaired electron may reside on the Mo atom of an MoO^{3+} containing impurity[28] which is commonly observed in the molybdenum compounds. We conclude that this low apparent magnetic moment of 0.54 μ_B most likely arises from the paramagnetic impurity and that the pure compound $K_3Mo_{14}O_{22}$ is spin-coupled between cluster units to give a diamagnetic susceptibility, even though the inter-cluster Mo-Mo bondings are weak. One possibility for this

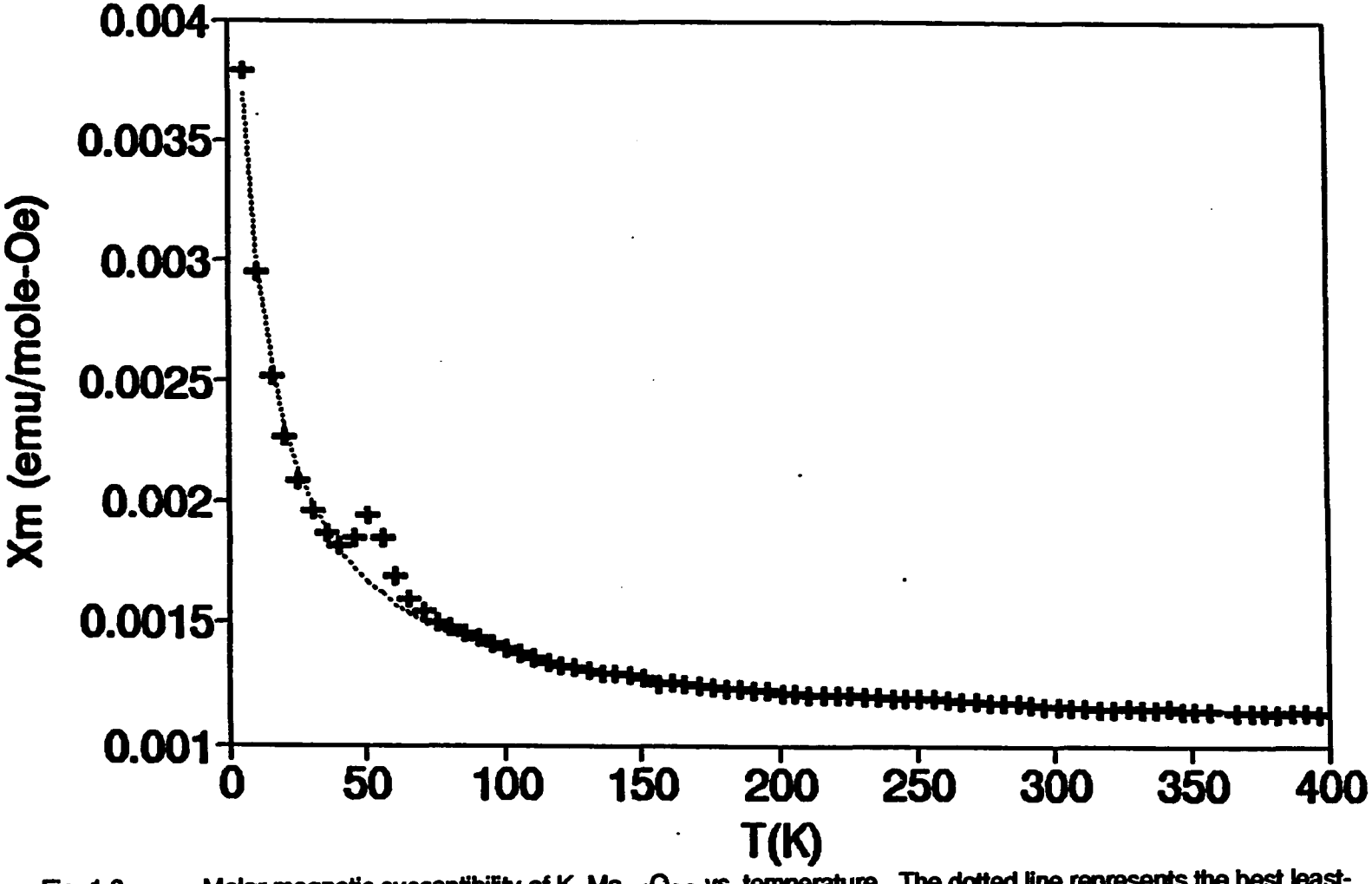

Fig. 1.8. Molar magnetic susceptibility of $K_3Mo_{14}O_{22}$ vs. temperature. The dotted line represents the best least-squares fit to the Curie-Weiss expression. The peak at ca. 50 K arises from the antiferromagnetic transition of adventitious adsorbed O_2.

diamagnetic behavior is the association with a charge disproportionation, forming clusters with 42 and 44 valence electrons. Further work, such as electron diffraction and low temperature x-ray diffraction, will be necessary to test this interpretation.

Resistivity Study

Fig. 1.9 shows the pressed pellet resistivity data of $K_3Mo_{14}O_{22}$ in the temperature range of 5 - 297 K. The pressed pellet resistivity at room temperature is ca. 2.0×10^{-2} ohm-cm, which falls into the resistivity range of a semiconductor. It can be seen from this figure that the resistivities are almost constant in the temperature range of 100 - 297 K and increase more rapidly with the decrease of temperature at $T < 100$ K. This increase of resistivity with the decrease of temperature is characteristic of a semiconductor and the leveling at higher temperatures (100 - 297 K) suggests that the band gap energy is small.

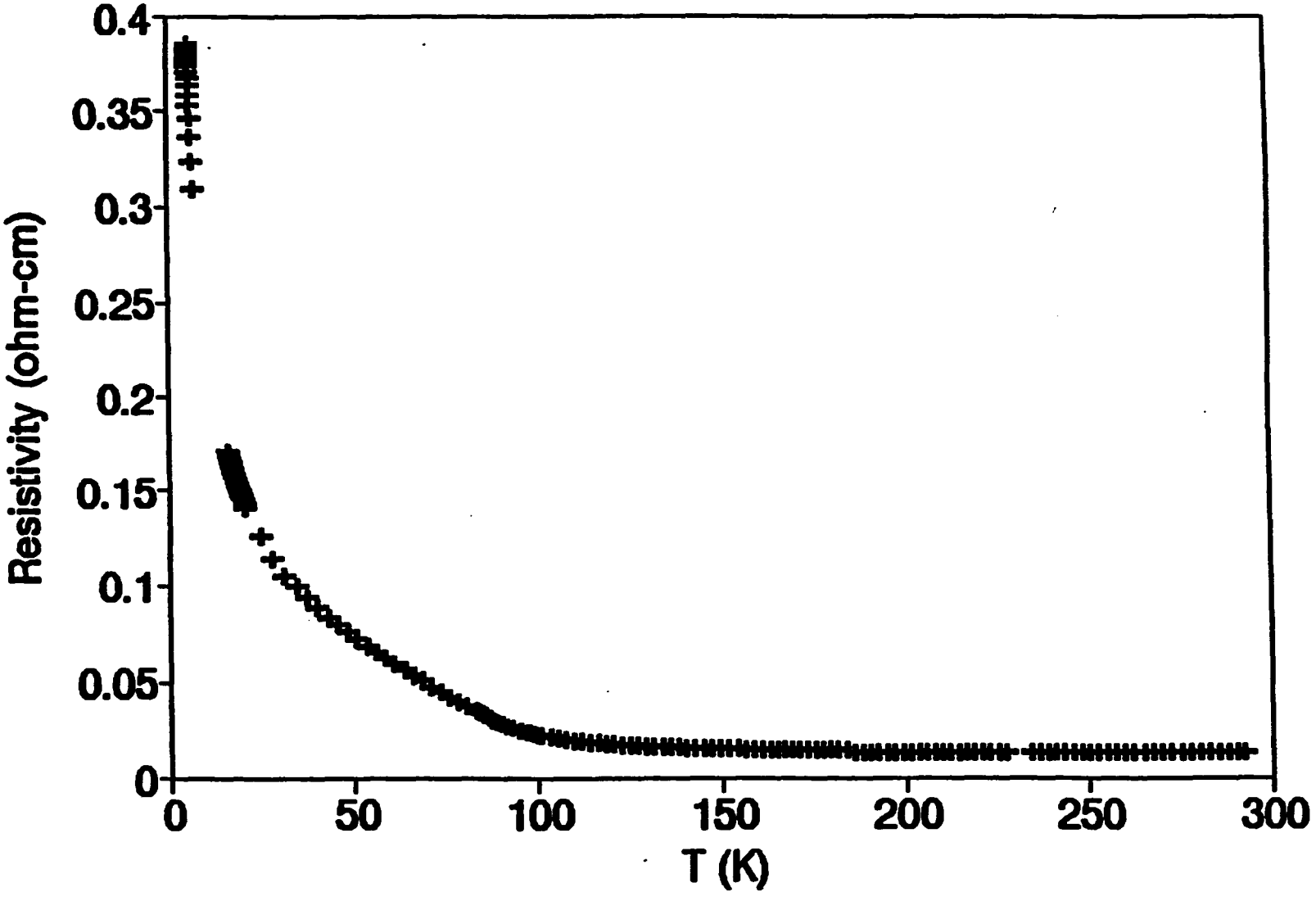

Fig. 1.9. Resistivity vs. temperature for a pressed and sintered pellet of $K_3Mo_{14}O_{22}$.

CONCLUSION

Discrete oligomeric cluster units in the $Mo_{4n+2}O_{6n+2}O_{4/2}$ series with n in the range from 3 to 5 show the similar bond alternations between Mo atoms located in the basal planes and between shared edges of the Mo_6 octahedra along the chain axis. The $Mo_{14}O_{22}^{3-}$ cluster unit is more favorable in the structure of the alternating pairing between apical molybdenum atoms by a sliding motion than by a tilting distortion of the octahedra. Although it is possible that the Mo-Mo bonding is unusually strong in this compound, the selection of a value for d(1)(Mo-Mo) = 2.614 Å which is too large for the lower average coordination number of Mo atoms may be responsible for the unusually high total Mo-Mo bond order in $K_3Mo_{14}O_{22}$ calculated from bond order - bond length relations. From the magnetic susceptibility and ESR studies, it appears that the low apparent magnetic moment of 0.54 μ_B in $K_3Mo_{14}O_{22}$ most likely arises from a paramagnetic impurity and that the pure compound $K_3Mo_{14}O_{22}$ is spin-coupled between cluster units to give a diamagnetic susceptibility.

The comparisons of Mo-Mo bond distances in compounds containing the discrete oligomeric cluster unit with n = 1 to 5 in the $Mo_{4n+2}O_{6n+2}O_{4/2}$ series, as given in Table 1.8, suggest that the intra-cluster Mo-Mo distances are scarcely affected by the degree of cluster condensation, whereas the inter-cluster Mo-Mo distances markedly increase as the degree of cluster condensation increase and the size of the counterions increase (or their charge decreases).

Table 1.8. Intra- and inter-cluster Mo-Mo distances in $Mo_{4n+2}O_{6n+2}O_{4/2}$ series with n = 1, 2, 3, 4, and 5

n	Compound	Mo-Mo(intra)[a] Å	Mo-Mo(inter) Å
1	$BaMo_6O_{10}$	2.759	2.727, 2.890, 3.015
2	$BaMo_5O_8$	2.752	2.778, 3.053, 3.099
	$PbMo_5O_8$	2.75	2.78, 3.03, 3.08
	$LaMo_5O_8$	------	2.733, 2.921, 3.065
3	$K_3Mo_{14}O_{22}$	2.764	3.191, 3.194, 3.234
	$Tl_{0.8}Sn_{0.6}Mo_7O_{11}$	2.78	2.99, 3.04, 3.12
4&5	$In_{11}Mo_{40}O_{62}$	2.79	≥ 3.20

[a]Average intra-cluster Mo-Mo distance

REFERENCES

1. Torardi, C.C.; McCarley, R.E. J. Am. Chem. Soc., 1979, 101, 3963.
2. Chen, S.C., Ph.D. Dissertation, Sect. 3, Iowa State University, Ames, Iowa, 1991.
3. Lii, K.H., Ph.D. Dissertation, Sect. 2, Iowa State University, Ames, Iowa, 1985.
4. Aufdembrink, B.A., Ph.D. Dissertation, Sect. 3, Iowa State University, Ames, Iowa, 1985.
5. Torardi, C.C.; McCarley, R.E. J. Less-Common Metals, 1986, 116, 169.
6. Lii, K.H.; Wang, C.C. Inorg. Chem., 1988, 77, 407.
7. Hibbie, S.J.; Cheetham, A.K.; Bogle, A.R.L.; Wakerley, H.R.; Cox, D.E. J. Am. Chem. Soc., 1988, 110, 3295.
8. Dronskowski, R; Simon, A. Angew. Chem. Int. Ed. Engl., 1989, 28, 758.
9. Mattausch, Hj; Simon, A.; Peters, E.-M. Inorg. Chem., 1986, 25, 3428.
10. Hughbanks, T.; Hoffmann, R. J. Am. Chem. Soc., 1983, 105, 3528.
11. Wheeler, R.A.; Hoffmann, R. J. Am. Chem. Soc., 1988, 110, 7315.
12. Van der Pauw, L.J. Pillips Research Reports, 1958, 13, 1.
13. Torardi, C.C., Ph.D. Dissertation, Sect. 5, Iowa State University, Ames, Iowa, 1981.
14. Aleandri, L.E., Ph.D. Dissertation, Sect. 4, Iowa State University, Ames, Iowa, 1987.
15. Main, P.; Friske, S.J.; Hull, S.E.; Lessinger, L.; Germain, G.; Declercq, J-P.; Woolfson, M.M. MULTAN 80. A System of Computer Programs for the Automatic Solution of Crystal Structures from X-ray Diffraction Data, University of York, York, England, 1980.

16. TEXSAN - TEXRAY Structure Analysis Package, Molecular Structure Corporation (1985).

17. Powell, D.R.; Jacobson, R.A., "Four: A Generalized Crystallographic Fourier Program", U.S. DOE Report IS-4737, Iowa State University, Ames, Iowa, 1980.

18. Lapp, R.L.; Jacobson, R.A., "ALLS: A Generalized Crystallographic Least-square Program", U.S. DOE Report, IS-4708, Iowa State University, Ames, Iowa, 1979.

19. McCarley, R.E. Philos. Trans. R. Soc. London, A, 1982, 308, 141.

20. The calculations were performed based on the method developed by Wheeler and Hoffmann in reference 11.

21. Chen, S.C., Ph.D. Dissertation, Sect. 2, Iowa State University, Ames, Iowa, 1991.

22. Hughbanks, T.; Corbett, J.D. Inorg. Chem., 1989, 28, 631.

23. Shannon, R.D. Acta Crystallogr., 1976, A32, 751.

24. McCarley, R.E. Polyhedron, 1986, 5, 51.

25. Pauling, L. "The Nature of the Chemical Bond", 3rd Edn, P. 400, Cornell University Press, Ithaca, NY (1960).

26. Brown, I.D.; Wu, K.K. Acta Crystallogr., 1976, B32, 1957.

27. Bart, J.C.; Ragaini, V. Inorg. Chim. Acta, 1979, 36, 262.

28. Goodman, B.A.; Raynor, J.B. Elctron Spin Resonance of Transition Metal Complexes. In Advances in Inorganic Chemistry and Radiochemistry, 1970, 13, 251.

SECTION 2. SYNTHESIS, STRUCTURE, AND PHYSICAL PROPERTIES OF $BaMo_5O_8$ - AN OXIDE CONTAINING Mo_{10} EDGE-SHARED BIOCTAHEDRAL CLUSTERS

INTRODUCTION

The formation of reduced ternary molybdenum oxides containing infinite chains of trans-edge-shared octahedra is well established.[1] Six different crystallographic structure types have been discovered in this class of compounds, which include $M_xMo_4O_6$,[2] $M_2Mo_4O_7$,[3] $M_xMo_8O_{11}$,[4] $Ca_{5.45}Mo_{18}O_{32}$,[5] MMo_8O_{10},[6] and $M_4Mo_4O_{11}$.[7] Each of these structures is dominated by Mo-Mo bonding in infinite chains composed of trans-edge-shared octahedral cluster repeat units. But examples of discrete oligomeric clusters are rather scarce. In 1986, $In_{11}Mo_{40}O_{62}$[8] was the first compound reported having finite chains of octahedral cluster units; in this case units with both four and five trans-edge-shared Mo_6 octahedra (n = 4 and 5) were observed. The compound $BaMo_6O_{10}$[9] containing a discrete Mo_6 octahedron (n = 1) has been more recently discovered by Lii and Wang. Compounds containing a chain fragment of n = 3 are realized in the structure of $K_3Mo_{14}O_{22}$[10] and $Tl_{0.6}Sn_{0.6}Mo_7O_{11}$.[11] An x-ray powder investigation on $LaMo_5O_8$[12] indicated that this compound featured the existence of a chain fragment with n = 2. A further compound analogous to $LaMo_5O_8$ with a slightly different electron balance, $PbMo_5O_8$,[11], was recently reported containing the discrete oligomeric cluster with n = 2.

All the examples of oligomeric cluster units thus far reported, where the fragments of the Mo_4O_6 chain (n = 1 to 5 condensed octahedra) have been identified as building blocks, show an identical coupling of the clusters and can be described by the general formula $Mo_{4n+2}O_{6n+2}O_{4/2}$, where n is the number of Mo_6 octahedra trans-edge shared together. The synthesis, structure, and physical properties of $BaMo_5O_8$, an oxide

containing discrete Mo_{10} trans-edge-shared bioctahedral clusters, will be discussed in this section.

EXPERIMENTAL

Materials

Molybdenum powder (99.99%) was used as obtained from Aldrich Chemical Company. Molybdenum tubing was obtained from Thermo-Electron Corp. (99.97%), and molybdenum sheet from Rembar Co. (99.95%). Prior to use, the powder was dried at 120 ^{o}C under dynamic vacuum for 24 hrs and stored in a desiccator. MoO_3 (Fisher Certified A.C.S.) was fired at 550^{o} C for 12 hrs and stored in a desiccator. Barium molybdate was prepared by mixing an aqueous solution of $BaCl_2 \cdot 2H_2O$ (Baker Analyzed Reagent, 99.6%) with an aqueous solution containing the stoichiometric quantity of sodium molybdate dihydrate (Fischer Certified A.C.S.). The white precipitate was filtered, washed with water, dried at 120^{o} C under dynamic vacuum overnight, and then stored in a desiccator.

Physical Measurements

The magnetic susceptibility measurements were carried out on a sintered pressed pellet sample with a SQUID magnetosusceptometer. The magnetic field strength was set at 10 KG. Prior to the measurement, the pellet was demagnetized first by manually bringing the magnetic field to 40 KG, then to -40 KG, and then back to zero G in oscillation mode. In the normal procedure, before data-taking was begun the pellet was held at 380 K for 3 hrs under vacuum to remove the O_2 molecules adsorbed on the

surface of the pellet. The magnetic data were measured every 3 degrees from 5 to 45 K and every 5 degrees from 50 to 400 K. Measurements of magnetization versus field strength at constant temperature were also taken and the resulting data were later used to calculate the amount of ferromagnetic impurity in the sample. The temperatures were set at 10, 100, 150, 200, 300, and 380 K and the field strength was varied in the following order, 100, 400, 700, 1000, 2000, 3000, 4000, 7000, 10000, 15000, 20000, 25000, 30000, 35000, and 40000 G. X-band ESR spectra were recorded on both single crystal and powdered sample with a Bruker ER200-SRC instrument equipped with an Oxford Instruments ESR 900 flow-through cryostat and a DTC-2 digital temperature controller. A Hewlett-Packard 5342 Å microwave frequency counter was used to accurately measure the frequency of the spectrometer. Data were taken at 107, 292, and 400 K.

Electrical resistivity measurements were carried out on a pressed pellet sintered in an evacuated quartz tube at 1100^{o} C for 1 day using a standard four-probe a.c. method. Four platinum wires, which served as the voltage and current leads, were attached to the pellet with Epo-Tech silver epoxy. The temperature was monitored by means of platinum and carbon glass resistance thermometers. The voltage across a standard calibrated resistor was measured periodically and showed no significant change during the course of the experiment.

Synthesis

In an attempt to prepare $BaMo_5O_8$, barium molybdate, molybdenum trioxide, and molybdenum powder, in mole ratio 3:4:8 (i.e. aiming at $BaMo_5O_8$), were ground together in a mortar, pressed into a pellet, placed in a basket made from Mo sheet, sealed in an evacuated quartz tube which, in turn, was sealed in another evacuated quartz tube, and then held at 1180° C for 8 days. Needle crystals of $Ba_{0.62}Mo_4O_6$ and hexagonal pyramidal crystals of Mo metal were found to be transported to the cold end of the reaction tube and left the pellet behind at the hot end. A Guinier x-ray powder diffraction pattern of this pellet indicated a single phase. Chunk crystals of $BaMo_5O_8$ were obtained from the further reaction of loose powder from this pellet held in evacuated double quartz tubes at 1180° C for 8 days. Crystals had grown on the wall of the reaction tube. Guinier x-ray powder patterns of the bulk powder and crystals were thus taken individually to assure that a single phase product was obtained. A single phase $BaMo_5O_8$ can also be prepared by the same procedure at 1200°C for 5 days.

X-ray Powder Diffraction Data

An Enraf Nonius Delft triple focusing Guinier x-ray powder diffraction camera was used with Cu $K\alpha_1$ radiation (λ = 1.54056 Å) to obtain d-spacings. National Bureau of Standards silicon powder was mixed with the sample as an internal standard. The observed versus calculated d-spacings are listed in Table 2.1. The diffraction pattern could be indexed based on cell dimensions determined from the single crystal diffraction

data. The cell parameters computed by a least squares method using the 15 strongest diffraction lines are a = 7.55(2) Å, b = 9.28(2) Å, c = 10.03(3) Å, and $\beta = 108.6(2)^{o}$. The relatively broad diffraction lines and the line overlap are most likely responsible for this poor precision of cell parameters.

Table 2.1. X-ray powder diffraction data for $BaMo_5O_8$

d-spacings (Å)		Intensities[a]	h k l
observed	calculated[b]		
6.79(1)	6.878	s	-1 0 1
4.913(6)	5.001	vw	1 0 1
4.660(5)	4.638	w	0 2 0
2.963(2)	2.940	m(br)	0 3 1
2.705(2)	2.697	m	-1 2 3
2.489(1)	2.500	w	2 0 2
2.401(1)	2.392	s	-3 1 2
2.300(1)	2.300	m	0 1 4
2.099(1)	2.101	wm(br)	-2 2 4
2.083(1)	2.084	w	0 4 2
2.029(1)	2.017	w(br)	2 1 3
1.942(1)	1.944	s	2 3 2
1.827(1)	1.831	w(br)	-4 0 3, 0 5 1
1.805(1)	1.804	w	-2 4 3, -2 2 5
1.701(1)	1.700	m	2 4 2

[a]Intensities: s = strong, m = medium, wm = weak medium, w = weak, and vw = very weak. br = broad

[b]Refined monoclinic cell parameters a = 7.55(2) Å, b = 9.28(2) Å, c = 10.03(3) Å, and $\beta = 108.6(2)^o$

X-ray Single Crystal Data Collection

A black rectangular crystal of $BaMo_5O_8$ having approximate dimensions of 0.09 x 0.04 x 0.02 mm was mounted on a glass fiber. Data were collected with a Rigaku AFC6R diffractometer at room temperature up to $2\theta = 50^{o}$ by using graphite-monochromated Mo Kα radiation and a 12 KW rotating anode generator. A scan mode of ω-2θ was used. Cell constants and an orientation matrix for data collection, obtained from a least-squares refinement of 20 carefully centered reflections with $14^{o} < 2\theta < 17^{o}$, corresponded to a monoclinic cell with dimensions: a = 7.566(1) Å, b = 9.276(2) Å, c = 10.025(1) Å, β=108.70(1)^{o}, and V = 666.4(2) Å^3. Three standard reflections which were measured after every 150 reflections showed no apparent variation in intensity during the data collection. The linear absorption coefficient for Mo Kα is 73.8 cm^{-1}. The intensity data were corrected for Lorentz and polarization effects. An empirical absorption correction, based on azimuthal scans of several reflections, was applied which resulted in transmission factors in the range from 0.62 to 1.00. A correction for secondary extinction was also applied and gave a coefficient of 0.342(1) x 10^{-5}. In the quadrant (h, k, $\pm$l), 1255 reflections were collected, and 856 of them were considered as observed ($I > 3\sigma(I)$).

Structure Solution and Refinement

The space group of $P2_1/c$ (#14) was chosen based on the systematic absences of h0l: $l \neq 2n$ and 0k0: $k \neq 2n$. All efforts to solve the structure by direct methods (MITHRIL[13] and SHELXS[14]) using the TEXRAY Structure Analysis Package (TEXSAN)[15] failed. The structure was then solved using the (SHELXS-86)[16] direct methods in the CAD4-SDP program package and refined on $|F|$ by using the full matrix least-square techniques in the TEXSAN program package. All the atoms were refined anisotropically except O(4), O(5), O(6), O(7), and O(8) which were refined isotropically. The structure, based on 856 observed reflections and 104 variable parameters,was then refined to R = 0.032 and Rw = 0.039. The final electron density difference map was flat with a maximum of 1.46 $e^-/Å^3$ close to Ba and a minimum of -1.59 $e^-/Å^3$ next to the symmetry related Ba.

Details of the data collection and refinement of $BaMo_5O_8$ are given in Table 2.2. Final positional parameters of $BaMo_5O_8$ are listed in Table 2.3 and corresponding selected bond distances and angles are given in Table 2.4 and 2.5, respectively. In Table 2.6 are given the anisotropic thermal parameters of atoms. Tables of observed and calculated structure factors are available as supplementary materials.

Table 2.2. X-ray crystallographic data for $BaMo_5O_8$

empirical formula	$BaMo_5O_8$
formula weight	745.03
crystal system	monoclinic
space group	$P2_1/c$ (#14)
a, Å	7.566(1)
b, Å	9.276(2)
c, Å	10.025(1)
β, deg	108.696(9)
V, $Å^3$	666.4(4)
Z	4
calcd density, g/cm^3	7.426
F000	660
crystal size, mm	0.09 x 0.04 x 0.02
μ(Mo Kα), cm^{-1}	73.81
diffractometer	Rigaku AFC6R
λ, Å, graphite-monochromated	0.71069
T, °C	23
2θ range, deg	0-50
scan mode	ω-2θ
No. reflections collected	1255
No. observations ($I > 3\sigma(I)$)	856
No. variables	104
goodness of fit indicator[a]	1.31
max. shift in final cycle	0.02
largest peak in final diff. map, $e/Å^3$	1.46
transmission coefficient	0.62-1.00
R[b], Rw[c]	0.032, 0.039

[a] Quality-of-fit = $[\Sigma\omega(|Fo| - |Fc|)^2/(N_{obs}-N_{parameters})]^{1/2}$

[b] $R = \Sigma||Fo| - |Fc||/\Sigma|Fo|$

[c] $Rw = [\Sigma\omega(|Fo| - |Fc|)^2/\Sigma\omega|Fo|^2]^{1/2}$; $\omega = 1/\sigma^2(|Fo|)$

Table 2.3. Positional parameters and B_{eq} for $BaMo_5O_8$

ATOM	X	Y	Z	B_{eq}[a], Å^2
Ba	0.7449(1)	0.5030(1)	0.54394(8)	0.63(4)
Mo1	0.5025(2)	0.1209(1)	0.4138(1)	0.44(5)
Mo2	0.8888(2)	0.1130(1)	0.5173(1)	0.44(4)
Mo3	0.3208(2)	0.1247(1)	0.6121(1)	0.42(5)
Mo4	0.1231(2)	0.1173(1)	0.3197(1)	0.44(5)
Mo5	0.6864(2)	0.1305(1)	0.7004(1)	0.44(5)
O1	0.494(1)	0.000(1)	0.240(1)	0.7(3)
O2	0.891(1)	0.496(1)	0.335(1)	0.7(3)
O3	0.902(1)	0.256(1)	0.678(1)	0.7(4)
O4	0.097(1)	0.238(1)	0.481(1)	0.8(2)
O5	0.304(1)	0.249(1)	0.284(1)	0.6(2)
O6	0.700(1)	0.246(1)	0.379(1)	0.5(2)
O7	0.890(1)	-0.001(1)	0.3362(9)	0.4(2)
O8	0.495(1)	0.270(1)	0.565(1)	0.5(2)

[a] $B_{eq} = 8\pi^2/3\ \Sigma U_{ij} a_i^* a_j^* a_i \cdot a_j$, where the temperature factors are defined as $\exp(-2\pi^2\ \Sigma h_i h_j a_i^* a_j^* U_{ij})$

Table 2.4. Selected bond distances (Å) for $BaMo_5O_8$

Mo1-Mo1'	2.839(2)	Mo1-Mo2	2.771(2)
Mo1-Mo3	2.756(2)	Mo1-Mo3'	2.695(2)
Mo1-Mo4	2.719(2)	Mo1-Mo5	2.763(2)
Mo1-Mo5'	2.783(2)	Mo2-Mo2(Inter)[a]	2.778(3)
Mo2-Mo3(Inter)	3.099(2)	Mo2-Mo3	2.782(2)
Mo2-Mo4(Inter)	3.053(2)	Mo2-Mo4'	2.708(2)
Mo2-Mo5'	2.747(2)	Mo3-Mo4'	2.833(2)
Mo3-Mo5	2.621(2)	Mo4-Mo5	2.755(2)
Mo1-O1	2.06(1)	Mo1-O5	2.03(1)
Mo1-O6	2.01(1)	Mo1-O8	2.066(9)
Mo2-O3	2.06(1)	Mo2-O4	2.08(1)
Mo2-O6	2.05(1)	Mo2-O7	2.105(9)
Mo2-O7(Inter)	2.111(9)	Mo3-O1	2.05(1)
Mo3-O4	2.07(1)	Mo3-O5	2.120(9)
Mo3-O7	2.155(9)	Mo3-O8	2.04(1)
Mo4-O2	1.89(1)	Mo4-O3	2.16(1)
Mo4-O4	2.03(1)	Mo4-O5	1.95(1)
Mo4-O7	2.131(9)	Mo5-O1	2.06(1)
Mo5-O2	2.06(1)	Mo5-O3	2.08(1)
Mo5-O6	2.10(1)	Mo5-O8	2.08(1)
Ba-O1	3.135(9)	Ba-O1'	2.84(1)
Ba-O2	2.666(9)	Ba-O2'	2.631(9)
Ba-O3	2.73(1)	Ba-O4	2.73(1)
Ba-O5	2.968(9)	Ba-O6	2.86(1)
Ba-O7	2.780(9)	Ba-O8	2.93(1)
Ba-O8'	2.77(1)	Ba•••Ba	3.524(2)

[a]Inter-cluster bond distance

Table 2.5. Selected bond angles (deg) for $BaMo_5O_8$

Mo1'-Mo1-Mo2	88.26(6)	Mo1'-Mo1-Mo3'	57.58(5)
Mo1'-Mo1-Mo3	59.66(5)	Mo1'-Mo1-Mo4	89.02(6)
Mo1'-Mo1-Mo5'	59.55(5)	Mo1'-Mo1-Mo5	58.88(5)
Mo2-Mo1-Mo3'	116.14(6)	Mo2-Mo1-Mo3	61.16(5)
Mo2-Mo1-Mo4	117.28(6)	Mo2-Mo1-Mo5'	59.51(4)
Mo2-Mo1-Mo5	118.22(6)	Mo3'-Mo1-Mo3	117.25(5)
Mo3'-Mo1-Mo4	62.31(4)	Mo3'-Mo1-Mo5'	56.70(4)
Mo3'-Mo1-Mo5	89.91(5)	Mo4-Mo1-Mo5'	119.00(5)
Mo4-Mo1-Mo5	60.07(4)	Mo5-Mo1-Mo5'	118.44(5)
Mo1-Mo2-Mo2	125.54(7)(Inter)[a]	Mo1-Mo2-Mo3	58.07(4)
Mo1-Mo2-Mo4'	90.66(5)	Mo1-Mo2-Mo5'	60.10(5)
Mo3-Mo2-Mo4'	54.84(4)	Mo3-Mo2-Mo5'	123.51(6)
Mo4'-Mo2-Mo5'	60.65(4)	Mo1'-Mo3-Mo1	62.75(5)
Mo1'-Mo3-Mo2	89.73(5)	Mo1'-Mo3-Mo4'	58.22(4)
Mo1'-Mo3-Mo5	61.80(5)	Mo1-Mo3-Mo2	60.76(5)
Mo1-Mo3-Mo4'	89.62(5)	Mo1-Mo3-Mo5	63.11(5)
Mo2-Mo3-Mo4'	57.68(4)	Mo2-Mo3-Mo5	123.80(6)
Mo4'-Mo3-Mo5	120.02(5)	Mo1-Mo4-Mo2'	92.06(5)
Mo1-Mo4-Mo2	122.87(6)(Inter)	Mo1-Mo4-Mo3'	59.47(4)
Mo1-Mo4-Mo5	61.11(5)	Mo2'-Mo4-Mo3'	60.22(4)
Mo2'-Mo4-Mo2	57.29(5)(Inter)	Mo2'-Mo4-Mo5	60.36(4)
Mo3'-Mo4-Mo5	88.91(5)	Mo1'-Mo5-Mo1	61.56(5)
Mo1'-Mo5-Mo2'	60.39(4)	Mo1'-Mo5-Mo3	61.50(5)
Mo1'-Mo5-Mo4	89.86(5)	Mo1-Mo5-Mo2'	89.89(5)
Mo1-Mo5-Mo3	59.75(4)	Mo1-Mo5-Mo4	58.82(5)

[a] Inter-cluster bond angle

Table 2.5. (continued)

Mo2'-Mo5-Mo3	121.81(6)	Mo2'-Mo5-Mo4	58.99(4)
Mo3-Mo5-Mo4	118.57(6)	Mo1-O1-Mo3	82.1(4)
Mo2-O3-Mo4	134.3(5)(inter)	Mo1-O1-Mo5	85.1(3)
Mo4-O3-Mo5	134.5(5)(inter)	Mo3-O1-Mo5	79.4(4)
Mo2-O4-Mo3	96.7(4)(inter)	Mo4-O2-Mo5	88.3(4)
Mo2-O4-Mo4	95.9(4)(inter)	Mo2-O3-Mo5	83.1(4)
Mo1-O5-Mo3	128.2(5)(inter)	Mo3-O4-Mo4'	87.5(4)
Mo3-O5-Mo4	136.5(5)(inter)	Mo1-O5-Mo4	86.2(4)
Mo1-O6-Mo5	128.8(5)(inter)	Mo1-O6-Mo2	86.0(4)
Mo2-O6-Mo5	137.7(5)(inter)	Mo2-O7-Mo3	81.5(3)
Mo2-O7-Mo2	82.4(3)(inter)	Mo2'-O7-Mo4	79.3(3)
Mo2-O7-Mo4	92.2(4)(inter)	Mo1-O8-Mo3	84.3(4)
Mo2-O7-Mo3	93.2(4)(inter)	Mo1-O8-Mo5	83.5(4)
Mo3'-O7-Mo4	170.9(5)(inter)	Mo3-O8-Mo5	78.9(3)

Table 2.6. Anisotropic temperature factors ($Å^2$) for $BaMo_5O_8$[a]

ATOM	U11	U22	U33	U12	U13	U23
Ba	0.0072(5)	0.0075(5)	0.0079(5)	0.0002(4)	0.0007(3)	-0.0001(4)
Mo1	0.0055(7)	0.0051(7)	0.0056(6)	-0.0006(5)	0.0012(5)	0.0000(5)
Mo2	0.0055(6)	0.0054(6)	0.0056(6)	0.0000(5)	0.0015(5)	0.0002(5)
Mo3	0.0041(6)	0.0051(7)	0.0059(6)	-0.0005(5)	0.0007(5)	-0.0001(5)
Mo4	0.0059(7)	0.0045(7)	0.0055(6)	-0.0001(5)	0.0008(5)	-0.0007(5)
Mo5	0.0055(6)	0.0057(7)	0.0050(6)	0.0001(5)	0.0009(5)	-0.0004(5)
O1	0.002(5)	0.016(5)	0.011(5)	-0.002(5)	0.003(4)	-0.002(5)
O2	0.001(5)	0.012(5)	0.010(5)	-0.001(4)	-0.001(4)	0.000(5)
O3	0.012(6)	0.007(5)	0.007(5)	-0.001(4)	0.003(4)	0.002(4)
O4	0.010(2)					
O5	0.007(2)					
O6	0.006(2)					
O7	0.006(2)					
O8	0.007(2)					

[a]The form of the anisotropic displacement parameter is $\exp[-2\pi^2\{h^2a^2\ U(1,1) + k^2b^2\ U(2,2) + l^2c^2\ U(3,3) + 2hkab\ U(1,2) + 2hlac\ U(1,3) + 2klbc\ U(2,3)\}]$, where a, b, and c are reciprocal lattice constants

RESULTS AND DISCUSSION

Description of Structure

As shown in Fig. 2.1, the molecular structure of the trans-edge-shared Mo_{10} bioctahedral cluster in $BaMo_5O_8$ is centrosymmetric. The structure of $Mo_{10}O_{16}^{4-}$ shows that the cluster is distorted such that the apical Mo atoms are moved toward each other to give a short bond distance of 2.621(2) Å between Mo3 and Mo5. This Mo3-Mo5 bond distance is the shortest Mo-Mo bond distance in $BaMo_5O_8$. The longest Mo-Mo bond distance is that of 2.839(2) Å for Mo1-Mo1'. The structure of the $Mo_{10}O_{16}^{4-}$ cluster unit (n = 2) shows the alternating long-short Mo-Mo bond distance along the chain axis both between the shared edges and between the Mo atoms located in the basal planes of the octahedra. The Mo2-Mo4' bond distance of 2.708(2) Å is 0.131 Å shorter than the shared edge of Mo1-Mo1' and results in an alternating S-L-S pattern of Mo-Mo bonds along the chain axis. The bond distance of 2.771(2) Å between Mo1 and Mo2 is longer than that between Mo1 and Mo4, 2.719(2) Å. Similar structural distortions are observed in the discrete oligomeric cluster units with n = 3,[10,11] 4,[8] and 5[8] in the $(Mo_{4n+2}O_{6n+2})O_{4/2}$ series. The Mo-O distances in $BaMo_5O_8$ range from 1.89(1) Å (Mo4-O2) to 2.16(1) Å (Mo4-O3) and are averaged to a distance of 2.06 Å. The unusually short bond distance of Mo4-O2 most likely arises from the low coordination number of 2 around the O2 atoms. The longer Mo5-O2 distance of 2.06(1) Å may be explained by the displacement of Mo5 toward Mo3. The relatively long Mo-O7 bond distances (ave. 2.125 Å) can be understood in terms of the higher coordination number

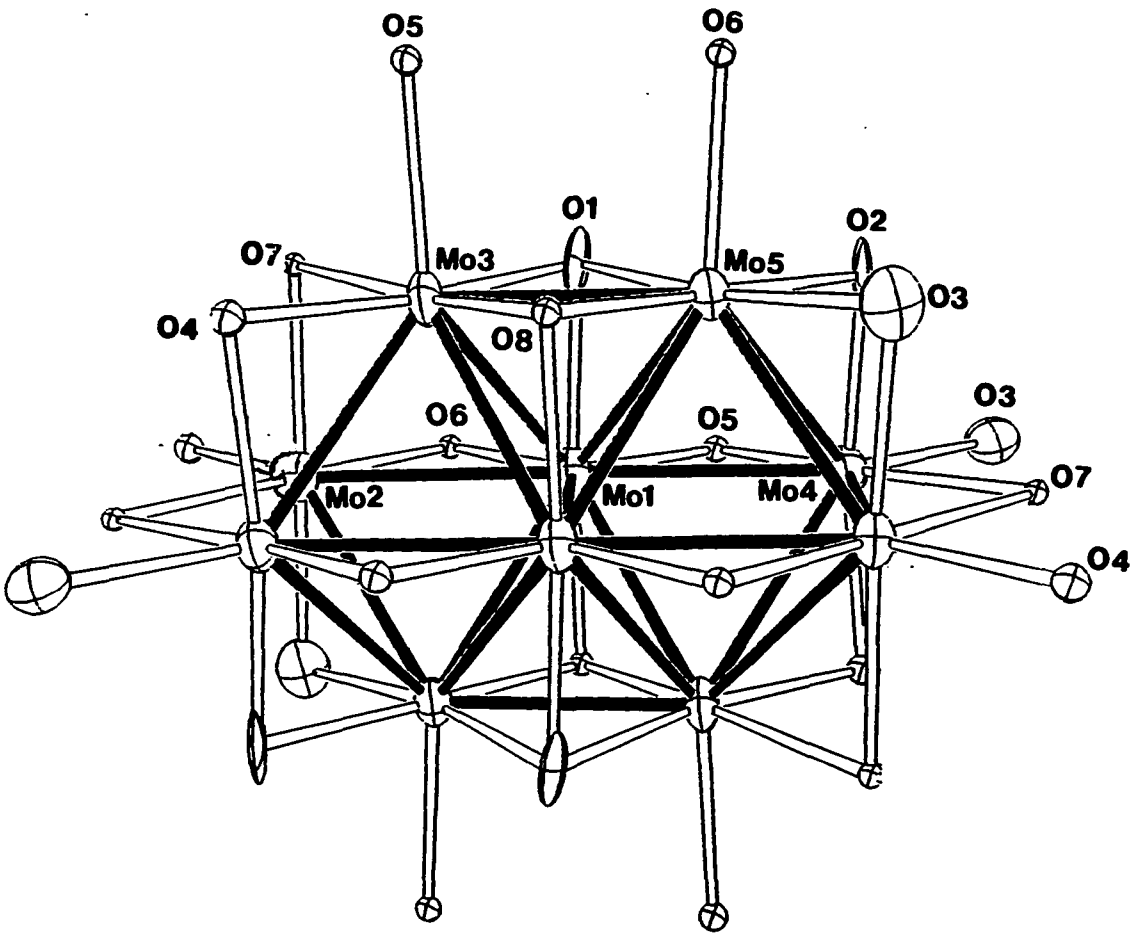

Fig. 2.1. ORTEP drawing (50 % thermal ellipsoids) of a trans-edge-shared bioctahedral cluster in $BaMo_5O_8$ showing the complete coordination by oxygen to form the $Mo_{10}O_{26}$ unit. Solid lines represent Mo-Mo bonds and open lines represent Mo-O bonds.

(CN = 4) around O7 atoms. A long distance like that of Mo4-O3 is also observed in the structure of $K_3Mo_{14}O_{22}$. The average distances of Mo-O and of Mo-Mo in $BaMo_5O_8$ are the same as those in the analogous compound $PbMo_5O_8$[11] and agree well with those in $K_3Mo_{14}O_{22}$,[10] $Tl_{0.8}Sn_{0.6}Mo_7O_{11}$,[11] and $In_{11}Mo_{40}O_{62}$.[8]

Fig. 2.2 shows the intercluster connection in $BaMo_5O_8$. The $Mo_{10}O_{16}^{4-}$ clusters are connected through a short inter-cluster Mo2-Mo2 bond distance of 2.778(3) Å to give an infinite chain along the a-axis. Notably, such short inter-cluster Mo-Mo bonding in the structures of members in the $Mo_{4n+2}O_{6n+2}O_{4/2}$ series is only observed when n = 1[9] and 2.[11,12] Other inter-cluster Mo-Mo distances in $BaMo_5O_8$ are 3.053(2) (Mo2-Mo4) and 3.099(2) Å (Mo2-Mo3). These inter-cluster Mo-Mo distances are longer than those in $BaMo_8O_{10}$ (n = 1) but shorter than those in the discrete oligomeric clusters with n = 3, 4, and 5. As previously noted,[10] this comparison indicates that the intra-cluster Mo-Mo distances are scarcely affected by the degree of cluster condensation, whereas the inter-cluster Mo-Mo distances significantly decrease with a lower degree of cluster condensation.

The oxygen atoms O1, O2, and O8 are edge-bridging only between Mo atoms in the same cluster unit (O^i). O3, O4, O5, and O6 are either edge-bridging between Mo atoms or terminal to apical Mo atoms and also bonded to the neighboring clusters through either terminal or edge-bridging positions (O^{i-a} or O^{a-i}), as observed in the structure of $K_3Mo_{14}O_{22}$. Atom O7 is edge-shared between two neighboring $Mo_{10}O_{16}^{4-}$ clusters (O^{i-i}). Subsequently, the structure of $BaMo_5O_8$ may be described by the connectivity formula of $Ba_2^{2+}[(Mo_{10}O_6{}^iO_{4/2}{}^{i-i}O_{8/2}{}^{i-a})O_{8/2}{}^{a-i}]^{4-}$. A three-dimensional view down the a-axis of $BaMo_5O_8$ is given in Fig. 2.3, showing the inter-linkages between clusters. The

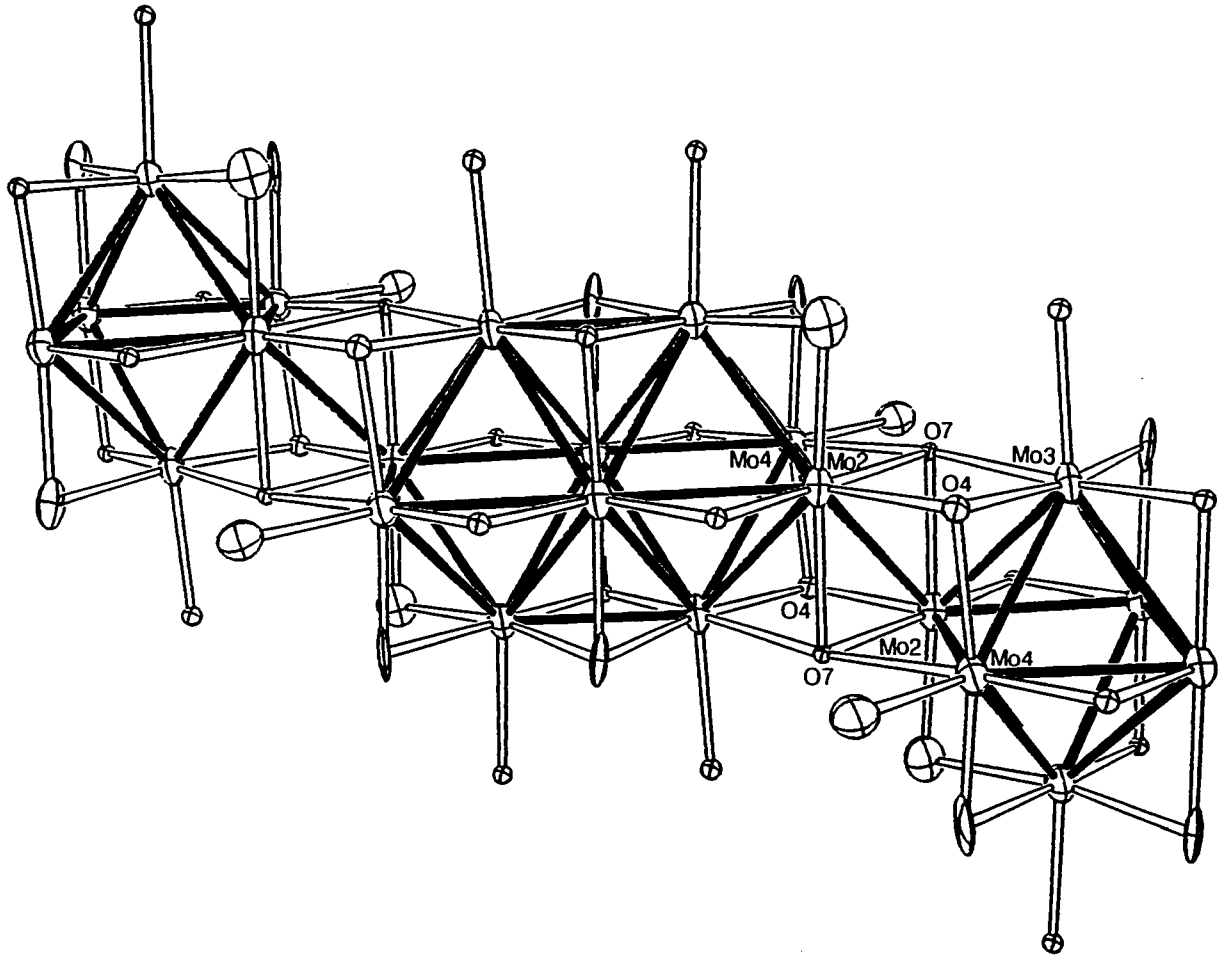

Fig. 2.2. ORTEP drawing (50 % thermal ellipsoids) of a perspective view along the a-axis of the $BaMo_5O_8$ structure showing the intercluster connections. Solid lines are Mo-Mo bonds and open lines are Mo-O bonds.

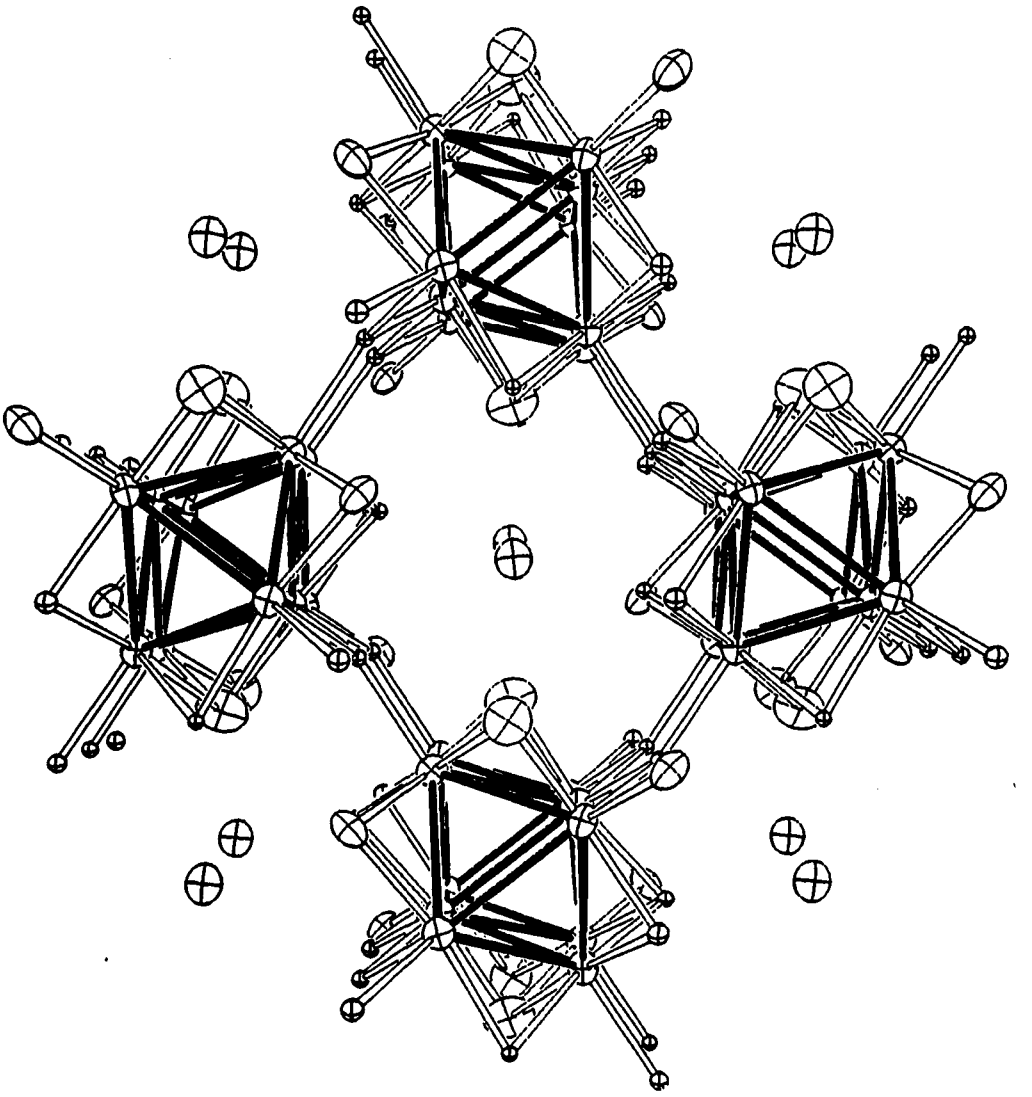

Fig. 2.3. ORTEP drawing (50 % thermal ellipsoids) of the unit cell of $BaMo_5O_8$ as viewed down the a-axis showing the cross-linking of clusters by Mo-O-Mo bridge bonding and the pockets formed for the Ba atoms (shown as unconnected ellipsoids). Mo-Mo bondings are represented by solid lines and Mo-O bondings by open lines.

structure of $BaMo_5O_8$ consists of two $Mo_{10}O_{16}^{4-}$ clusters per unit cell which are linked in the b and c directions through trigonally bonded oxygen atoms. The Ba^{2+} ions are located in the channels provided by four cross-linked clusters.

Fig. 2.4 shows the [001] projection of metal-atom substructure for $BaMo_5O_8$, from which the layered stacking of bioctahedral units (Mo_{10}) and the inter-cluster connection leading to the chain structure are clearly recognizable. The Mo_{10} clusters are centered at (0, 1/2, 0) and (0, 0, 1/2) and the Ba atoms are located roughly at z = 1/2. The coordination around Ba^{2+} ions is shown in Fig. 2.5. The Ba^{2+} ion is 11-coordinated with Ba-O distances between 2.631(9) and 3.135(9) Å. This is different from $BaMo_6O_{10}$ where Ba^{2+} is 12-coordinated with Ba-O distances in the range of 2.757-2.986 Å. The La atoms in $LaBa_5Mo_8$[9] are also 11-coordinated. The average Ba-O distance of 2.822 Å is a little shorter than the calculated Ba-O distance of 2.95 Å, based on Ba^{2+} (1.57 Å, CN = 11) and O^{2-} (1.38 Å, CN = 4).[17] The Ba^{2+} ion is therefore tightly bonded to the oxygen atoms and does not exhibit large thermal parameters. The bond valence calculations for Ba^{2+} ion, based on the empirical equation (eq 1.) developed by Brown and Wu,[18] give poor sums of 2.78(9) v.u. in $BaMo_5O_8$ and 2.6(1) v.u. in $BaMo_6O_{10}$. Poor bond valence sums for Ba^{2+} ion are frequently observed, especially in the perovskite related structure.[19]

$$S(Ba\text{-}O) = [\, d(Ba\text{-}O)/2.297 \,]^{-7.0} \qquad (1)$$

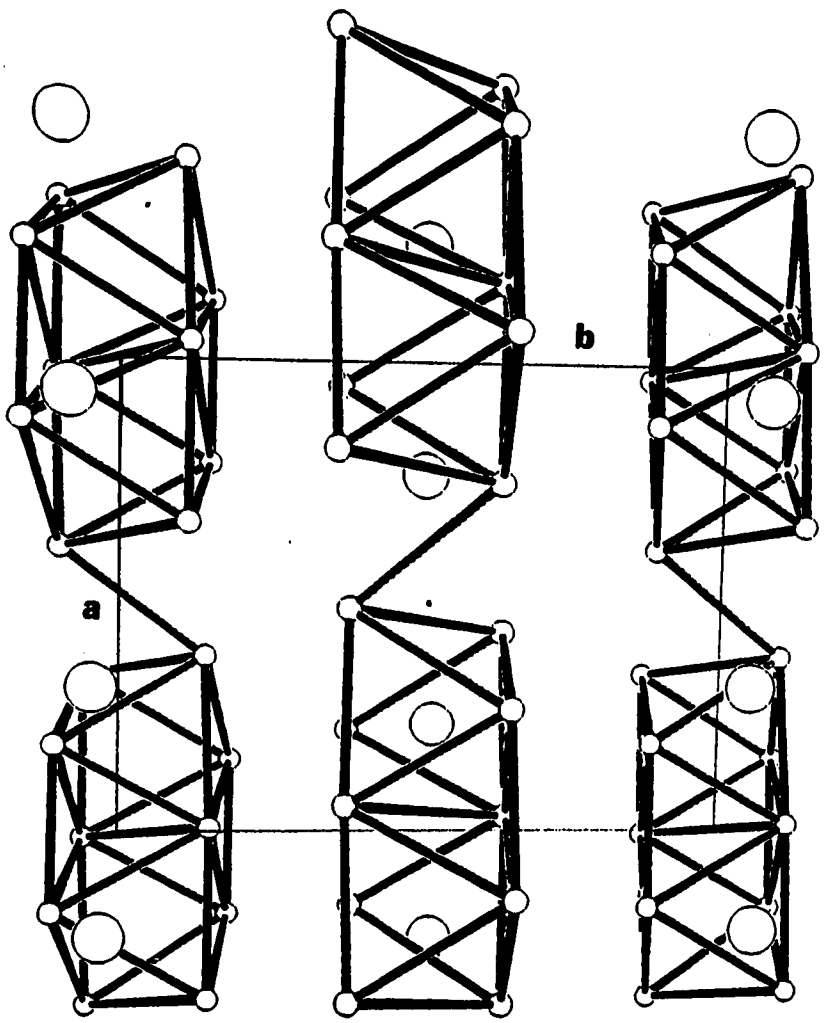

Fig. 2.4. A perspective view of the condensed cluster units and Ba atoms in $BaMo_5O_8$ along [001]; Mo atoms as small circles, Ba atoms as large circles. Clusters are centered at (0, 1/2, 0) and (0, 0, 1/2).

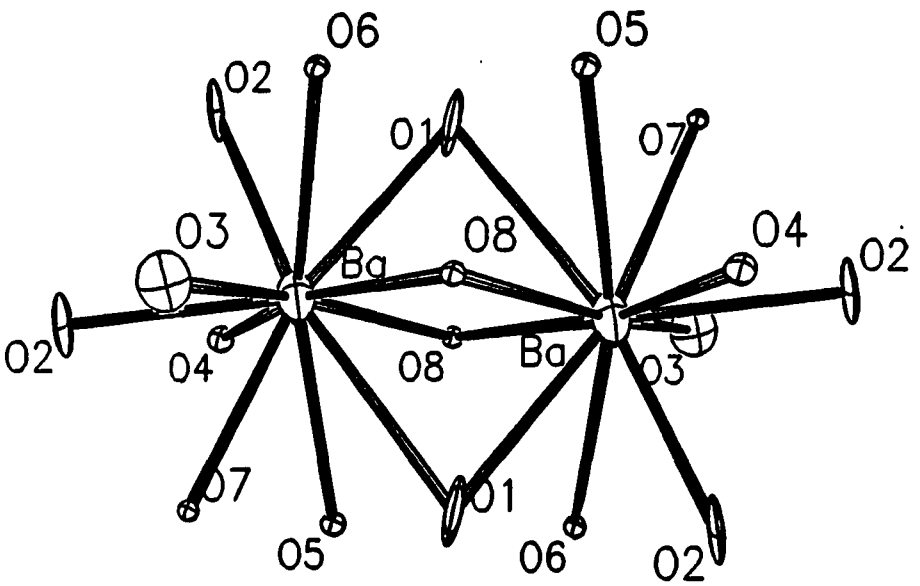

Fig. 2.5. An ORTEP drawing (50% thermal ellipsoids) showing the coordination around the Ba^{2+} ions in $BaMo_5O_8$.

Bond Length-Bond Order Relationships

The numerical values resulting from bond length-bond order calculations, as discussed in Section 1, for $BaMo_5O_8$ are tabulated in Table 2.7. The number of metal-centered electrons (MCE) per $Mo_{10}O_{16}^{4-}$ cluster unit is estimated from the sum of the intra-cluster metal-metal bond orders and results in MCE(Σn) = 30.5(2) e^-. The total Mo-O valence of the $Mo_{10}O_{16}^{4-}$ cluster unit is 28.0(4) v.u., assessed from the summation of individual Mo-O valence on each Mo atom in the $Mo_{10}O_{16}^{4-}$ cluster unit. The number of electrons utilized for metal-metal bonding is then calculated by subtraction of 28.0(4) from 60, the maximum number of valence electrons of ten Mo atoms in the $Mo_{10}O_{16}^{4-}$ cluster. The resulting MCE(Σs) value of 32.0(4) e^- agrees well with MCE(f) = 32 e^-, derived from the formula and the expected values of Ba and O in $BaMo_5O_8$. The low value of MCE(Σn), as compared to those of MCE(Σs) and MCE(f), is in part explained by the strong inter-cluster Mo-Mo bonds observed in this structure. Ideally, the number of electrons utilized in inter-cluster Mo-Mo bonding can be estimated from the difference (1.5(2) e^-) between MCE(Σn) and MCE(f). The utilizing of the metal-centered electrons in inter-cluster metal-metal bondings is evidenced by MCE(Σn) = 31.6(2) e^-, in which the shortest inter-cluster Mo-Mo bond order is included in calculation. From the total number of electrons about each Mo atom estimated from Ne = Σn + Σs, the calculations show an average Ne/Mo of 5.96(1) (inter-cluster Mo2-Mo2 bond included), which agrees well with the ideal value of 6.0. The total valence electrons per Mo atom should equal the periodic group number, 6, if all electrons are involved in the bonding Mo-Mo or Mo-O interactions.

Table 2.7. Bond length - bond order relationships in $BaMo_5O_8$

Atom	d(Mo-Mo)		n	d(Mo-O)		s
Mo1	2.839(2)		0.421(4)	2.06(1)		0.58(2)
	2.771(2)		0.547(4)	2.03(1)		0.64(2)
	2.756(2)		0.580(4)	2.01(1)		0.67(2)
	2.695(2)		0.73(5)	2.066(9)		0.57(1)
	2.719(2)		0.668(4)		Σs	2.46(7)
	2.763(2)		0.564(4)			
	2.783(2)		0.523(4)			
		Σn	4.04(3)			
Mo2	2.771(2)		0.547(4)	2.06(1)		0.58(2)
	2.782(2)		0.525(4)	2.08(1)		0.55(2)
	2.708(2)		0.697(4)	2.05(1)		0.60(2)
	2.747(2)		0.600(4)	2.105(9)		0.51(1)
		Σn	2.37(2)	2.111(9)		0.50(2)
	2.778(3)(inter)[a]		0.533(6)		Σs	2.74(9)
	Σn(inter)		2.90(2)	2.05(1)		0.60(2)
Mo3	2.756(2)		0.580(4)	2.07(1)		0.57(2)
	2.695(2)		0.733(5)	2.120(9)		0.49(1)
	2.782(2)		0.525(4)	2.155(9)		0.44(1)
	2.833(2)		0.432(4)	2.04(1)		0.62(2)
	2.621(2)		0.974(8)		Σs	2.72(8)
		Σn	3.24(3)			
Mo4	2.719(2)		0.668(4)	1.89(1)		0.98(4)
	2.708(2)		0.697(4)	2.16(1)		0.44(1)
	2.633(2)		0.432(4)	2.03(1)		0.64(2)
	2.755(2)		0.582(4)	1.95(1)		0.81(2)
		Σn	2.38(2)	2.131(9)		0.47(1)
					Σs	3.3(1)
Mo5	2.763(2)		0.564(4)	2.06(1)		0.58(2)
	2.783(2)		0.523(4)	2.06(1)		0.58(2)
	2.747(2)		0.600(4)	2.08(1)		0.55(2)
	2.621(2)		0.974(8)	2.10(1)		0.52(2)
	2.755(2)		0.582(4)	2.08(1)		0.55(2)
		Σn	3.24(2)		Σs	2.8(1)

$MCE(\Sigma n) = 2\ \Sigma(\Sigma n) = 30.5(2)\ e^-$

$MCE(\Sigma n) = 2\ \Sigma(\Sigma n) = 31.6(2)\ e^-$ (shortest inter-cluster Mo-Mo included)

Total valence of Mo_{10} unit $= 2\ \Sigma(\Sigma s) = 28.0(4)$ v.u.

$MCE(\Sigma s) = 6\ e^- \times 10 - 28.0(4) = 32.0(4)\ e^-$

[a]Shortest inter-cluster Mo-Mo bond

Magnetic Properties

$BaMo_5O_8$ is ESR silent. This indication of the diamagnetic property of $BaMo_5O_8$ is further confirmed by the pressed pellet magnetic susceptibility data shown in Fig. 2.6. The upper data curve is the corrected raw data, which depicts the paramagnetic impurity with an apparent moment of 0.0823 μ_B/Mo (0.324 μ_B/molecule). The least square fitting to the Curie-Weiss law shown by the solid line through the data gives the fitting parameter $\chi^o = 1.17 \times 10^{-5}$ cm^3/Mo, $c = 8.47 \times 10^{-4}$ cm^3/Mo, and $\theta = -3.04$ K. The lower curve shows the data corrected for the paramagnetic impurity. The essentially diamagnetic character of $BaMo_5O_8$ is illustrated by the constant susceptibility within the temperature range of measurement. The temperature independent term of susceptibility (χ_{TIP}) was calculated as 3.47×10^{-5} cm^3/Mo (5.39×10^{-4} cm^3/molecule). The small hump around 50 K arises from the antiferromagnetic transition in crystalline O_2, a trace amount of which condensed on the sample and was very difficult to remove. The ferromagnetic impurity calculated from the plot of magnetic moment vs. field strength corresponds to 26.9 ppm Fe/Mo.

Resistivity Study

The D.C. resistivity measurements on a pressed pellet of $BaMo_5O_8$ is given in Fig. 2.7. The resistivity increases gradually with the decrease of temperature in the temperature range of 296-100 K and then increases dramatically at temperatures below 100 K. This increase of resistivity with the decrease of temperature indicates that

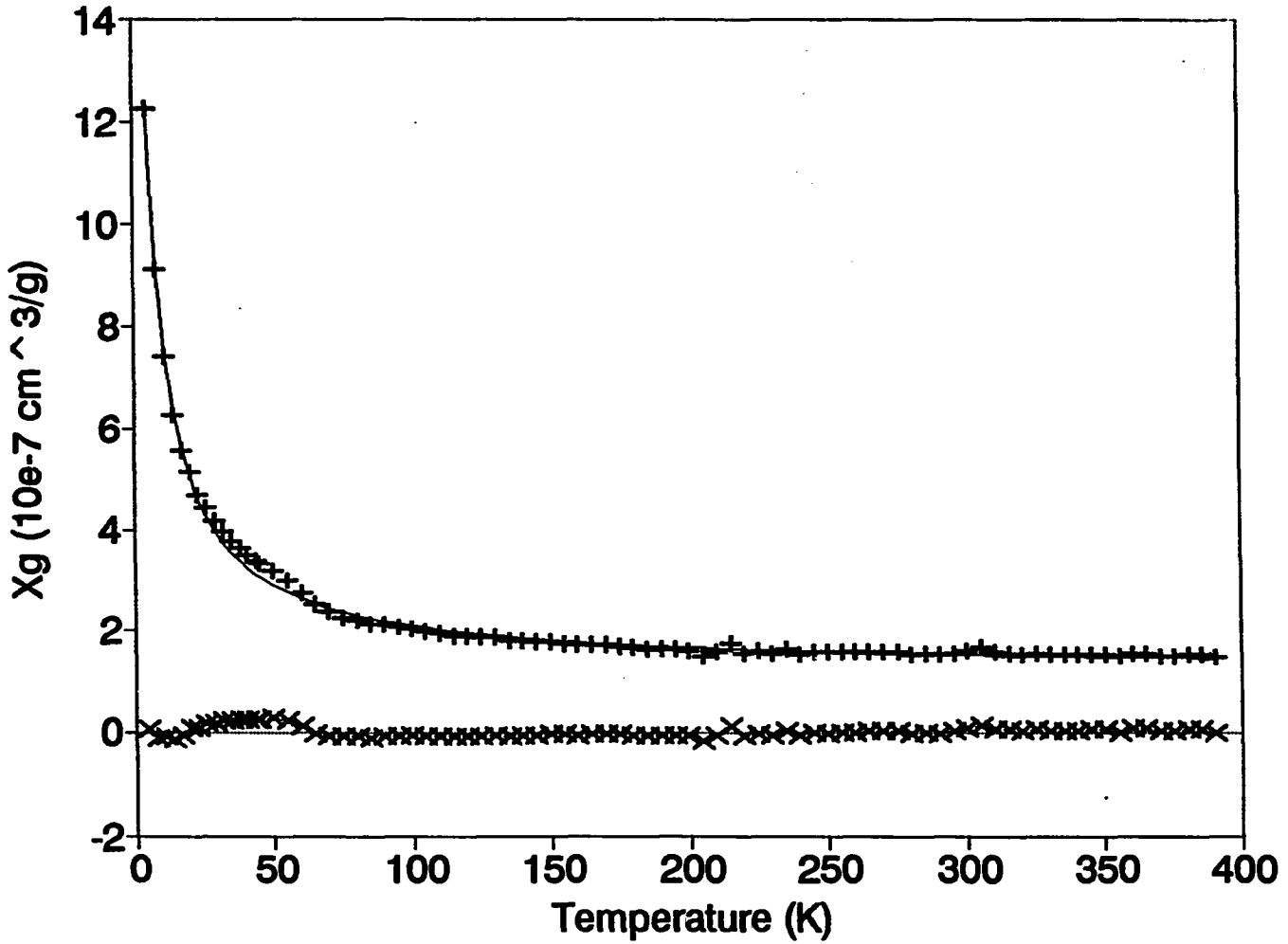

Fig. 2.6. A plot of gram magnetic susceptibility of $BaMo_5O_8$ as a function of temperature. The upper curve is the data corrected for sample holder and ferromagnetic impurity. The lower curve is the data further corrected for paramagnetic impurity. The solid line represents the best least squares fitting of data.

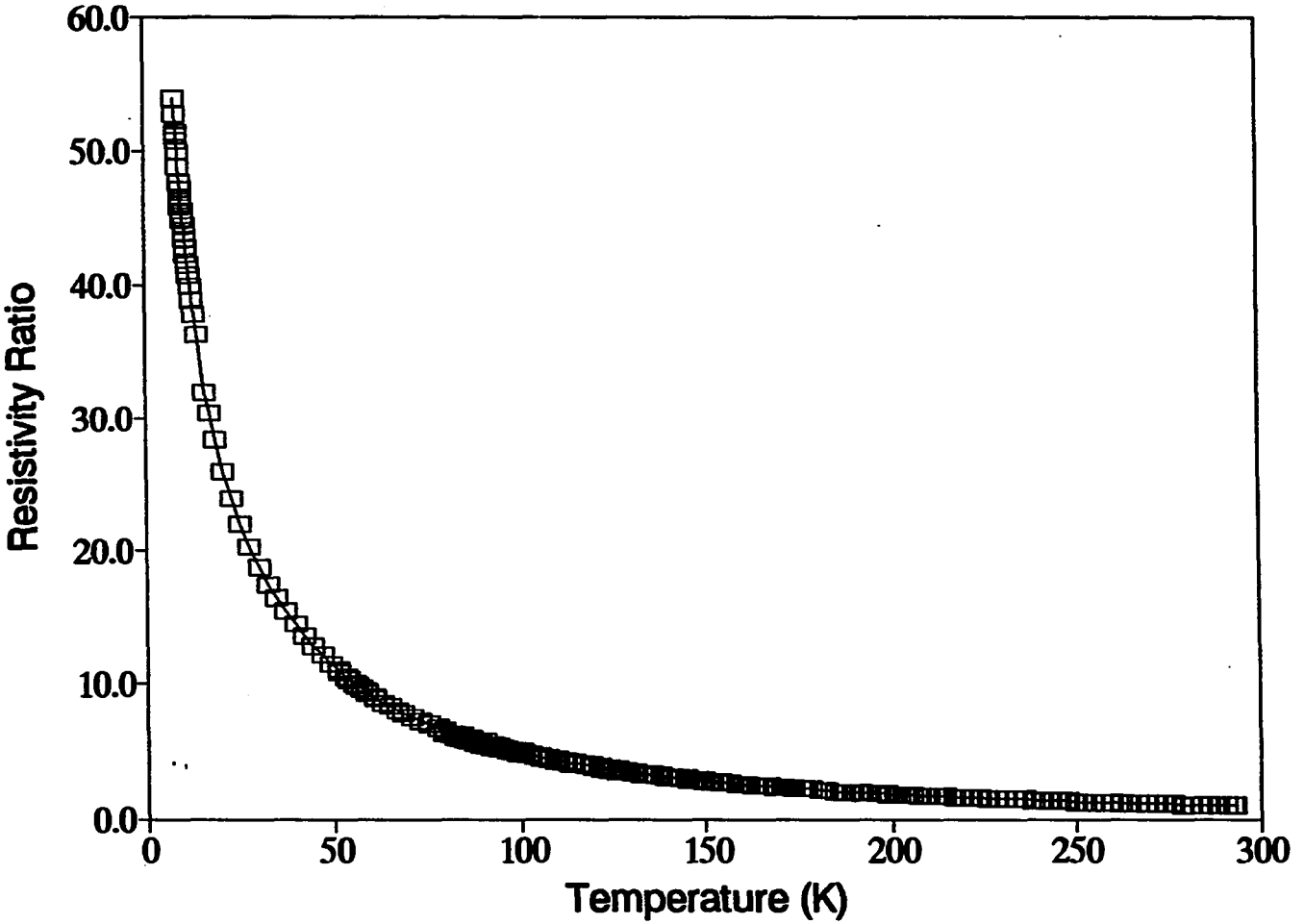

Fig. 2.7. Resistivity ratio (ρ(T)/ρ(R.T.)) vs. temperature for a pressed and sintered pellet of $BaMo_5O_8$.

$BaMo_5O_8$ is a semiconductor. The room temperature resistivity of $BaMo_5O_8$ is 0.145 ohm-cm. Fig. 2.8 shows the plot of logarithmic resistivity vs. reciprocal temperature for $BaMo_5O_8$. Ideally, a semiconductor will give a straight line in the plot of log(p) vs. 1/T. The nonlinear behavior in the plot of Fig. 2.8 reflects the presence of impurity levels in the semiconductor energy gap. The energy gap calculated from 190 to 296 K is 0.064 ev. This value of 0.064 eV is 0.036 eV smaller than the lowest intrinsic semiconductor energy gap known in grey Sn and suggests that the value of 0.0641 eV might not be the intrinsic energy gap but the energy gap between impurity level and the conduction band. This is also reflected by the continued decrease of resistivity at room temperature, as shown in Fig. 2.7. High temperature resistivity measurements on $BaMo_5O_8$ may thus allow us to elucidate the intrinsic semiconductor energy gap and to detect any possible transition from semiconductor to conductor.

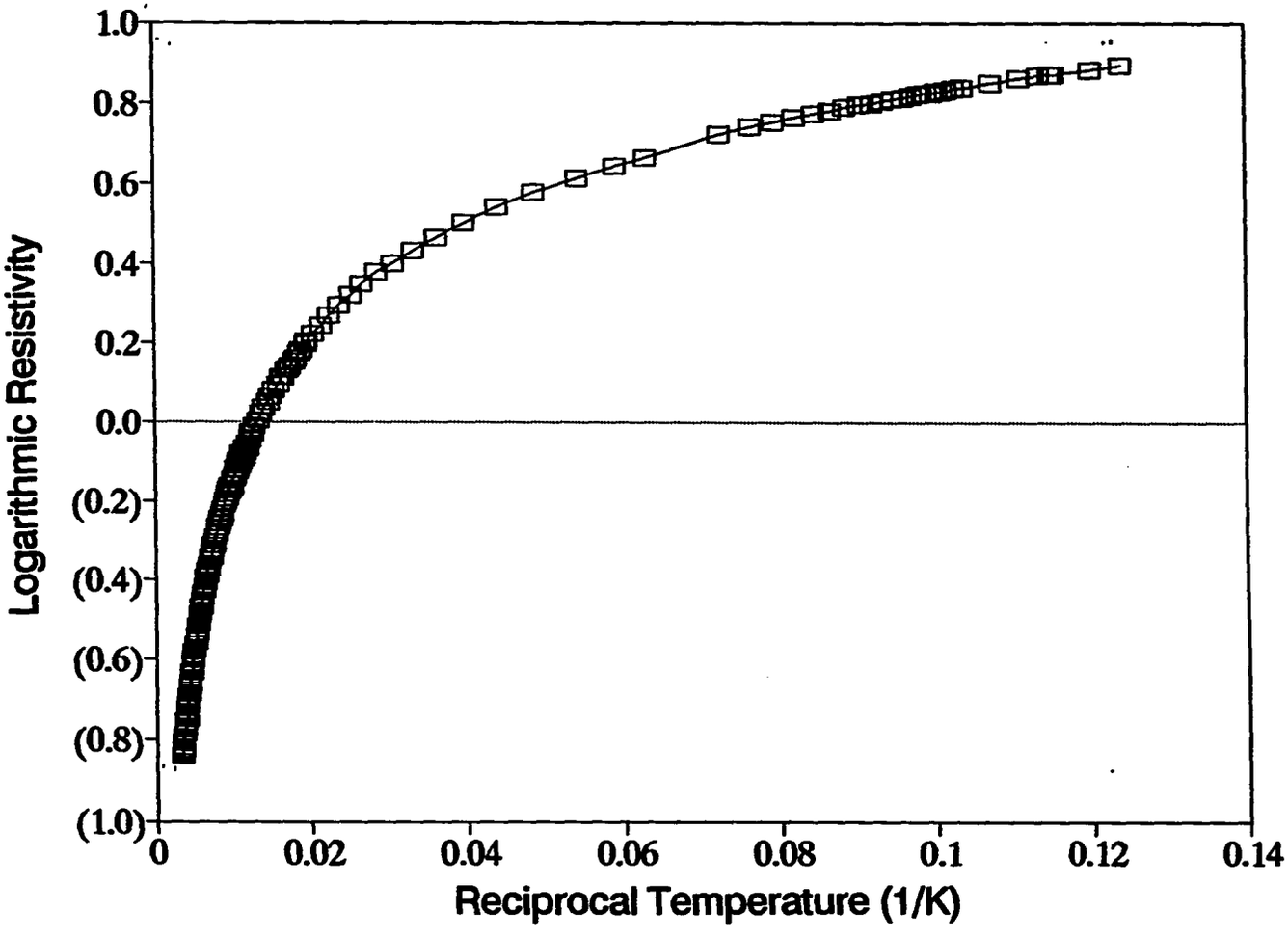

Fig. 2.8. A plot of log(ρ) vs. 1/T for $BaMo_5O_8$.

CONCLUSION

A novel compound that consists of discrete oligomeric cluster units belong to the $Mo_{4n+2}O_{6n+2}O_{4/2}$ series has been reported, in which the fragment (n = 2, two condensed octahedra) of the $[Mo_4O_6]$ infinite chain has been identified as the building block. Unlike compounds[8,10,11] containing chain fragments of n = 3, 4, 5, $BaMo_5O_8$, like other compounds[11,12] containing chain fragment of n = 2, show a short Mo-Mo bond distance (2.778(3) Å) interconnecting clusters and therefore it can be thought of as compound that consists of one-dimensional infinite chains.

Considering the one-dimensional infinite chain structural feature and the low semiconducting energy gap (0.064 eV) that $BaMo_5O_8$ have, it is quite possible that $BaMo_5O_8$ is actually a metallic conductor and the weak semiconducting behavior observed from the sintered pressed pellet resistivity measurements probably arises from the energy barriers between the particles. The four-probe d.c. resistivity measurements on a single of $BaMo_5O_8$ should be able to depict whether this material is a conductor or not. In view of the difficulty in growing crystals big enough to do single crystal four-probe resistivity measurement, the following alternative ways are thus suggested: solid state Mo isotope NMR measurement, in which a linear relationship between the reciprocal relaxation time and the temperature (Korriga relation) or, for this particular compound, a constant Knight shift with respect to temperature would be observed on electron conducting materials;[20] Q-factor measurements of the a.c. resistivity, in which the Q-factor measured on the electron conducting materials is lower than the one without conductor.[21]

REFERENCES

1. McCarley, R.E. Polyhedron, 1986, 5, 51.
2. (a). Torardi, C.C.; McCarley, R.E. J. Am. Chem. Soc., 1979, 101, 3963; (b). Torardi, C.C.; McCarley, R.E. J. Less-Common Meals, 1986, 116, 169; (c). Chen, S.C.; Lii, K.H.; Aufdembrink, B.A.; McCarley, R.E. unpublished research.
3. (a). McCarley, R.E. Philos. Trans. R. Soc. London A, 1982, 308, 141; (b). McCarley, R.E. Am. Chem. Soc. Symp. Ser., 1983, 211, 273; (c). Lii, K.H.; McCarley, R.E. unpublished research.
4. Calson, C.D.; Brough, L.F.; Edwards, P.A.; McCarley, R.E. J. Less-Common Meals, 1989, 156, 325.
5. McCarley, R.E.; Lii, K.H.; Edwards, P.A.; Brough, L.F. J. Solid State Chem., 1985, 57, 17.
6. Lii, K.H.; McCarley, R.E.; Kim, S.; Jacobson, R.A. J. Solid State Chem., 1986, 64, 347.
7. (a). Gougeon, P.; Gall, P.; McCarley, R.E. Acta Crystallogr. C in press; (b). Gougeon, P.; Lee, K.H.; Schimek, G.; McCarley, R.E. unpublished results.
8. Mattausch, Hj; Simon, A.; Peters, E.-M. Inorg. Chem., 1986, 25, 3428.
9. Lii, K.H.; Wang, C.C. Inorg. Chem., 1988, 77, 407.
10. Chen, S.C. Ph.D. Dissertation, Sect. 1, Iowa State University, Ames, Iowa, 1991.
11. Dronskowski, R.; Simon, A. Angew. Chem. Int. Ed. Engl., 1989, 28, 758.
12. Hibble, S.J.; Cheetham, A.K.; Bogle, A.R.L.; WAkerley, H.R.; Cox, D.E. J. Am. Chem. Soc., 1988, 110, 3295.

13. Gilmore, C.J. J. Appl. Cryst., 1984, 17, p.42-46.

14. A menu driven interface to the SHELXS/PATSEE system is distributed with TEXSAN, which will create a reflection file in a proper SHELXS format as well as different input files that are necessary to run the program. But the SHELXS/PATSEE structure solution package is not distributed as part of the TEXSAN package.

15. TEXSAN - TEXRAY Structure Analysis Package, Molecular Structure Corporation (1985).

16. Sheldrick, G.M. In: Crystallographic Computing3, Eds., Sheldrick, G.M.; Kruger, C.; Goddard, R. Oxford University Press, 1985, p. 175-189.

17. Shannon, R.D. Acta Crystallogr., 1976, A32, 751.

18. Brown, I.D.; Wu, K.K. Acta Crystallogr., 1976, B32, 1957.

19. Bart, J.C.;Ragaini, V. Inorg. Chim. Acta, 1979, 36, 262.

20. (a). Wolf, D. Spin-Temperature and Nuclear-Spin Relaxation in Matter; Oxford University Press: London, 1979; Chapter 15; (b). Carter, G.C.; Bennett, L.H.; Kahan, D.J. Metallic shifts in NMR, part I. In Progress in Materials Science, 1977, 20, Chapter 2.

21. (a). Shinar, J.; Dehner, B.; Beaudry, B.J.; Peterson, D.T. Phys. Rev. B, 1988, 37, 2066; (b). Shinar, J.; Dehner, B.; Beaudry, B.J. Phys. Rev. Lett., 1990, 64, 563.

SECTION 3. SYNTHESES AND CRYSTAL STRUCTURES OF TERNARY MOLYBDENUM OXIDES HAVING THE $NaMo_4O_6$ STRUCTURE TYPE: KMo_4O_6 AND $Sr_{0.62}Mo_4O_6$

INTRODUCTION

Compounds containing M_6 octahedral metal cluster chains may be classified into two different types based on their building blocks, namely the M_6X_8 and the M_6X_{12} clusters. Chains based on M_6X_8 clusters may be subclassified into two groups; one is trans-face-sharing octahedra, another is trans-edge-sharing octahedra.

Compounds belonging to the former group (well-known as Chevrel phases) can be described by the formula of $Mo_{3n+3}X_{3n+5}$, where X and n represent chalcogenides and number of Mo_6 octahedra, respectively. The end member of this group was discovered in MMo_3X_3 (M = Li - Cs, In, Tl, Ag),[1-5] in which the infinite chains of trans-face-sharing Mo_6X_8 octahedra were observed. Infinite chains of trans-edge-sharing M_6X_8 octahedra were first found in the prototype compounds Gd_2Cl_3[6] and Sc_7Cl_{10}.[7]

Chains based on Mo_6X_{12} type building blocks were observed both in reduced binary lanthanide halides and in reduced ternary and quaternary molybdenum oxides. The first member observed in this oxide system is $NaMo_4O_6$,[8] which is more electron-rich (13 e^-/Mo4) and more tightly bound than the analogous lanthanide halides (7 e^-/Mo4). The repeat distance along the cluster chain is considerably shorter in the oxides than those in the halides.

The discovery of $Ba_{0.62}Mo_4O_6$[9] along with $NaMo_4O_6$ indicated that there may be a wide variety of new structures present in this family. Experiments have therefore been designed to synthesize analogous compounds with different counterions to find the upper limit of Metal-Centered Electrons (MCE) per Mo_4O_6 repeat unit. Another reason

for this is to investigate the possible change of structure and physical properties that may arise from different counterions, as already seen in the compounds $Sn_{0.9}Mo_4O_6$,[10] $Pb_{0.77}Mo_4O_6$,[11] and $InMo_4O_6$.[11] Reported here are the syntheses and structural characterizations of KMo_4O_6 and $Sr_{0.62}Mo_4O_6$ whose structures belong to the $NaMo_4O_6$ structure type.

EXPERIMENTAL

Materials

Potassium molybdate was prepared by the reaction of KOH (Fisher Certified A.C.S.) with a stoichiometric quantity of MoO_3 (Fisher Certified A.C.S.) in deionized water. The molybdate solution was filtered, its volume reduced by heating, and the precipitate collected on a glass frit. The product was finally dried at 120°C and stored in a dry box. Strontium molybdate was prepared by the reaction of $SrCO_3$ (Baker Analyzed, 99.6%) with a stoichiometric quantity of MoO_3 at 550°C in an open crucible. The resulting white powder was air cooled to room temperature and then stored in a dessicator. Molybdenum tubing was obtained from Thermo-Electron Corp. (99.97%), molybdenum metal powder from Aldrich Chemical Co. (99.99%), and molybdenum sheet from Rembar Co. (99.95%).

Synthesis

KMo_4O_6

Needle crystals of KMo_4O_6 were discovered in a mixture resulting from the reaction of stoichiometric amounts of MoO_3, Mo, and a two-fold excess of K_2MoO_4 needed for formation of $KMo_{11}O_{17}$. The reactants were weighed and ground together in a dry box. The loose powder was electron beam welded in an evacuated Mo tube (3

cm long x 0.8 cm inner diameter), and held under Ar(g) at 1430°C for 4 days. The outer surface of the Mo-tube was oxidized to MoO_2 but the inner surface was still shiny and remained intact. The reaction mixture was washed with water to remove the unreacted K_2MoO_4. The other phases identified in the product mixture were $K_3Mo_{14}O_{22}$ (discussed in Section 1) and Mo.

$\underline{Sr_{0.62}Mo_4O_6}$

This crystalline compound was discovered as small needle crystals growing on the walls of the quartz tube used in the reaction of K_2MoO_4, $SrMoO_4$, MoO_3, and Mo in mole ratio 3:6:16:29 (aiming at $K_2Sr_2Mo_{18}O_{28}$). The reactant mixture was ground, pelletized under 700 Kg/cm^2, placed in a basket made from Mo sheet, and sealed in an evacuated quartz tube which, in turn, was sealed in an evacuated quartz protection tube. The reaction was conducted at 1270°C for 10 days. A Guinier x-ray powder diffraction pattern of the bulk sample indicated that it was a single phase corresponding to $K_{0.5}M_{1.9}Mo_{14}O_{22}$ ($M = M^{2+}$) which will be discussed in Section 6, and was free of Mo, MoO_2, K_2MoO_4, and $SrMoO_4$.

X-ray Single Crystal Analysis for KMo_4O_6

A black needle crystal of KMo_4O_6 having approximate dimensions of 0.10 x 0.03 x 0.02 mm was mounted on a glass fiber. Data were collected with a Rigaku AFC6R diffractometer at room temperature up to $2\theta = 50^\circ$ by using graphite-monochromated Mo

Kα radiation and a 12 KW rotating anode generator. A scan mode of ω-2θ was used. Lattice parameters were measured from a least-squares refinement of 25 carefully centered reflections with $14^{o} < 2\theta < 27^{o}$ and gave a tetragonal cell with dimensions: a = b = 9.613(2) Å, c = 2.878(1) Å, and V = 265.9(2) $Å^3$. Three standard reflections which were measured after every 150 reflections showed no apparent variation in intensity during the data collection. The linear absorption coefficient for Mo Kα is 48.73 cm^{-1}. The intensity data were corrected for Lorentz and polarization effects. An empirical absorption correction, based on azimuthal scans of several reflections, was applied which resulted in transmission factors in the range 0.886 - 1.000. In the octant (h,k,l), 178 reflections were collected and 139 of them were considered as observed ($I > 3\sigma(I)$).

The space group of P4/mbm (#127) was chosen based on the systematic absences of 0kl: $k \neq 2n$. The structure was solved by starting with the coordinates of the atoms from the isostructural compound, $NaMo_4O_6$, and refined on $|F|$ by full matrix least-square techniques. All the atoms were refined anisotropically to R = 0.032 and Rw = 0.039. The final electron density difference map was flat with a maximum peak of 0.991 $e^-/Å^3$ and a minimum peak of -1.429 $e^-/Å^3$; both are close to Mo1.

X-ray Single Crystal Analysis for $Sr_{0.62}Mo_4O_6$

A black needle crystal of $Sr_{0.62}Mo_4O_6$ having approximate dimensions of 0.34 x 0.01 x 0.01 mm was mounted on a glass fiber. Data were collected on a Rigaku AFC6R diffractometer with graphite monochromated Mo Kα radiation and a 12 KW rotating anode

generator. The data were collected at room temperature up to $2\theta = 50^{o}$ and a scan mode of ω-2θ was used. Lattice parameters obtained from a least-squares refinement of 15 carefully centered reflections with $13^{o} < 2\theta < 21^{o}$ corresponded to a orthorhombic cell with dimensions: a = 9.432(4) Å, b = 9.706(3) Å, c = 2.852(4) Å, and V = 261.1(4) $Å^3$. Three standard reflections which were measured after every 150 reflections showed no apparent variation in intensity during the data collection. The linear absorption coefficient for Mo Kα is 94.8 cm^{-1}. The intensity data were corrected for Lorentz and polarization effects. An empirical absorption correction, based on azimuthal scans of several reflections, was applied which resulted in transmission factors in the range 0.840 - 1.000. A correction for secondary extinction was applied and gave a coefficient of 0.2968×10^{-6}. In the octant (h,k,l), 326 reflections were collected and 172 of them were considered as observed ($I > 3\,\sigma(I)$).

A space group of Pbam (#55) was chosen based on the systematic absences of 0kl: $k \neq 2n$ and h0l: $h = 2n$. The structure was solved by inputting the coordinates of the atoms from the isostructural compound, $Ba_{0.62}Mo_4O_6$ and refined on $|F|$ by full matrix least-square techniques. All the heavy atoms were refined anisotropically and oxygen atoms isotropically to R = 0.038 and Rw = 0.041. The final electron density difference map was flat with a maximum of 1.42 $e^{-}/Å^3$ and a minimum of -1.72 $e^{-}/Å^3$; both are near Mo2.

Details of the data collection and refinement of KMo_4O_6 and $Sr_{0.62}Mo_4O_6$ are given in Table 3.1. and 3.2, respectively. Final positional parameters for both compounds are listed in Table 3.3. The selected bond distances and angles of KMo_4O_6 and

$Sr_{0.62}Mo_4O_6$ are given in Table 3.4 and 3.5, respectively, and Table 3.6 lists out the anisotropic thermal parameters of atoms for both compounds. Tables of observed and calculated structure factors are available as supplementary materials.

Table 3.1. X-ray crystallographic data for KMo_4O_6

empirical formula	KMo_4O_6
formula weight	518.85
crystal system	tetragonal
space group	P4/mbm (#127)
a, Å	9.613(2)
c, Å	2.878(1)
V, $Å^3$	265.93(2)
Z	2
calcd density, g/cm^3	6.48
F000	235
crystal size, mm	0.10 x 0.03 x 0.02
μ(Mo Kα), cm^{-1}	48.73
diffractometer	Rigaku AFC6R
λ, Å, graphite-monochromated	0.71069
T, ^oC	23
2θ, deg	0-50
scan mode	ω-2θ
No. reflections collected	178
No. observations (I > 3 σ(I))	139
No. variables	22
goodness of fit indicator[a]	1.15
max. shift in final cycle	0.00
largest peak in final diff. map, $e/Å^3$	0.99
transmission coefficient	0.886-1.00
R[b], Rw[c]	0.029, 0.038

[a] Quality-of-fit = $[\Sigma\omega(|Fo| - |Fc|)^2/(N_{obs} - N_{parameters})]^{1/2}$

[b] $R = \Sigma||Fo| - |Fc||/\Sigma|Fo|$

[c] $Rw = [\Sigma\omega(|Fo| - |Fc|)^2/\Sigma\omega|Fo|^2]^{1/2}$; $\omega = 1/\sigma^2(|Fo|)$

Table 3.2. X-ray crystallographic data for $Sr_{0.62}Mo_4O_6$

empirical formula	$Sr_{0.62}Mo_4O_6$
formula weight	534.08
crystal system	orthorhomic
space group	Pbam (#55)
a, Å	9.432(4)
b, Å	9.706(3)
c, Å	2.852(4)
V, $Å^3$	261.1(4)
Z	2
calcd density, g/cm^3	6.79
F000	254
crystal size, mm	0.34 x 0.010 x 0.010
μ(Mo Kα), cm^{-1}	94.77
diffractometer	Rigaku AFC6R
λ, Å, graphite-monochromated	0.71069
T, °C	23
2θ, deg	0-50
scan mode	ω-2θ
No. reflections collected	326
No. observations ($I > 3\sigma(I)$)	172
No. variables	29
goodness of fit indicator[a]	1.00
max. shift in final cycle	0.00
largest peak in final diff. map, $e/Å^3$	1.42
transmission coefficient	0.84-1.00
R[b], Rw[c]	0.038, 0.041

[a] Quality-of-fit = $[\Sigma\omega(|Fo| - |Fc|)^2/(N_{obs}-N_{parameters})]^{1/2}$

[b] $R = \Sigma||Fo| - |Fc||/\Sigma|Fo|$

[c] $Rw = [\Sigma\omega(|Fo| - |Fc|)^2/\Sigma\omega|Fo|^2]^{1/2}$; $\omega = 1/\sigma^2(|Fo|)$

Table 3.3. Atomic coordinates and B_{eq}[a] for KMo_4O_6 and $Sr_{0.62}Mo_4O_6$

ATOM	Position[b]	Multiplier	X	Y	Z	B_{eq}, Å^2
$\underline{KMo_4O_6}$						
Mo1	4g	0.250	0.6010(1)	0.1010	0.00	0.27(4)
Mo2	4h	0.250	0.1428(1)	0.6428	0.50	0.50(4)
O1	4h	0.250	0.2931(8)	0.7931	0.50	0.7(3)
O2	8i	0.50	0.0458(8)	0.7591(9)	0.00	0.8(4)
K	2b	0.127(8)	0.00	0.00	0.50	1.3(1)
$\underline{Sr_{0.62}Mo_4O_6}$						
Mo1	4g	0.50	0.6089(2)	0.0942(9)	0.00	0.3(1)
Mo2	4h	0.50	0.3634(2)	0.1492(2)	-0.50	0.6(1)
O1	4h	0.50	0.721(2)	0.190(2)	-0.50	1.4(5)
O2	4g	0.50	0.476(2)	0.260(2)	0.00	0.3(4)
O3	4g	0.50	0.238(2)	0.058(2)	0.00	1.1(4)
Sr	4e	0.156(4)	0.00	0.00	0.374(3)	0.9(5)

[a] $B_{eq} = 8\pi^2/3\ \Sigma U_{ij} a_i^* a_j^* a_i \cdot a_j$, where the temperature factors are defined as $\exp(-2\pi^2\ \Sigma h_i h_j a_i^* a_j^* U_{ij})$

[b] Space group P4/mbm (no. 127) for KMo_4O_6 and Pbam (no. 55) for $Sr_{0.62}Mo_4O_6$

Table 3.4. Interatomic distances and angles in KMo_4O_6

	Interatomic Distances (Å)		
Mo1a-Mo1b	2.745(3)	Mo1a-O2a	2.074(8)
Mo1a-Mo2	2.779(1)	Mo1a-O1a	2.036(8)
Mo1a-Mo1c	2.878(1)	Mo2-O1c	2.04(1)
Mo1a-Mo1d	3.977(2)	Mo2-O2a	2.047(6)
Mo2-Mo2	3.883(3)		
O1a-O2a	2.868(8)	O1c-O2a	2.80(1)
O2a-O2b	2.90(2)	K-O1	3.449(2)
O2a-O2e	2.878(1)	K-O2	2.762(7)
	Bond Angles (deg)		
Mo1a-Mo1b-Mo1d	90.00	O1a-Mo1a-O2a	88.5(2)
Mo1a-Mo2-Mo1b	59.20(6)	O2a-Mo1a-O2c	175.7(5)
Mo1a-Mo2-Mo1c	62.37(3)	O1c-Mo2-O2a	86.3(2)
Mo1b-Mo1a-Mo2	60.40(3)	O2a-Mo2-O2b	90.2(3)
Mo1c-Mo1a-Mo2	58.82(2)	O2a-Mo2-O2e	89.3(3)
Mo1a-O2a-Mo2	84.8(3)	O2a-Mo2-O2f	173.2(5)
Mo1a-O1a-Mo1c	89.9(4)		

Table 3.5. Interatomic distances and angles in $Sr_{0.62}Mo_4O_6$

Interatomic Distances (Å)			
Mo1a-Mo1b	2.751(5)	Mo1a-O2a	2.03(2)
Mo1a-Mo2a	2.772(3)	Mo1a-O1a	2.00(2)
Mo1a-Mo1c	2.852(5)	Mo1a-O3b	2.07(2)
Mo1a-Mo1d	3.977(2)	Mo2a-O1c	2.06(2)
O1a-O2a	2.84(2)	Mo2a-O2a	2.08(1)
O1a-O3b	2.82(3)	Mo2a-O3a	2.05(1)
O1c-O2a	2.80(2)	Sr-O1	3.23(2)
O1c-O3a	2.84(3)	Sr-O2	2.95(1)
O2a-O2c	2.852(5)	Sr-O2	2.58(2)
O2a-O3a	2.98(2)	Sr-O3	2.92(2)
		Sr-O3	2.55(2)

Bond Angles (deg)			
Mo1a-Mo1c-Mo1d	90.00	O1a-Mo1a-O2a	87.7(7)
Mo1a-Mo1c-Mo2a	59.04(6)	O1a-Mo1a-O3b	87.8(7)
Mo1a-Mo1c-Mo2b	59.04(6)	O2a-Mo1a-O3b	173.6(7)
Mo1a-Mo1b-Mo2a	60.24(9)	O2a-Mo2a-O3a	92.4(5)
Mo1a-Mo2a-Mo1b	59.49(9)	O2a-Mo2a-O1c	86.7(6)
Mo1a-Mo2a-Mo1c	61.9(4)	O2a-Mo2a-O2c	86.7(6)
Mo1a-Mo2b-Mo1c	59.49(9)	O2a-Mo2a-O3c	174.0(7)
Mo1b-Mo1a-Mo2a	60.26(9)	O3a-Mo2a-O3c	88.0(7)
Mo2a-Mo1a-Mo2b	88.76(9)	O3a-Mo2a-O1c	87.3(8)
Mo1a-O1a-Mo1c	90.7(9)	Mo1a-O2a-Mo2a	84.8(5)
Mo1a-O3b-Mo2b	86.7(7)		

Table 3.6. Thermal parameters ($Å^2$) for KMo_4O_6 and $Sr_{0.62}Mo_4O_6$[a]

ATOM	U11	U22	U33	U12
KMo_4O_6				
Mo1	0.0030(6)	0.0030	0.0043(9)	-0.0001(5)
Mo2	0.0030(6)	0.0030	0.013(1)	-0.0007(5)
O1	0.008(4)	0.008	0.008(7)	-0.003(5)
O2	0.005(4)	0.008(4)	0.017(5)	-0.000(3)
K	0.019(2)	0.019	0.013(3)	0.00
$Sr_{0.62}Mo_4O_6$				
Mo1	0.005(1)	0.003(1)	0.005(1)	0.0008(8)
Mo2	0.001(1)	0.002(1)	0.020(2)	0.0013(9)
Sr	0.012(4)	0.010(5)	0.01(1)	-0.005(3)
O1	0.017(6)			
O2	0.004(5)			
O3	0.014(5)			

[a]The form of the anisotropic displacement parameter is $\exp[-2\pi^2\{h^2a^2\ U(1,1) + k^2b^2\ U(2,2) + l^2c^2\ U(3,3) + 2hkab\ U(1,2) + 2hlac\ U(1,3) + 2klbc\ U(2,3)\}]$, where a, b, and c are reciprocal lattice constants. U13 = U23 = 0 by symmetry, pace group P4/mbm (no. 127) for KMo_4O_6 and Pbam (no. 55) for $Sr_{0.62}Mo_4O_6$

RESULTS AND DISCUSSION

Crystal Structure of KMo_4O_6

KMo_4O_6 is isostructural to $NaMo_4O_6$, $InMo_4O_6$, $Sn_{0.9}Mo_4O_6$, and $Pb_{0.77}Mo_4O_6$. Like those compounds the structure of KMo_4O_6 is dominated by Mo-Mo bonding in infinite chains composed of trans-edge-shared octahedral cluster repeat units along the tetragonal c-axis. These chains are connected through Mo-O-Mo interchain linkages to weave a square pattern and form tunnels parallel to the c-axis in which the ternary metal ions are located. A view of the structure of KMo_4O_6 as projected down the tetragonal c-axis is provided in Fig. 3.1. The four-fold symmetry is clearly evident from this view. Unlike the structure of $NaMo_4O_6$ in which Na^+ ions display unusually large thermal parameters in the a-b plane, the K^+ ions in KMo_4O_6 are tightly bonded to the oxygen atoms and do not have large thermal parameters. The K-O2 bond distance of 2.762(7) Å is significantly shorter than the calculated K-O distance (2.89 Å) based on K^+ (1.51 Å, CN = 8) and O^{2-} (1.38 Å, CN = 4).[12]

Fig. 3.2 is an ORTEP drawing of a repeat unit of one octahedral cluster chain in KMo_4O_6 along the c-axis. There are two distinct Mo atoms, Mo1 (waist) and Mo2 (apex), in this repeat unit. All Mo1 and O2 atoms lie in mirror planes perpendicular to the c-axis at z = 0 and 1, while the Mo2 and O1 atoms lie in a mirror plane at z = 1/2. Two other mirror planes are present in this unit; one contains all of the Mo1 atoms as well as O1a and O1b, the other contains the Mo2, O1c, and O1d atoms and bisects the

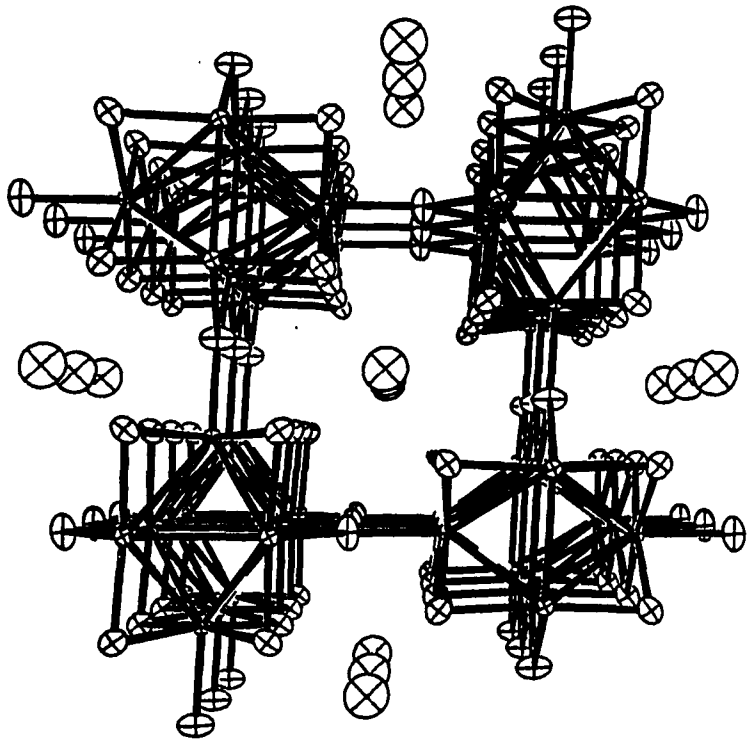

Fig. 3.1. ORTEP drawing (50% thermal ellipsoids) of a three dimensional view of the KMo_4O_6 structure as viewed down the tetragonal c-axis. Unconnected ellipsoids represent the K atoms.

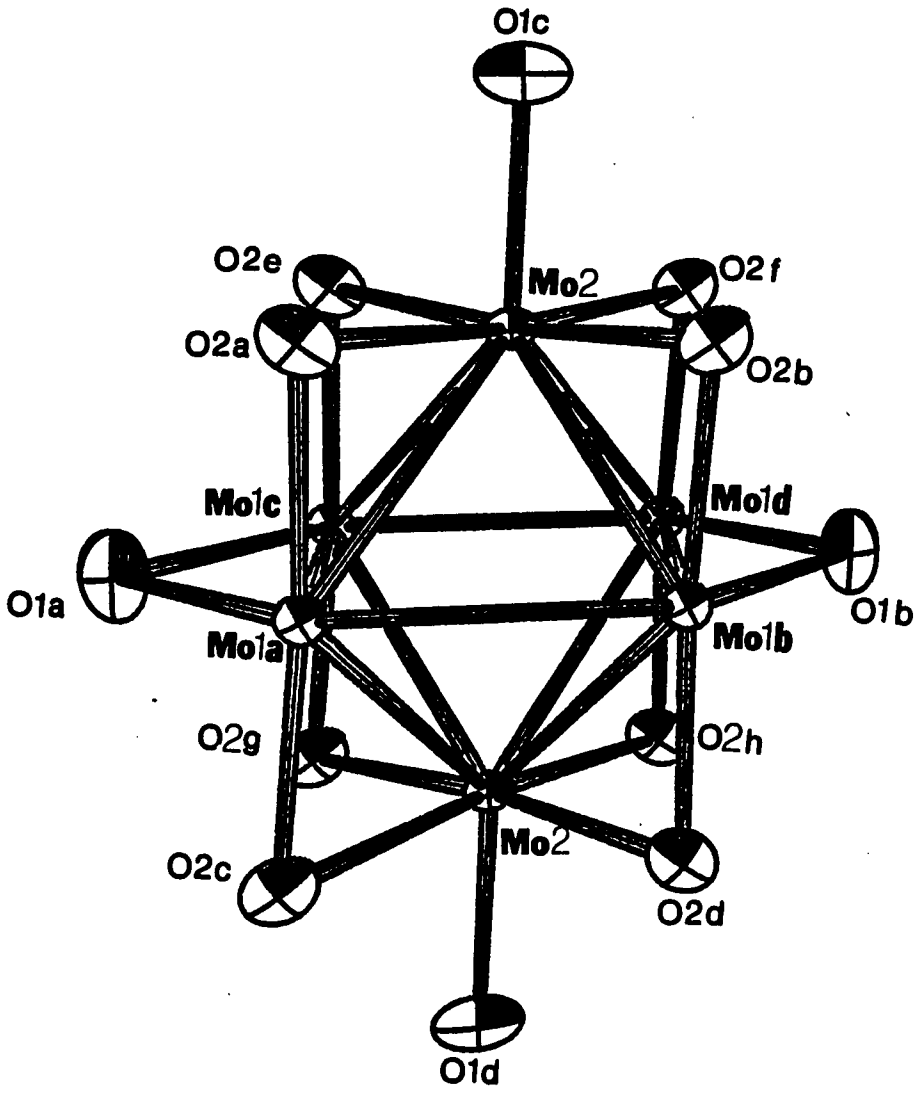

Fig. 3.2. ORTEP drawing (50% thermal ellipsoids) of a repeat unit of one molybdenum-oxide cluster chain in KMo_4O_6.

bonds between Mo1a-Mo1b and Mo1c-Mo1d. Consequently, the atoms Mo1, Mo2, and O1 lie on sites of mm symmetry while the O2 atoms reside on sites of m symmetry.

The structure of one cluster chain as viewed perpendicular to the chain direction is given in Fig. 3.3, which shows the trans-edge sharing of the repeating octahedral cluster units. The infinite chain is comprised of Mo_6O_{12} clusters fused at opposite edges by removal of two edge-bridging oxygen atoms and sharing of the metal and remaining oxygen atoms on those edges between cluster units. The unshared Mo atoms occupy the apex positions of the octahedra, while the shared Mo atoms occupy the waist positions along the chain. All O2 atoms are edge-bridged between two neighboring clusters ($O^{i\text{-}i}$). Oxygen O1c and O1d ($O^{a\text{-}i}$) are terminal to Mo2 atoms and connect to the neighboring clusters at the bridging sites of O1a and O1b ($O^{i\text{-}a}$). The connectivity within and between chains can therefore be represented by the formulation $K^+[(Mo_2Mo_{4/2}O_{8/2}{}^{i\text{-}i}O_{2/2}{}^{a\text{-}i})O_{2/2}{}^{a\text{-}i}]^-$.

It is notable that two compounds of composition KMo_4O_6 in different phases were recently reported by Hoffman and coworkers.[13] KMo_4O_6-I was prepared from a slow heating of KO_2 in a Mo cylinder to 1080°C at normal pressure. The unit cell of KMo_4O_6-I is orthorhombic, space group Pbam with a = 9.793(9) Å, b = 9.4764(8) Å, c = 2.8732(4) Å, and z = 2. KMo_4O_6-II was recovered after a high pressure decomposition of K_2MoO_4 in gold capsule at 1100°C, 30 Kbar for 30 minutes. KMo_4O_6-II crystallizes in the tetragonal system, space group P4/mbm, with unit cell dimensions a = 9.612(2) Å, c = 2.950(1) Å, and z = 2. The structural features of KMo_4O_6-I and KMo_4O_6-II are the same as those of $Ba_{0.62}Mo_4O_6$ and $NaMo_4O_6$, but the c-axis (2.950(1) Å) of

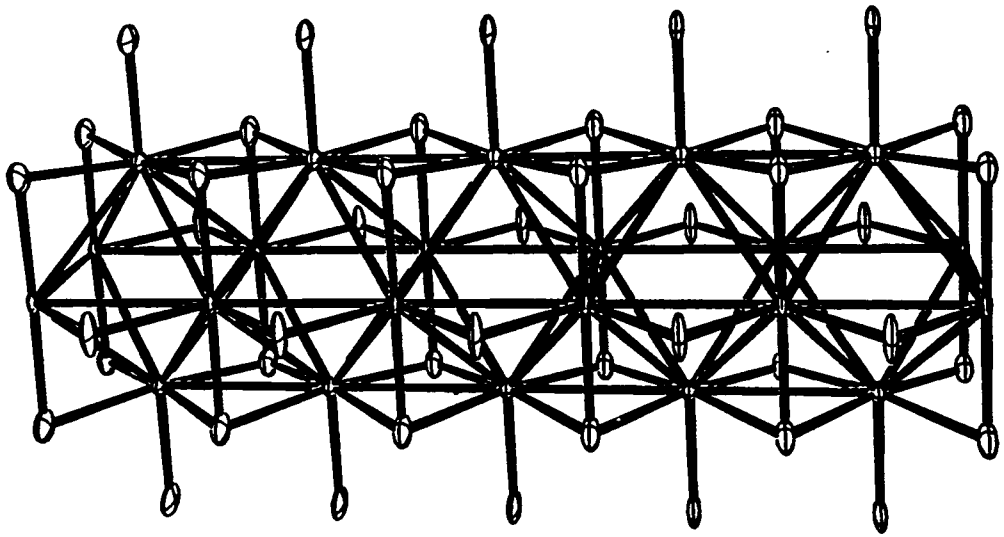

Fig. 3.3. ORTEP drawing (50% thermal ellipsoids) of a segment of one molybdenum-oxide cluster chain along the c-axis in KMo_4O_6. The O atoms connected to the apex Mo atoms above and below the chain and the coplanar O atoms connected to the waist Mo atoms also form the Mo-O-Mo linkages to neighboring chains.

KMo_4O_6-II is significantly longer than the usual Mo-Mo bond distance (2.65 to 2.85 Å). Interestingly, McCarroll and coworkers have more recently prepared and structurally characterized a compound of composition KMo_4O_6 by the electrolysis of fused salts mixture.[14] The unit cell of this compound is tetragonal, space group P4/m with c-axis ca. 2.88 Å.

Crystal Structure of $Sr_{0.62}Mo_4O_6$

The structure of $Sr_{0.62}Mo_4O_6$ belongs to the $NaMo_4O_6$ type structure, but with a lower symmetry. A compound isostructural and isoelectronic to $Sr_{0.62}Mo_4O_6$ has been previously reported as $Ba_{0.62}Mo_4O_6$, where Ba^{2+} ions are ordered in five of eight positions in the channel and lead to a supercell of $Ba_5(Mo_4O_6)_8$. Within the infinite trans-edge-shared octahedral cluster chains of $Ba_5(Mo_4O_6)_8$, Mo-Mo distances show a remarkable long-short-long pattern along the chain direction.

The structure of $Sr_{0.62}Mo_4O_6$ (subcell) as viewed down the c-axis is given in Fig. 3.4, which shows that the principal features of this subcell structure are exactly the same as those of $NaMo_4O_6$ except that the unit cell is distorted from tetragonal to orthorhombic symmetry. The square pattern weaved by the Mo-O-Mo interchain linkages is slightly puckered compared to that in $NaMo_4O_6$. This is, in part, a result of a slight rotation of each cluster chain about its own axis parallel to the c-axis. The rotation of each chain is in a direction opposite to that of its neighbors. The O-O distances between atoms in neighboring chains are thus reduced in one direction and increased in

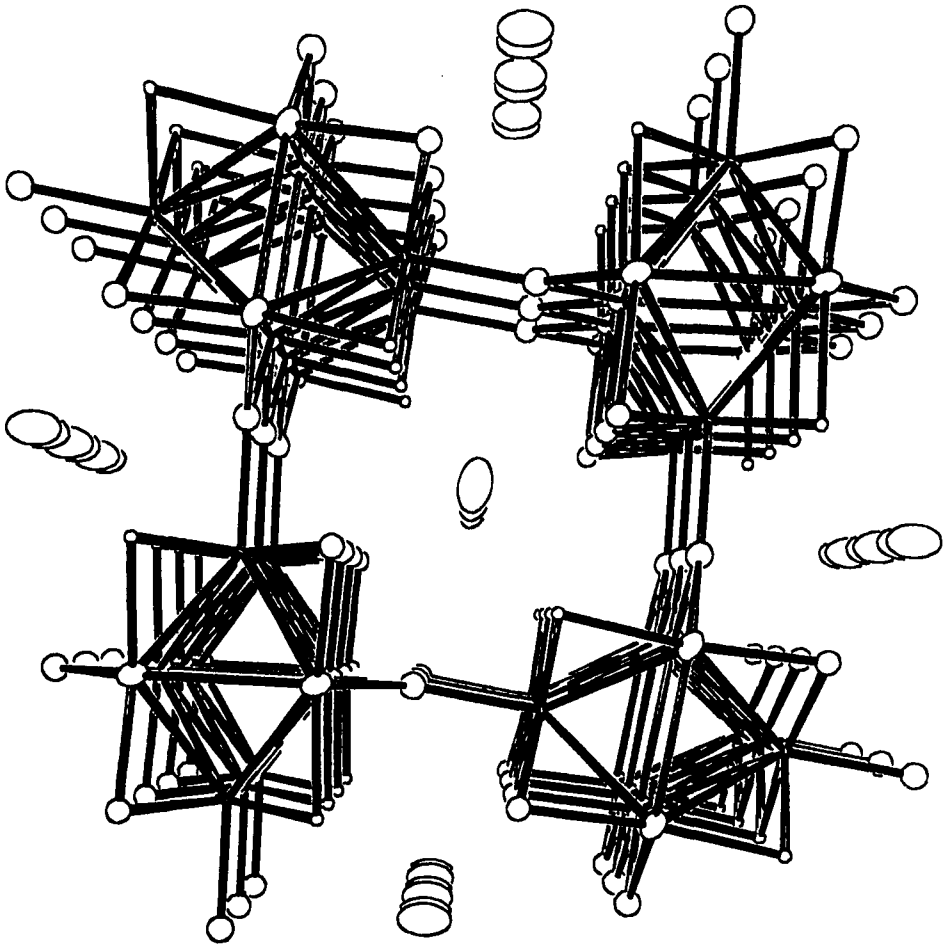

Fig. 3.4. ORTEP drawing (50% thermal ellipsoids) of the structure of $Sr_{0.62}Mo_4O_6$ as viewed down the c-axis showing the cross-linking of molybdenum-oxide chains by Mo-O-Mo bridge bondings and the pockets formed for the Sr atoms (shown as unconnected ellipsoids).

the other direction within the a,b plane. The cause of this distortion from tetragonal to orthorhombic is not obvious. It could be due to the presence of the larger and more highly charged Sr^{2+} and Ba^{2+} ions which weakly interact with the unhybridized p orbitals on the sp^2-like interchain O atoms surrounding the tunnel sites, as evidenced by Sr-O1 (3.23(2) Å) and Ba-O1 (3.19(2) Å) distances. In the structure of $NaMo_4O_6$ the lone pair p orbitals on the interchain O atoms evidently do not interact with Na^+ ions and thus the capability of pi bonding to the molybdenum chains is enhanced.

The Sr-O bond distances (ave. 2.846 Å) are relatively long compared to the calculated Sr-O distance of 2.74 Å based on Sr^{2+} (1.36 Å, CN = 10) and O^{2-} (1.38 Å, CN = 4), and yet Sr^{2+} ion has a small temperature factor of B_{eq} = 0.9 $Å^2$. The oxidation state of the Sr^{2+} ion assessed from the bond length-bond order relation,[15] $\Sigma s(Sr\text{-}O) = \Sigma[d(Sr\text{-}O)/2.143]^{-7.0}$ is 1.69 v.u.. Since there is only 0.62 Sr^{2+} ion per Mo_4O_6, this valence number is in a reasonably good agreement with the anion charges of -1.07 and -1.12, estimated from the bond order calculations of Mo-O and Mo-Mo, respectively.

Discussion

One of the most interesting features of the $M_xMo_4O_6$ structures is the variation in the position and occupancy of the tunnel cations. The Na^+ and the K^+ ion each fully occupies the tunnel site at (0, 0, 1/2) in $NaMo_4O_6$ and KMo_4O_6, respectively. The Na^+ ions in $NaMo_4O_6$ exhibited large temperature parameters along the a and b directions

and were positionally disordered in four off-center sites,[16] while the K^+ ions in KMo_4O_6 are rather isotropic with small temperature factors. The In^+ ion in $InMo_4O_6$ fully occupies the tunnel site but is displaced to (0, 0, 0.0987) along the tunnel direction. About eight-tenths and one-tenth of the Sn^{2+} ions in $Sn_{0.9}Mo_4O_6$ are each displaced from the cell center to (0, 0, 0.0148) and (0, 0, 0.3018), respectively. There is likely a vacancy every tenth subcell. In the structure of $Pb_{0.77}Mo_4O_6$, two-thirds of the Pb^{2+} ions are displaced to (0, 0, 0.28) and a vacancy exists every fourth subcell. In the subcell refinement, the Sr^{2+} ion in $Sr_{0.62}Mo_4O_6$ and the Ba^{2+} ion in $Ba_{0.62}Mo_4O_6$ are each displaced to (0, 0, 0.37) with an occupancy of about 60%.

These positional displacements and occupational variations observed in $M_xMo_4O_6$ structures presumably arise from the electrostatic repulsions or bonding interactions between counterions. The only exception to this is the structure of KMo_4O_6, in which the K^+ ion fully occupies the site at (0, 0, 1/2). It also appears that the state of ordering in the tunnels in $M_xMo_4O_6$ strongly depend upon the charge and size of the counterions, as well as the number of the electrons transferred to the molybdenum chains.

Table 3.7 is the selected structural parameters for $M_xMo_4O_6$ compounds. It is interesting that the Mo-Mo bond distance parallel to the chain axis in KMo_4O_6 is the longest one, while the Mo-Mo distance perpendicular to the chain axis in KMo_4O_6 is the shortest one for those in $M_xMo_4O_6$ compounds. From the comparisons of $NaMo_4O_6$ to KMo_4O_6 and of $Ba_{0.62}Mo_4O_6$ to $Sr_{0.62}Mo_4O_6$, the a and b cell parameters are likely dominated by the size of the counterions. A remarkable relationship between c cell

parameter and MCE(f) is observed. The c cell parameters apparently decrease with the increase of MCE(f). This implies that the Mo-Mo distance parallel to the chain axis is sensitive to the number of electrons available for metal-metal bonding in the cluster unit. The consistent observation of the smaller value of MCE(Σn) compare to those of MCE(Σs) or MCE(f) indicate that some of the MCE electrons enter the metal-metal antibonding states which then weaken the Mo-Mo bonding. The estimation of MCE in antibonding states of some reduced molybdenum oxides containing infinite chains of trans-edge-shared octahedral cluster units has been studied by McCarley.[17]

Table 3.7. Selected structural parameters for $M_xMo_4O_6$ compounds

compound	a, Å	b, Å	c, Å	size[a]	MCE(Σn)	MCE(Σs)	MCE(f)	Mo-Mo(//)	Mo-Mo(⊥)
$NaMo_4O_6$	9.570(3)	9.570	2.8618(2)	1.16	12.7(1)	12.8(2)	13.0	2.8618(2)	2.753(3)
KMo_4O_6	9.613(2)	9.613	2.878(1)	1.51	12.6	13.2	13.0	2.878(1)	2.745(3)
$InMo_4O_6$	9.6650(5)	9.6650	2.8633(3)	*	12.3(1)	13.1(2)	13.0	2.8633(3)	2.773(1)
$Sn_{0.9}Mo_4O_6$	9.621(2)	9.621	2.8369(6)	1.22	13.3(1)	13.4(2)	13.8	2.8369(6)	2.7770(8)
$Pb_{0.77}Mo_4O_6$	9.6119(5)	9.6119	2.8424(3)	1.29	12.7(1)	13.3(2)	13.5	2.8424(3)	2.775(2)
$Ba_{0.62}Mo_4O_6$	9.509(2)	9.825(2)	2.853(1)	1.42	12.4(1)	13.06	13.24	2.853(1)	2.787(4)
$Sr_{0.62}Mo_4O_6$	9.432(4)	9.706(3)	2.852(4)	1.25	13.12	13.07	13.24	2.852(4)	2.751(5)

[a]Ionic radii (Å) of counterions

REFERENCES

1. Potel, M.; Chevrel, R.; Sergent, M. Acta Crystallogr., 1980, B36, 1545.
2. Potel, M.; Chevrel, R.; Sergent, M.; Armici, J.C.; Decroux, M.; Fisher, O. J. Solid State Chem., 1980, 35, 286.
3. Honle, W.; Von Schnering, H.-G.; Lipka, A.; Yvon, K. J. Less Common Metals, 1980, 71, 135.
4. Huster, J.; Schippers, G.; Bronger, W. J. Less Common Metals, 1983, 91, 333.
5. Tarascon, J.M.; DiSalvo, F.J.; Waszczak, J.V. Solid State Commun., 1984, 52, 227.
6. Lokken, D.A.; Corbett, J.D.; Inorg. Chem., 1973, 12, 556.
7. Poeppelmeier, K.R.; Corbett, J.D.; Inorg. Chem., 1977, 16, 1107.
8. Torardi, C.C.; McCarley, R.E. J. Am. Chem. Soc., 1979, 101, 3963.
9. Torardi, C.C.; McCarley, R.E. J. Less Common Metals, 1986, 116, 169.
10. Aufdembrink, B.A.; McCarley, R.E. unpublished research.
11. Lii, K.H.; McCarley, R.E. unpublished research.
12. Shannon, R.D. Acta Crystallogr., 1976, A32, 751.
13. Hoffman, R.; Hoppe, R.; Bauer, K.; Range, K.-J. J. Less Common Metals, 1990, 161, 279.
14. Private communication with W.H. McCarroll, March, 1991.
15. Brown, I.D.; Wu, K.K. Acta Crystallogr., 1976, B32, 1957.
16. Chu, P.J.; Gerstein, B.C.; J. Chem. Phys., 1989, 90, 3713.
17. McCarley, R.E. Polyhedron, 1986, 5, 51.

SECTION 4. SYNTHESIS AND CHARACTERIZATION OF THREE COPPER(II) ALKOXIDE CHLORIDE DIMERS WITH THE ANION OF THE CHELATING LIGAND 2-(2-HYDROXYETHYL)PYRIDINE

ABSTRACT

The syntheses and structural characterizations are reported for the novel compounds $[CuCl(hep)]_2$ (1), $[CuCl(hep)(Hhep)]_2 \cdot 2CH_2Cl_2$ (2), and $[CuCl(hep)(py)]_2 \cdot CH_2Cl_2$ (3), where hep is the anion of 2-(2-hydroxyethyl)pyridine and py is pyridine. The magnetic properties of 1 are also reported. Compound 1 crystallizes in the triclinic system, space group $P\bar{1}$. The unit cell dimensions are a = 8.018(3) Å, b = 8.546(2) Å, c = 6.198(2) Å, $\alpha = 100.76(2)^o$, $\beta = 109.99(2)^o$, $\gamma = 89.77(2)^o$, V = 391.2(4) $Å^3$, and Z = 1. Compound 2 crystallizes in the monoclinic system, space group $P2_1/c$. The unit cell dimensions are a = 10.857(3) Å, b = 20.207(3) Å, c = 16.694(4) Å, $\beta = 95.09(1)^o$, V = 3648.0(1) $Å^3$, and Z = 4. Compound 3 crystallizes in the triclinic system, space group $P\bar{1}$. The unit cell dimensions are a = 9.434(7) Å, b = 20.718(6) Å, c = 8.233(6) Å, $\alpha = 101.42(4)^o$, $\beta = 115.61(5)^o$, $\gamma = 90.53^o$, V = 1414(2) $Å^3$, and Z = 2. The two halves of the binuclear structures in 1, 2, and 3 are held together by ethyloxo bridges between the two copper atoms. Compound 1 may also be described as a polymer of dimers. The dimers are linked through the intermolecular chloro bridges between the copper atoms in a stairstep fashion to give a polymer. The Cu-Cl separations are 2.255(1) Å (intradimer) and 2.947(2) Å (interdimer). The coordination geometry around the copper atoms can be described as square-based pyramidal with CuO_2NCl_2 ligation. Compound 2 consists of pseudo-centrosymmetric dimeric units that are well separated from one another in the crystal lattice The Hhep ligand binds only

through the N atom and leaves the 2-(2-hydroxyethyl) group free. The basal positions of the distorted square pyramidal coordination about Cu are occupied by N and O. The Cl atom is weakly bonded in the apical site at a distance of 2.597 Å. Compound 3 consists of two centrosymmetric dimeric units, one centered at (0, 0, 0) and another at (1/2, 1/2, 1/2). The molecular structure of 3 is the same as that of 1, except that the pyridine ligands are weakly bonded to Cu atoms at the apical position. The coordination geometry around Cu atom is thus a distorted square pyramid. Interestingly, when under reduced pressure, 2 and 3 are each convertible to 1.

INTRODUCTION

The chemistry of copper (II) alkoxides has not been well-developed. Most of these compounds have been found to be insoluble and polymeric, with essentially unknown structures.[1] Structural information has been derived in most cases from studies of spectroscopic and physical properties. There is thus a need to prepare new alkoxide derivatives which are soluble in a range of organic solvents and which can be definitively structurally characterized. The insoluble, polymeric structures of conventional copper(II) alkoxides are due to extensive alkoxide bridging.[2] The tendencies for bridging may be decreased and solubilities increased by using chelating alkoxide ligands.[3] Recently, one soluble monomeric copper(II) siloxide complex, $Cu[OSi(OCMe_3)_3]_2(py)_2$,[4] and two volatile monomeric copper(II) alkoxides, $Cu[OCHMeCH_2NMe_2]_2$ and $Cu[OCH_2CH_2NMeCH_2CH_2NMe_2]_2$,[5] have been structurally characterized. This section will discuss the synthesis, characterization, and physical properties of three new copper(II) alkoxide complexes, 1, 2, and 3, which contain the bidentate chelating alkoxide ligand, hep, the anion of 2-(2-hydroxyethyl)pyridine.

EXPERIMENTAL SECTION

Materials and Methods

All reactions and manipulations were carried out under inert atmospheres with the use of standard dry-box, vacuum, and Schlenk techniques. Copper(II) chloride was dried under vacuum at 130^{0} C for three days and further analyzed for chlorine and copper. Chlorine analyses were performed by bringing samples into solution with dilute nitric acid and titrating potentiometrically with a standard silver nitrate solution. Copper analyses were performed iodometrically.[6] 2-(2-hydroxyethyl)pyridine was used as commercially obtained. Tetrahydrofuran was stirred with sodium metal and benzophenone overnight, then degassed, vacuum distilled, and stored over outgassed 4A molecular sieves before use. Diethyl ether was dried in the same manner. In a similar manner, methanol and isopropanol were dried by addition of sodium metal and stirring overnight, followed by vacuum distillation. Pyridine was dried by refluxing with CaH_2, distilled and stored under vacuum over outgassed 4A molecular sieves. Dichloromethane was refluxed over P_2O_5 for 8 hrs., then distilled and stored in a similar manner.

Physical Measurements

Fourier-transform infrared spectra were recorded on an IBM IR98FT spectrometer, whose sample chamber was flushed with purified nitrogen. Samples were prepared as

Nujol mulls and mounted on CsI plates. The magnetic susceptibility measurements were carried out on solid polycrystalline samples with a SQUID magnetosusceptometer. The magnetic field strength was set at 5 KG. Data were taken every 3 degrees from 5 to 395 K. Measurements of magnetization versus field strength at constant temperature were also taken and the resulting data were later used to calculate the amount of ferromagnetic impurity contained in the sample. The temperatures were set at 10, 200, and 395 K and the field strength was varied in the range from 2000 to 50000 G. The ferromagnetic impurity calculated from the plot of magnetic moment vs. the field strength corresponds to 11.4 ppm of Fe/molecule. X-band ESR spectra were recorded on both powdered and solution samples with a Bruker ER200-SRC instrument equipped with an Oxford Instruments ESR 900 flow-through cryostat and a DTC-2 digital temperature controller. Spectra were taken at 107 and 297 K. The UV/visible spectra were taken with a Perkin-Elmer Lambda Array 3840 UV/vis Spectrophotometer.

Synthesis

[CuCl(hep)]$_2$ (1)

Dehydrated copper(II) chloride was allowed to react with two equivalents of Hhep in THF at room temperature for ca. 12 hrs.. The resulting blue mixture was filtered to recover the blue precipitate 4, which was then vacuum dried overnight. Analysis indicated that 4 was $CuCl_2(Hhep)(THF)_2$ (90.5 % yield). Anal. Calcd for $CuCl_2C_{15}H_{25}O_3N$: Cu, 15.8; Cl, 17.6. Found: Cu, 15.0; Cl, 17.6. Compound 1 was synthesized by dropwise addition of a hexane solution of 2.2 M n-butyllithium (4.4 ml,

9.68 mmol) into a suspension of 4 (1.945 g, 4.841 mmol) in THF. After 10 hr. stirring at room temperature, a yellow precipitate and a blue filtrate were separated by filtration. The blue compound obtained after vacuum removal of solvent from the filtrate was dissolved in a minimum amount of CH_2Cl_2. Green crystals of compound 1 were discovered after 16 hr. standing at room temperature under vacuum. These green crystals are slightly soluble in THF, CH_2Cl_2, and CH_3CN. Far IR(CsI): 573(m), 510(w), 440(sh), 432(m), 357(m), 323(w), 288(w), 266(m), 221(m). Compound 1 also can be prepared quantitatively by a stoichiometric reaction of $CuCl_2$ and Lihep in THF. The purity of 1 thus prepared was checked by x-ray powder pattern and elemental analysis (Calcd: Cu, 28.7; Cl, 16.0. Found: Cu, 27.4, Cl, 16.0.).

[CuCl(hep)(Hhep)]$_2$•2CH_2Cl_2 (2)

Lithium methoxide was prepared by dropwise reaction of 2.2M n-butyllithium in hexane with a slightly deficient amount of methanol in hexane. The yellowish white precipitate was separated from the filtrate and vacuum dried overnight, then stored in the dry box. By following Mehrotra's procedure,[1b] copper(II) methoxide was prepared from the reaction of dehydrated copper(II) chloride with two equivalents of lithium methoxide in methanol. The insoluble blue product obtained was filtered and washed with parent alcohol thoroughly. After removing excess of solvent and drying under vacuum, this blue solid was later found to contain 3% of Cl by analysis. Compound 2 was then synthesized by the alcoholysis reaction of this Cl-containing copper(II) methoxide with two equivalents of Hhep in THF. A green insoluble product and a dark green filtrate were obtained after filtration. An oily product was obtained after vacuum

removal of solvent from the filtrate. After dissolving this oily product in a small amount of CH_2Cl_2, green crystals of 2 were obtained after two weeks at -10° C, but the yield was low. In efforts to increase the yield of 2, reactions of 1 with excess Hhep in either THF or CH_2Cl_2 were tested and each gave an insoluble green solid and a dark green filtrate. The green solids were identified as 1 by x-ray powder diffraction pattern. The green crystals obtained from the filtrate of this procedure gave yields of 2 in the range from 25 to 40 %.

[CuCl(hep)(py)]$_2$•CH_2Cl_2 (3)

The preparations of lithium isopropoxide and copper(II) isopropoxide were similar to those of lithium methoxide and copper(II) methoxide, respectively. The green copper(II) isopropoxide thus prepared also contains a small amount of Cl. The reaction of this Cl-containing Cu(II) isopropoxide with 2 moles of Hhep in THF resulted in a green solid and a dark green filtrate. After vacuum removal of solvent from the filtrate, the residual oily product was then recrystallized from a mixed solvent (CH_2Cl_2/py = 1/9) at -20 °C for 3 weeks. The yield of 3 was low. In an attempt to increase the yield of 3, a reaction of 1 with neat pyridine in CH_2Cl_2 was thus conducted and resulted in a clear dark green solution. The crystals of 3 grown from this solution were obtained in an yield of 52.9 %.

Interestingly, upon pumping extensively under vacuum, crystals of 2 and 3 each undergo convertion to 1 by the loss of CH_2Cl_2 solvents and the apical ligands (Hhep for 2 and py for 3).

Single Crystal Crystallographic Study

[CuCl(hep)]$_2$ (1)

The green crystals obtained from CH_2Cl_2 were surprisingly stable and showed no sign of decomposition after a month in air. X-ray data were collected with a Rigaku AFC6 diffractometer at room temperature up to $2\theta = 50^o$ by using graphite-monochromated Mo Kα radiation. A scan mode of ω-2θ was used. No decay of the intensities of three standard reflections was observed. In the hemisphere (h, $\pm$k, $\pm$l), 1483 reflections were collected and 1081 of them were considered as observed ($I \geq 3\sigma(I)$). The absorption coefficient for Mo Kα is $\mu = 31.64\ cm^{-1}$. Intensity data were corrected for Lorentz and polarization effects as well as for absorption.

The intensity statistical test indicated a space group of P1, so both centrosymmetric and noncentrosymmetric models were tested. The structure was solved in either case by direct methods (Mithril)[7] and refined on $|F|$ by full-matrix least-square techniques (TEXSAN).[8] The centrosymmetric model gave a residual index $R = 0.034$, $R_w = 0.044$, and the noncentrosymmetric one, $R = 0.032$, $R_w = 0.041$. The structural features resulting from the two refinements are essentially the same except that in the noncentrosymmetric model, one of the bridging Cu-O distances is relatively long (2.00 Å) and another is relatively short (1.90 Å), when compared to the other Cu-O distances in the same model or in the centrosymmetric model (1.93-1.94 Å). The coordination geometry of one of the copper atoms in the noncentrosymmetric model also slightly deviates from a square planar arrangement (sum of angles = 350^o). Because the differences in bond distances, symmetry, and principal structural features derived from

the two models were small, and the acentric structure in general will show a lower R-value at a given stage of refinement than will the centric one,[9] the centrosymmetric model was chosen as the preferred one. The final electron density difference map was flat to less than ±0.68 e/Å^3. All the hydrogen atoms were introduced at calculated positions with C-H = 1.05 Å

[CuCl(hep)(Hhep)]$_2$•2CH$_2$Cl$_2$ (2)

Crystals of 2 are subject to loss of solvent under reduced pressure. Thus, a single crystal picked up from the solution contained in a Schlenk tube was immediately mounted on the diffractometer in the low temperature nitrogen stream (-75^o C). Data were collected with an Enraf-Nonius CAD4 diffractometer. Lattice parameters were measured from 16 reflections with $24^o \leq 2\theta \leq 34^o$. Graphite-monochromated Mo Kα radiation was employed to collect data with $4^o \leq 2\theta \leq 45^o$. The θ-2θ scan technique was used. Three standard reflections showed no apparent variation in intensity during the data collection. The absorption coefficient for Mo Kα is μ = 16.516 cm^{-1}.

The intensity data were corrected for Lorentz and polarization effects. The space group ($P2_1/c$) was chosen based on the systematic extinctions. Data collected in the hemisphere (±h, k, ±l) were then averaged to give a total of 4941 reflections of which 2161 reflections with $I > 3\sigma(I)$ were considered as observed. The ψ-scan transmission coefficients were 0.1436 to 0.9966. The usual empirical correction for absorption was thus not applied, but after the structure was solved, a θ-dependent numerical correction[10] for absorption was applied, which gave correction factors of 0.807 to 1.832. The structure was solved by Patterson methods (SHELXS-86)[11] and refined with the

CAD4-SDP program.[12] C(11) could not be refined anisotropically; all other nonhydrogen atoms were refined anisotropically to give R = 0.061 and R_w = 0.074. The structure was refined to R = 0.057 and R_w = 0.063 after deleting five reflections which appeared to be seriously in error with $F_o << F_c$. One of the hydrogen atoms on one of the uncoordinated hydroxo groups was located at (0.527, 0.135, 0.541) from the final ED map. The refinement also showed that the sites for the CH_2Cl_2 molecules were fully occupied. Hydrogen atoms introduced by calculation were at a C-H distance of 0.95 Å.

[CuCl(hep)(py)]$_2$·CH_2Cl_2 (3)

Like 2, crystals of 3 are subject to loss of solvent under reduced pressure. A single crystal picked up from the solution contained in a Schlenk tube was thus immediately mounted on the diffractometer in the low temperature nitrogen stream (-80° C). Data were collected with a Rigaku AFC6R diffractometer up to 2θ = 50° by using graphite-monochromated Mo Kα radiation and a 12 KW rotating anode generator. A scan mode of ω-2θ was used. Cell constants and an orientation matrix for data collection, obtained from a least-squares refinement of 20 carefully centered reflections with 13° < 2θ < 15°, corresponded to a triclinic cell with dimensions: a = 9.434(7) Å, b = 20.718(6) Å, c = 8.233(6) Å, α = 101.42(4)°, β = 115.61(5)°, γ = 90.53(5)°, and V = 1414(2) Å^3. Three standard reflections which were measured after every 150 reflections showed no apparent variation in intensity during the data collection. The linear absorption coefficient for Mo Kα is 19.19 cm^{-1}. The intensity data were corrected for Lorentz and polarization effects. An empirical absorption correction, based on azimuthal scans of several reflections, was applied which resulted in transmission

factors in the range from 0.57 to 1.00. In the hemisphere (h, ±k, ±l), 4986 reflections were collected, and 3832 of them were considered as observed ($I > 3\sigma(I)$).

The space group ($P\bar{1}$) was chosen based on the statistical analysis of intensity distribution. The structure was solved by direct methods (SHELXS-86)[11] and refined on $|F|$ by full-matrix least squares techniques (TEXSAN).[8] All nonhydrogen atoms were refined anisotropically to give R = 0.084 and Rw = 0.118. The final electron density different map was flat with a maximum of 0.97 $e^-/Å^3$ near Cu(2) and a minimum of -1.45 $e^-/Å^3$ close to Cu(1). The full occupancy of CH_2Cl_2 was proved by the refinement. All the hydrogen atoms were introduced at calculated positions with C-H = 0.95 Å

Details of the crystallographic data for 1, 2, and 3 are given in Table 4.1. Final positional parameters of 1, 2, and 3 are listed in Tables 4.2, 4.3, and 4.4, respectively. The selected bond distances and angles of 1, 2, and 3 are given in Tables 4.5, 4.6, and 4.7, respectively. The anisotropic thermal parameters for compound 1, 2, and 3 are listed in Table 4.8, 4.9, and 4.10. Information about the least squares planes of atoms and the observed and calculated structure factors for 1, 2, and 3 are available as supplementary materials.

Table 4.1. X-ray crystallographic data for $[CuCl(hep)]_2$(1), $[CuCl(hep)(Hhep)]_2 \cdot 2CH_2Cl_2$(2), and $[CuCl(hep)(py)]_2 \cdot CH_2Cl_2$(3)

	1	2	3
empirical formula	$Cu_2Cl_2O_2N_2C_{14}H_{16}$	$Cu_2Cl_6O_4N_4C_{30}H_{38}$	$Cu_2Cl_4O_2N_4C_{25}H_{28}$
formula weight	442.28	858.46	685.43
crystal system	triclinic	monoclinic	triclinic
space group	P-1	$P2_1/c$	P-1
a, Å	8.018(3)	10.857(3)	9.434(7)
b, Å	8.546(2)	20.207(3)	20.718(6)
c, Å	6.198(2)	16.694(4)	8.233(6)
α, deg	100.76(2)	90.0	101.42(4)
β, deg	109.99(2)	95.09(1)	115.61(5)
γ, deg	89.77(2)	90.0	90.53(5)
V, $Å^3$	391.2(4)	3648.0(1)	1414(2)
Z,	1	4	2
calcd density, g/cm^3	1.88	1.563	1.610
crystal size, mm	0.19x0.10x0.10	0.15x0.24x0.36	0.84x0.84x0.10
μ(Mo Kα), cm^{-1}	31.64	16.516	19.19
diffractometer	Rigaku AFC6R	Enraf-Nonius CAD4	Rigaku AFC6R

Table 4.1. (continued)

λ^a, Å	0.71069	0.71069	0.71069
T, ^oC	23	-75	-80
2θ, deg	0-50	4-45	0-50
No. reflections collected	1483	4941	4986
No. observations (I>3.0σI)	1081	2161	3832
No. variables	100	410	334
goodness of fit indicator[b]	1.24	1.293	4.50
max. shift in final cycle	0.02	0.03	0.08
max. in final diff. map e/Å^3	0.68	0.823	0.97
scan mode	ω-2θ	θ-2θ	ω-2θ
transmission coeff. (ϕ-scan)	0.8719-1.000	0.1436-0.9966	0.570-1.00
correction factors(numerical)	----	0.807-1.832	----
R[c]; Rw[d]	0.034; 0.044	0.057; 0.063	0.084; 0.118

[a]Graphite-monochromated

[b]Quality-of-fit = $[\Sigma\omega(|Fo|-|Fc|)^2/(N_{obs} - N_{parameters})]^{1/2}$

[c]$R=\Sigma||Fo|-|Fc||/\Sigma|Fo|$

[d]$Rw=[\Sigma\omega(|Fo|-|Fc|)^2/\Sigma\omega|Fo|^2]^{1/2}$; $\omega=1/\sigma^2(|Fo|)$

Table 4.2. Positional parameters and B_{eq} for $[CuCl(hep)]_2$(1)

atom	x	y	z	B_{eq}[a], Å^2
Cu	0.59934(8)	0.49942(6)	0.3264(1)	2.44(2)
Cl	0.6394(2)	0.6828(1)	0.1265(2)	3.09(4)
O	0.5633(5)	0.3803(4)	0.5457(6)	2.9(1)
N	0.7911(5)	0.3584(4)	0.2738(7)	2.5(1)
C1	0.9288(7)	0.4208(6)	0.2329(9)	3.0(2)
C2	1.0677(7)	0.3355(7)	0.208(1)	3.7(2)
C3	1.0663(8)	0.1756(7)	0.222(1)	4.0(2)
C4	0.9252(8)	0.1098(6)	0.261(1)	3.7(2)
C5	0.7887(7)	0.2027(5)	0.2890(8)	2.8(2)
C6	0.6406(7)	0.1369(6)	0.345(1)	3.4(2)
C7	0.6278(8)	0.2293(6)	0.573(1)	3.4(2)

[a] $B_{eq} = 8\pi^2/3\ \Sigma U_{ij} a_i^* a_j^* a_i \cdot a_j$, where the temperature factors are defined as $\exp(-2\pi^2\ \Sigma h_i h_j a_i^* a_j^* U_{ij})$

Table 4.3. Positional parameters and B_{eq} for $[CuCl(hep)(Hhep)]_2 \cdot 2CH_2Cl_2$(2)[a]

atom	x	y	z	B_{eq}[b], Å^2
Cu(1)	0.18243(8)	0.20495(5)	0.42321(7)	1.35(2)
Cu(2)	0.39923(8)	0.29866(5)	0.46424(7)	1.31(2)
Cl(1)	0.5252(2)	0.2322(1)	0.5770(2)	1.95(5)
Cl(2)	0.0521(2)	0.2749(1)	0.3146(2)	2.11(5)
Cl(3)	0.3178(3)	0.0386(2)	0.6895(2)	5.21(9)
Cl(4)	0.0855(3)	0.4892(2)	0.0971(3)	6.1(1)
Cl(5)	-0.1449(3)	0.3647(2)	0.6254(3)	6.31(9)
Cl(6)	-0.2860(3)	0.3553(2)	0.7647(3)	5.63(9)
O(1)	0.3400(4)	0.2295(3)	0.3867(4)	1.3(1)
O(2)	0.2397(4)	0.2738(3)	0.4988(4)	1.2(1)
O(3)	0.5470(5)	0.0869(3)	0.5244(6)	3.8(2)
O(4)	0.0354(5)	0.4225(4)	0.3617(6)	3.8(2)

[a]Starred atoms were refined isotropically

[b]$B_{eq} = 8\pi^2/3 \Sigma U_{ij} a_i^* a_j^* a_i \cdot a_j$, where the temperature factors are defined as $\exp(-2\pi^2 \Sigma h_i h_j a_i^* a_j^* U_{ij})$

Table 4.3. (continued)

atom	x	y	z	B_{eq}[b], Å^2
N(1)	0.5445(5)	0.3149(3)	0.4013(5)	1.5(2)
N(2)	0.0400(6)	0.1826(3)	0.4857(5)	1.6(2)
N(3)	0.4028(6)	0.3863(4)	0.5244(5)	1.8(2)
N(4)	0.1831(5)	0.1179(3)	0.3614(5)	1.4(2)
C(1)	0.6567(7)	0.3238(5)	0.4410(6)	2.0(2)
C(2)	0.7620(8)	0.3340(5)	0.4012(7)	2.5(2)
C(3)	0.7494(7)	0.3359(5)	0.3191(6)	2.2(2)
C(4)	0.6350(7)	0.3250(4)	0.2775(6)	1.8(2)
C(5)	0.5317(7)	0.3147(4)	0.3209(6)	1.4(2)
C(6)	0.4087(7)	0.2956(4)	0.2787(6)	1.7(2)
C(7)	0.3682(7)	0.2297(5)	0.3036(6)	2.1(2)
C(8)	-0.0697(7)	0.1651(5)	0.4448(7)	2.6(2)
C(9)	-0.1721(8)	0.1521(5)	0.4859(8)	3.2(3)
C(10)	-0.1648(7)	0.1573(5)	0.5674(7)	2.5(2)
C(11)	-0.0526(7)	0.1752(5)	0.6088(6)	2.0(2)*
C(12)	0.0475(7)	0.1883(4)	0.5667(6)	1.7(2)
C(13)	0.1701(7)	0.2099(4)	0.6088(6)	1.8(2)

Table 4.3. (continued)

atom	x	y	z	B_{eq}[b], Å^2
C(14)	0.2084(8)	0.2778(5)	0.5793(6)	2.2(2)
C(15)	0.4739(7)	0.3945(4)	0.5939(6)	1.7(2)
C(16)	0.4776(8)	0.4507(5)	0.6359(7)	2.3(2)
C(17)	0.4067(8)	0.5047(5)	0.6077(7)	3.2(3)
C(18)	0.3350(8)	0.4965(5)	0.5366(6)	2.4(2)
C(19)	0.3339(7)	0.4379(5)	0.4978(6)	2.0(2)
C(20)	0.2504(8)	0.4288(5)	0.4196(8)	3.0(3)
C(21)	0.1121(8)	0.4301(6)	0.4361(9)	4.0(3)
C(22)	0.1163(8)	0.1104(5)	0.2882(7)	2.2(2)
C(23)	0.1209(9)	0.0549(5)	0.2443(8)	3.4(3)
C(24)	0.1958(9)	0.0032(5)	0.2716(9)	4.1(3)
C(25)	0.2622(8)	0.0097(5)	0.3432(8)	3.1(3)
C(26)	0.2574(7)	0.0679(5)	0.3887(7)	2.0(2)
C(27)	0.3354(8)	0.0751(5)	0.4641(7)	2.9(2)
C(28)	0.4739(8)	0.0812(5)	0.4513(8)	3.2(3)
C(29)	0.156(1)	0.4704(7)	0.1921(8)	5.2(3)
C(30)	-0.209(1)	0.1892(5)	0.1952(9)	3.9(3)

Table 4.4. Positional parameters and B_{eq} for $[CuCl(hep)(py)]_2 \cdot CH_2Cl_2$(3)

atom	x	y	z	B_{eq}[a], Å^2
Cu(1)	0.3621(2)	0.45089(7)	0.4618(2)	2.57(5)
Cu(2)	0.1386(2)	0.04923(7)	0.1492(2)	2.51(5)
Cl(1)	0.1711(3)	0.3854(2)	0.1933(4)	3.1(1)
Cl(2)	0.3291(3)	0.1147(1)	0.1368(4)	3.0(1)
Cl(3)	0.4119(4)	0.2820(2)	0.8661(5)	4.6(1)
Cl(4)	0.0895(4)	0.2187(2)	0.6735(5)	4.6(1)
O(1)	0.5113(9)	0.5228(4)	0.651(1)	2.8(3)
O(2)	-0.0126(9)	-0.0224(4)	0.1117(1)	2.8(3)
N(1)	0.231(1)	0.4517(5)	0.601(1)	2.5(3)
N(2)	0.507(1)	0.3664(5)	0.565(1)	3.0(4)
N(3)	0.265(1)	0.0474(4)	0.415(1)	2.3(3)
N(4)	-0.012(1)	0.1332(4)	0.190(1)	2.7(3)
C(1)	0.159(1)	0.3948(6)	0.593(2)	3.2(4)
C(2)	0.060(1)	0.3932(7)	0.675(2)	4.0(5)
C(3)	0.040(1)	0.4517(7)	0.770(2)	3.4(5)
C(4)	0.113(1)	0.5075(7)	0.778(2)	3.6(5)
C(5)	0.216(1)	0.5094(6)	0.700(2)	2.9(4)
C(6)	0.313(2)	0.5724(6)	0.721(2)	3.6(5)

[a] $B_{eq} = 8\pi^2/3 \Sigma U_{ij} a_i^* a_j^* a_i \cdot a_j$, where the temperature factors are defined as $\exp(-2\pi^2 \Sigma h_i h_j a_i^* a_j^* U_{ij})$

Table 4.4. (continued)

atom	x	y	z	B_{eq}[a], Å^2
C(7)	0.484(1)	0.5636(6)	0.787(2)	2.9(4)
C(8)	0.480(1)	0.3020(6)	0.471(2)	3.2(4)
C(9)	0.576(1)	0.2562(6)	0.530(2)	3.3(4)
C(10)	0.713(1)	0.2717(7)	0.696(2)	3.9(5)
C(11)	0.749(1)	0.3365(7)	0.795(2)	3.8(5)
C(12)	0.639(1)	0.3809(6)	0.723(2)	3.4(5)
C(13)	0.343(1)	0.1032(6)	0.540(2)	2.8(4)
C(14)	0.443(1)	0.1052(6)	0.724(2)	3.5(5)
C(15)	0.466(2)	0.0465(8)	0.778(2)	4.4(5)
C(16)	0.384(1)	-0.0101(6)	0.654(2)	3.0(4)
C(17)	0.288(1)	-0.0102(6)	0.475(2)	2.8(4)
C(18)	0.195(1)	-0.0710(6)	0.338(2)	3.5(5)
C(19)	0.016(2)	-0.0659(7)	0.237(2)	4.3(5)
C(20)	0.015(1)	0.1971(6)	0.187(2)	3.2(4)
C(21)	-0.075(1)	0.2456(6)	0.200(2)	3.4(5)
C(22)	-0.212(1)	0.2262(7)	0.210(2)	3.6(5)
C(23)	-0.247(1)	0.1641(6)	0.210(2)	3.3(4)
C(24)	-0.141(1)	0.1197(6)	0.203(2)	3.3(4)
C(25)	0.252(2)	0.2476(7)	0.890(2)	4.4(5)

Table 4.5. Selected bond distances (Å) and angles (deg.) for $[CuCl(hep)]_2$(1)

		bond distances	
Cu-O	1.935(3)	O···O'	2.359(6)[a]
Cu-O'	1.945(3)	Cu···Cu'	3.081(2)[b]
Cu-N	2.028(4)	Cu-Cl	2.947(2)[c]
Cu-Cl	2.255(1)	Cu···Cu'	3.805(2)[c]
		bond angles	
O-Cu-O'	74.9(1)	Cl-Cu-O	168.1(1)
O-Cu-N	92.5(1)	N-Cu-O'	165.4(1)
N-Cu-Cl	96.0(1)	Cu-O-Cu'	105.2(1)
Cl-Cu-O'	95.6(1)	Cu···Cl···Cu'	93.11(6)[c]

[a]Nonbonded distance

[b]Intradimer distance

[c]Interdimer distances or angle

Table 4.6. Selected bond distances (Å) and angles (deg.) for $[CuCl(hep)(Hhep)]_2 \cdot 2CH_2Cl_2$(2)

		bond distances	
Cu(1)-Cl(2)	2.614(3)	Cu(2)-Cl(1)	2.579(3)
Cu(1)-O(1)	1.932(5)	Cu(2)-O(2)	1.929(5)
Cu(1)-O(2)	1.943(6)	Cu(2)-O(1)	1.945(6)
Cu(1)-N(4)	2.040(7)	Cu(2)-N(3)	2.070(8)
Cu(1)-N(2)	1.993(7)	Cu(2)-N(1)	2.006(7)
O(1)•••O(2)	2.419[a]	Cu(1)•••Cu(2)	3.026[b]
Cu(1)•••Cu(2)	8.213[c]		
		bond angles	
Cl(2)-Cu(1)-O(1)	94.7(2)	Cl(1)-Cu(2)-O(1)	104.9(2)
Cl(2)-Cu(1)-O(2)	100.7(2)	Cl(1)-Cu(2)-O(2)	95.3(2)
Cl(2)-Cu(1)-N(2)	95.1(2)	Cl(1)-Cu(2)-N(1)	94.8(2)
Cl(2)-Cu(1)-N(4)	98.1(2)	Cl(1)-Cu(2)-N(3)	95.8(2)
O(1)-Cu(1)-O(2)	77.3(2)	O(1)-Cu(2)-O(2)	77.3(2)
O(1)-Cu(1)-N(4)	91.1(3)	O(1)-Cu(2)-N(1)	90.5(3)
N(2)-Cu(1)-N(4)	96.2(3)	N(3)-Cu(2)-N(1)	96.4(3)
O(2)-Cu(1)-N(2)	92.3(3)	O(2)-Cu(2)-N(3)	92.5(3)
Cu(1)-O(1)-Cu(2)	102.6(3)	Cu(1)-O(2)-Cu(2)	102.8(3)

[a]Nonbonded distance

[b]Intradimer distance

[c]Interdimer distance

Table 4.7. Selected bond distances (Å) and angles (deg.) for $[CuCl(hep)(py)]_2 \cdot CH_2Cl_2$(3)

		bond distances	
Cu(1)-Cl(1)	2.301(4)	Cu(2)-Cl(2)	2.292(3)
Cu(1)-O(1)	1.942(7)	Cu(2)-O(2)	1.946(7)
Cu(1)-O(1)'	1.929(7)	Cu(2)-O(2)'	1.941(7)
Cu(1)-N(1)	2.012(9)	Cu(2)-N(3)	2.000(8)
Cu(1)-N(2)	2.30(1)	Cu(2)-N(4)	2.32(1)
O(1)•••O(1)'	2.39(1)[a]	O(1)•••O(1)'	2.39(1)[a]
Cu(1)•••Cu(1)'	3.048(3)[b]	Cu(2)•••Cu(2)'	3.066(4)[b]
Cu(1)•••Cu(2)	8.17[c]		
		bond angles	
Cl(1)-Cu(1)-O(1)'	95.3(2)	Cl(2)-Cu(2)-O(2)'	95.4(2)
Cl(1)-Cu(1)-N(1)	93.9(3)	Cl(2)-Cu(2)-O(3)	94.8(3)
Cl(1)-Cu(1)-N(2)	96.0(3)	Cl(2)-Cu(2)-N(4)	96.6(2)
O(1)-Cu(1)-N(1)	91.9(3)	O(2)-Cu(2)-N(3)	91.2(3)
O(1)-Cu(1)-O(1)'	76.1(3)	O(2)-Cu(2)-O(2)'	75.9(3)
O(1)-Cu(1)-N(2)	96.5(4)	O(2)-Cu(2)-N(4)	95.2(3)
N(1)-Cu(1)-N(2)	97.3(3)	N(3)-Cu(2)-N(4)	97.8(3)
O(1)'-Cu(1)-N(2)	95.2(3)	O(2)'-Cu(2)-N(4)	94.9(3)
Cu(1)-O(1)-Cu(1)'	103.9(3)	Cu(2)-O(2)-Cu(2)'	104.1(3)

[a]Nonbonded distances

[b]Intradimer distances

[c]Interdimer distance

Table 4.8. Anisotropic temperature parameters for $[CuCl(hep)]_2$(1)[a]

Atom	U11	U22	U33	U12	U13	U23
Cu	0.0414(4)	0.0259(3)	0.0371(4)	0.0041(2)	0.0275(3)	0.0079(2)
Cl	0.0548(8)	0.0316(6)	0.0450(7)	0.0022(5)	0.0330(6)	0.0111(5)
O	0.056(2)	0.027(2)	0.048(2)	0.012(2)	0.039(2)	0.015(1)
N	0.037(2)	0.032(2)	0.034(2)	-0.001(2)	0.022(2)	0.003(2)
C(1)	0.039(3)	0.050(3)	0.031(3)	-0.002(2)	0.020(2)	0.004(2)
C(2)	0.040(3)	0.073(4)	0.033(3)	0.004(3)	0.022(2)	0.005(3)
C(3)	0.052(3)	0.068(4)	0.041(3)	0.022(3)	0.026(3)	0.013(3)
C(4)	0.057(3)	0.045(3)	0.044(3)	0.019(3)	0.027(3)	0.007(2)
C(5)	0.049(3)	0.033(3)	0.030(3)	0.003(2)	0.022(2)	0.003(2)
C(6)	0.057(3)	0.024(2)	0.062(4)	0.008(2)	0.036(3)	0.010(2)
C(7)	0.064(4)	0.033(3)	0.054(3)	0.012(2)	0.043(3)	0.017(2)

[a]The form of the anisotropic displacement parameter is:
$\exp[-2\pi^2 \{h^2 a^2 U(1,1) + k^2 b^2 U(2,2) + l^2 c^2 U(3,3) + 2hkab\, U(1,2) + 2hlac\, U(1,3) + 2klbc\, U(2,3)\}]$ where a, b, and c are reciprocal lattice constants

Table 4.9. Anisotropic temperature parameters for $[CuCl(hep)(Hhep)]_2 \cdot 2CH_2Cl_2$(2)[a]

Atom	U11	U22	U33	U12	U13	U23
Cu(1)	0.0144(4)	0.0207(5)	0.0166(6)	-0.0027(5)	0.0031(4)	-0.0035(6)
Cu(2)	0.0151(4)	0.0195(5)	0.0157(6)	-0.0039(5)	0.0039(4)	-0.0021(6)
Cl(1)	0.028(1)	0.027(1)	0.018(1)	0.002(1)	-0.001(1)	0.004(1)
Cl(2)	0.025(1)	0.034(1)	0.021(1)	0.004(1)	-0.000(1)	0.004(1)
Cl(3)	0.084(2)	0.056(2)	0.058(3)	0.001(2)	0.001(2)	0.006(2)
Cl(4)	0.082(2)	0.064(2)	0.084(3)	0.005(2)	0.005(2)	0.005(2)
Cl(5)	0.074(2)	0.087(2)	0.071(3)	-0.030(2)	-0.034(2)	0.023(2)
Cl(6)	0.076(2)	0.065(2)	0.066(3)	0.025(2)	-0.030(2)	-0.018(2)
O(1)	0.016(2)	0.028(3)	0.004(3)	-0.009(3)	-0.000(2)	-0.004(3)
O(2)	0.012(2)	0.027(3)	0.008(3)	-0.007(2)	0.004(2)	-0.013(3)
O(3)	0.029(3)	0.038(4)	0.072(7)	0.005(3)	-0.031(4)	-0.001(4)
O(4)	0.036(3)	0.048(4)	0.057(6)	-0.001(3)	-0.019(4)	0.011(5)
N(1)	0.013(3)	0.025(4)	0.021(5)	-0.001(3)	0.006(3)	-0.007(4)
N(2)	0.025(3)	0.024(4)	0.012(5)	-0.011(3)	0.003(3)	-0.000(4)

[a]The form of the anisotropic displacement parameter is:
$\exp[-2\pi^2 \{h^2 a^2 U(1,1) + k^2 b^2 U(2,2) + l^2 c^2 U(3,3) + 2 hkab\, U(1,2) + 2 hlac\, U(1,3) + 2 klbc\, U(2,3)\}]$ where a, b, and c are reciprocal lattice constants

Table 4.9. (continued)

Atom	U11	U22	U33	U12	U13	U23
N(3)	0.016(3)	0.020(4)	0.034(5)	0.004(3)	0.006(3)	-0.001(4)
N(4)	0.011(3)	0.020(4)	0.023(5)	-0.001(3)	0.001(3)	0.000(4)
C(1)	0.023(4)	0.039(5)	0.015(6)	-0.002(4)	-0.003(4)	-0.001(5)
C(2)	0.025(4)	0.029(5)	0.045(7)	-0.011(4)	0.012(4)	0.001(6)
C(3)	0.024(4)	0.026(5)	0.035(6)	-0.001(4)	0.016(4)	-0.006(5)
C(4)	0.035(4)	0.023(4)	0.012(5)	-0.010(4)	0.006(4)	0.003(5)
C(5)	0.019(4)	0.023(4)	0.012(5)	0.002(4)	0.001(4)	0.004(5)
C(6)	0.027(4)	0.023(5)	0.014(5)	0.000(4)	0.004(4)	-0.001(5)
C(7)	0.018(4)	0.039(5)	0.022(6)	0.006(4)	0.010(4)	-0.010(5)
C(8)	0.019(4)	0.051(6)	0.029(6)	-0.008(5)	0.003(4)	0.002(6)
C(9)	0.025(5)	0.041(6)	0.053(8)	-0.008(5)	-0.001(5)	-0.006(6)
C(10)	0.019(4)	0.037(5)	0.037(7)	-0.010(4)	0.008(4)	-0.010(6)
C(11)	0.0					
C(12)	0.015(4)	0.023(5)	0.027(6)	-0.002(4)	0.001(4)	0.002(5)
C(13)	0.028(4)	0.025(5)	0.013(5)	-0.001(4)	-0.000(4)	-0.004(5)
C(14)	0.028(4)	0.034(5)	0.024(6)	-0.005(4)	0.007(4)	-0.007(5)
C(15)	0.031(4)	0.014(4)	0.018(6)	-0.002(4)	-0.005(4)	-0.004(4)

Table 4.9. (continued)

Atom	U11	U22	U33	U12	U13	U23
C(16)	0.036(5)	0.029(5)	0.021(6)	-0.005(5)	-0.012(5)	0.001(5)
C(17)	0.047(6)	0.024(5)	0.049(8)	-0.001(5)	0.005(6)	-0.003(6)
C(18)	0.042(5)	0.035(5)	0.011(6)	0.009(5)	-0.002(5)	-0.006(5)
C(19)	0.023(4)	0.037(5)	0.017(6)	-0.010(4)	0.012(4)	-0.004(5)
C(20)	0.032(5)	0.029(5)	0.053(8)	0.008(5)	0.007(5)	-0.003(6)
C(21)	0.025(5)	0.049(6)	0.08(1)	-0.009(5)	0.007(6)	0.000(7)
C(22)	0.027(4)	0.034(5)	0.021(6)	0.002(4)	-0.000(4)	-0.003(5)
C(23)	0.051(6)	0.041(6)	0.035(8)	0.004(5)	-0.011(6)	-0.018(6)
C(24)	0.050(6)	0.036(6)	0.069(9)	0.008(5)	0.004(6)	-0.021(6)
C(25)	0.031(5)	0.028(5)	0.059(9)	0.005(5)	-0.002(5)	-0.021(6)
C(26)	0.019(4)	0.029(5)	0.029(6)	-0.006(4)	0.010(4)	-0.003(5)
C(27)	0.026(4)	0.029(5)	0.055(8)	-0.001(4)	0.005(5)	0.022(6)
C(28)	0.020(4)	0.028(5)	0.074(9)	0.005(4)	0.008(5)	-0.012(6)
C(29)	0.077(7)	0.10(1)	0.019(8)	0.005(8)	-0.003(6)	0.001(9)
C(30)	0.060(6)	0.037(6)	0.051(8)	-0.001(6)	-0.004(6)	-0.007(7)

Table 4.10. Anisotropic temperature parameters for $[CuCl(hep)(py)]_2 \cdot CH_2Cl_2$(3)[a]

Atom	U11	U22	U33	U12	U13	U23
Cu(1)	0.0340(8)	0.0397(9)	0.0301(8)	-0.0007(6)	0.0221(6)	0.0022(6)
Cu(2)	0.0336(8)	0.0370(9)	0.0269(7)	-0.0020(6)	0.0160(6)	0.056(6)
Cl(1)	0.034(2)	0.053(2)	0.033(2)	0.003(1)	0.020(1)	0.003(1)
Cl(2)	0.032(1)	0.049(2)	0.038(2)	-0.000(1)	0.018(1)	0.013(1)
Cl(3)	0.057(2)	0.059(2)	0.065(2)	0.002(2)	0.036(2)	0.006(2)
Cl(4)	0.060(2)	0.057(2)	0.056(2)	0.004(2)	0.024(2)	0.014(2)
O(1)	0.039(4)	0.040(5)	0.034(4)	-0.009(4)	0.027(4)	-0.006(3)
O(2)	0.038(4)	0.043(5)	0.026(4)	0.001(4)	0.014(3)	0.011(3)
N(1)	0.033(5)	0.042(6)	0.029(5)	0.008(4)	0.020(4)	0.007(4)
N(2)	0.035(5)	0.052(7)	0.031(5)	0.002(5)	0.019(4)	0.008(5)
N(3)	0.028(5)	0.034(5)	0.024(5)	0.001(4)	0.010(4)	0.006(4)
N(4)	0.028(5)	0.036(6)	0.034(5)	-0.008(4)	0.014(4)	0.001(4)

[a]The form of the anisotropic displacement parameter is:

$\exp[-2\pi^2 \{h^2 a^2 U(1,1) + k^2 b^2 U(2,2) + l^2 c^2 U(3,3) + 2 hkab U(1,2) + 2 hlac U(1,3) + 2 klbc U(2,3)\}]$ where a, b, and c are reciprocal lattice constants

Table 4.10. (continued)

Atom	U11	U22	U33	U12	U13	U23
C(1)	0.040(7)	0.055(8)	0.032(6)	0.002(6)	0.021(5)	0.008(6)
C(2)	0.041(7)	0.07(1)	0.053(8)	0.005(7)	0.028(6)	0.029(7)
C(3)	0.036(7)	0.053(8)	0.050(8)	-0.003(6)	0.032(6)	-0.001(6)
C(4)	0.043(7)	0.007(1)	0.037(7)	0.017(7)	0.028(6)	0.007(6)
C(5)	0.041(7)	0.048(8)	0.030(6)	0.016(6)	0.020(5)	0.013(5)
C(6)	0.060(8)	0.037(7)	0.049(8)	0.003(6)	0.039(7)	-0.004(6)
C(7)	0.039(7)	0.034(7)	0.033(6)	-0.017(5)	0.021(5)	-0.013(5)
C(8)	0.036(7)	0.051(8)	0.040(7)	-0.001(6)	0.026(6)	-0.001(6)
C(9)	0.038(7)	0.043(8)	0.048(7)	0.006(6)	0.026(6)	0.004(6)
C(10)	0.039(7)	0.06(1)	0.058(8)	0.009(6)	0.033(7)	0.009(7)
C(11)	0.032(7)	0.08(1)	0.035(7)	-0.007(6)	0.013(5)	0.009(6)
C(12)	0.041(7)	0.050(8)	0.046(7)	0.008(6)	0.028(6)	0.008(6)
C(13)	0.032(6)	0.039(7)	0.037(7)	0.003(5)	0.016(5)	0.007(5)
C(14)	0.039(7)	0.043(8)	0.044(7)	0.006(6)	0.019(6)	-0.006(6)

Table 4.10. (continued)

Atom	U11	U22	U33	U12	U13	U23
C(15)	0.058(9)	0.08(1)	0.029(7)	0.004(8)	0.015(6)	0.026(7)
C(16)	0.030(6)	0.045(8)	0.042(7)	-0.000(5)	0.018(5)	0.013(6)
C(17)	0.030(6)	0.053(8)	0.035(6)	0.004(5)	0.023(5)	0.014(6)
C(18)	0.045(7)	0.048(8)	0.044(7)	0.014(6)	0.017(6)	0.022(6)
C(19)	0.07(1)	0.07(1)	0.030(7)	-0.019(8)	0.032(7)	0.005(6)
C(20)	0.031(6)	0.056(9)	0.030(6)	-0.007(6)	0.011(5)	0.007(6)
C(21)	0.050(8)	0.039(7)	0.046(7)	0.015(6)	0.025(6)	0.016(6)
C(22)	0.034(7)	0.051(8)	0.053(8)	0.013(6)	0.019(6)	0.013(6)
C(23)	0.026(6)	0.053(8)	0.043(7)	-0.005(6)	0.016(5)	0.004(6)
C(24)	0.034(7)	0.041(7)	0.048(7)	-0.003(6)	0.017(6)	0.008(6)
C(25)	0.059(9)	0.06(1)	0.050(8)	-0.014(7)	0.028(7)	0.006(7)

RESULTS AND DISCUSSION

Description of the Structures

Compound 1

The structure of 1 consists of two monomeric units CuCl(hep) held together by two ethyloxo bridges between the copper atoms. The structure of the molecule and its orientation in the unit cell of 1 is given in Fig. 4.1. The dimeric unit is centrosymmetric and the Cu_2O_2 moiety is exactly planar owing to crystallographic inversion symmetry. The Cu(II) atoms are each 4-coordinate with the ligation CuO_2NCl in roughly square-planar geometry, as shown by the sum of the bond angles about Cu equal to 359.0° and the dihedral angle, τ, of 5.56° between Cu_2O_2 and $Cu_2N_2Cl_2$ planes. This roughly planar geometry of copper coordination is unusual for the analogous compounds, $[CuX(OR)]_2$ (5),[13-15] where X = Cl or Br; OR = anion of aminoalcohol or Schiff base ligand. The common structural feature of compounds 5 is that the copper coordination geometry is considerably distorted from planar toward tetrahedral, where the τ angles range from 20 to 40°.

As illustrated in Fig. 4.2, the structure of 1 may be described more accurately as consisting of oxygen-bridged dimers held together in an infinite chain by weak chloride bridges. The dimers are linked in a stairstep fashion along [111] through bridging of the equatorial Cl atoms of the dimers to axial positions above or below Cu atoms of adjacent dimers. The coordination around copper is therefore described roughly as square-based pyramidal, with the apical Cu-Cl distance, 2.947(2) Å, much longer than the basal

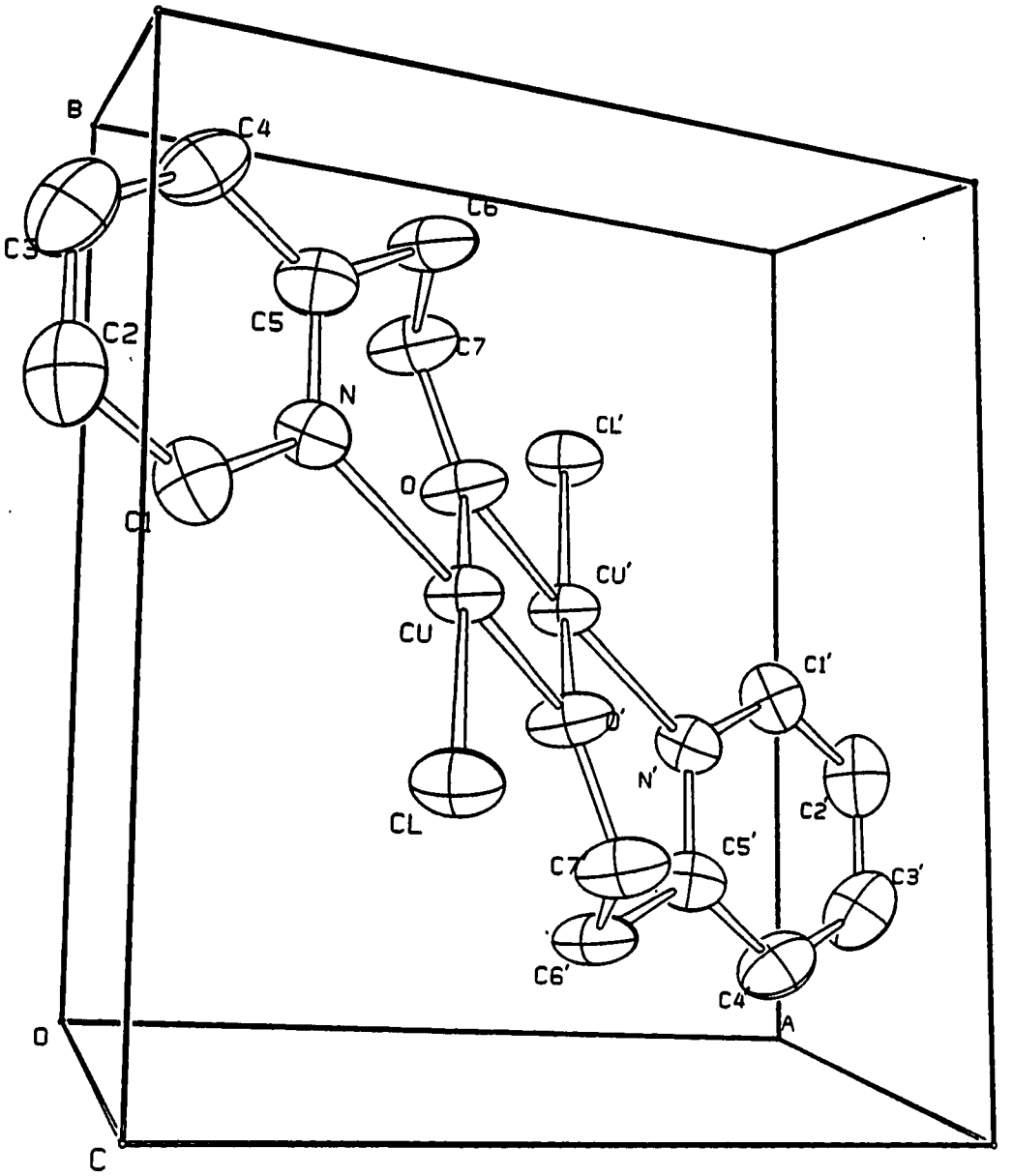

Fig. 4.1. ORTEP drawing (50 % thermal ellipsoids) of the $[CuCl(hep)]_2$ (1) molecule and its orientation in the unit cell. Interdimer Cu-Cl-Cu bridges are not shown.

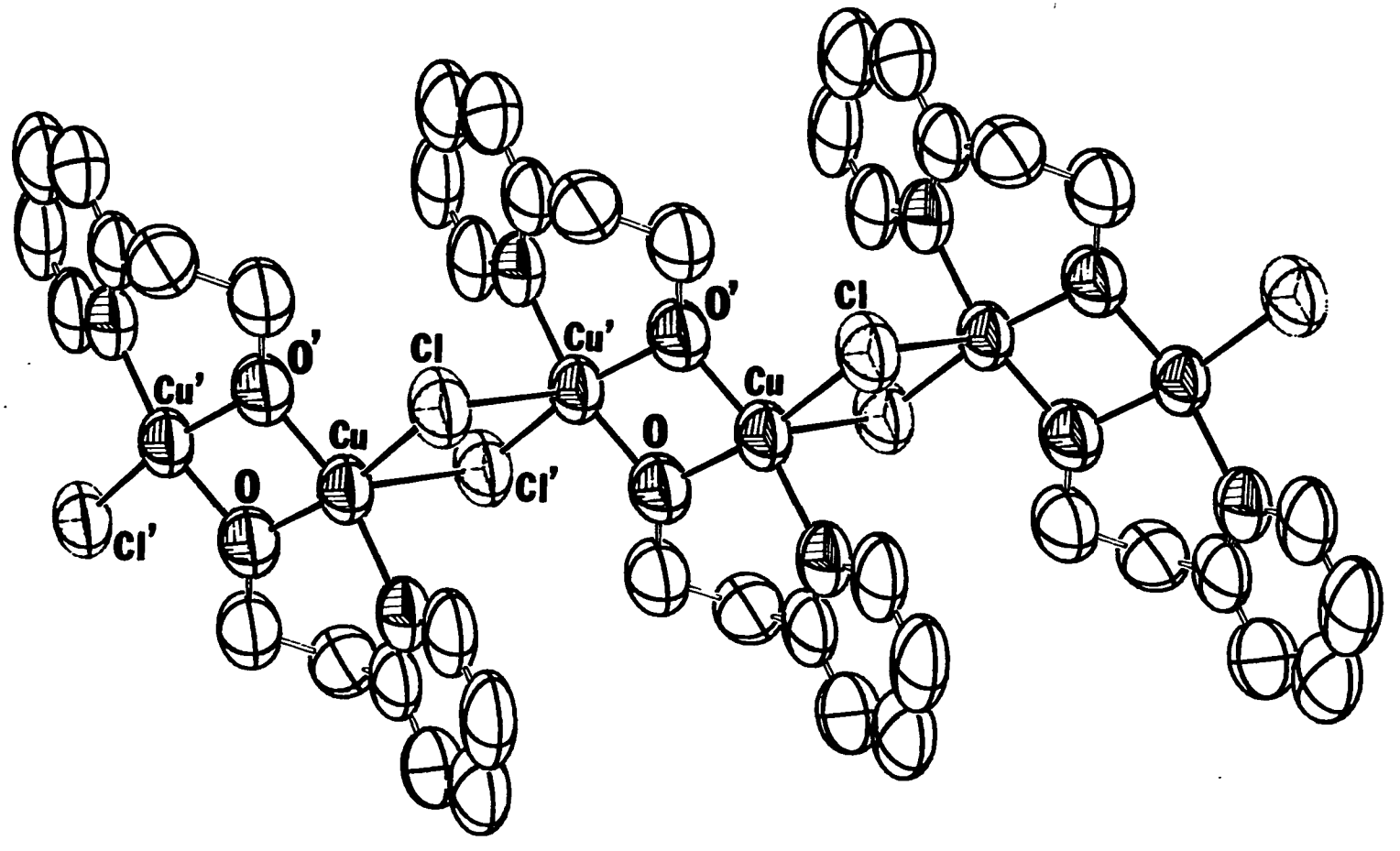

Fig. 4.2. ORTEP drawing (50 % thermal ellipsoids) showing the interdimer Cu-Cl-Cu linkages of $[CuCl(hep)]_2$(1) to form a chain polymer along the [111] direction. The coordination geometry about the Cu atoms is square pyramidal with the Cu-Cl' or Cu'-Cl bonds in the axial positions.

distance, 2.255(1) Å. The bridging CuClCu angle is 93.11(6)^{o} and the interdimer Cu to Cu distance is 3.805(2) Å. The polymeric nature of 1 caused by this CuClCu interlinking could explain the unusual stability of 1 in the air. This polymer of dimers is like that previously observed in the complex of $[CuCl_2(pyO)]_2$ (6),[16-18] where pyO = pyridine N-oxide. The chloride ions in 6 that form the Cu-Cl-Cu interdimer linkages give a shorter Cu-Cl (apical) distance, 2.836(5) Å, than those in 1, 2.947(2) Å and the Cu-O distances (ave. 2.01(1) Å) in 6 are longer than those (ave. 1.940 Å) in 1. The basal Cu-Cl separation of 2.255(1) Å in 1 is longer than those reported for 5 (2.202-2.209 Å)[11] and for 6 (2.206 Å; 2.217 Å).[16,18]

Compound 2

In contrast to 1, compound 2 consists of pseudo-centrosymmetric dimeric units that are well separated from one another. Two monomeric units CuCl(hep)(Hhep) are held together in the same way as in 1. The structure of the dimeric unit is given in Fig. 4.3 and a view of the unit cell is shown in Fig. 4.4. As reflected by the presence of the pseudo-inversion center, the Cu_2O_2 moiety is still planar with the maximum deviation of ±0.013 Å by any atom from the least-square plane. The dihedral angle, τ, between the planes Cu(1)O(1)Cu(2)O(2) and Cu(1)N(2)N(4)Cu(2)N(1)N(3) is 11.45^{o}. In regard to the uncoordinated hydroxyl groups, O(3) is 4.172(8) Å below the Cu_2O_2 plane and O(4) is 4.265(8) Å above it. The coordination geometry about copper may be described as distorted square pyramidal with the Cu atom located an average 0.2531 Å, and the Cl atom an average 2.8467 Å out of the basal plane. The Cl(1) and Cl(2) atoms are slightly tilted away from O(2) and O(1), respectively. These tiltings most likely arise from

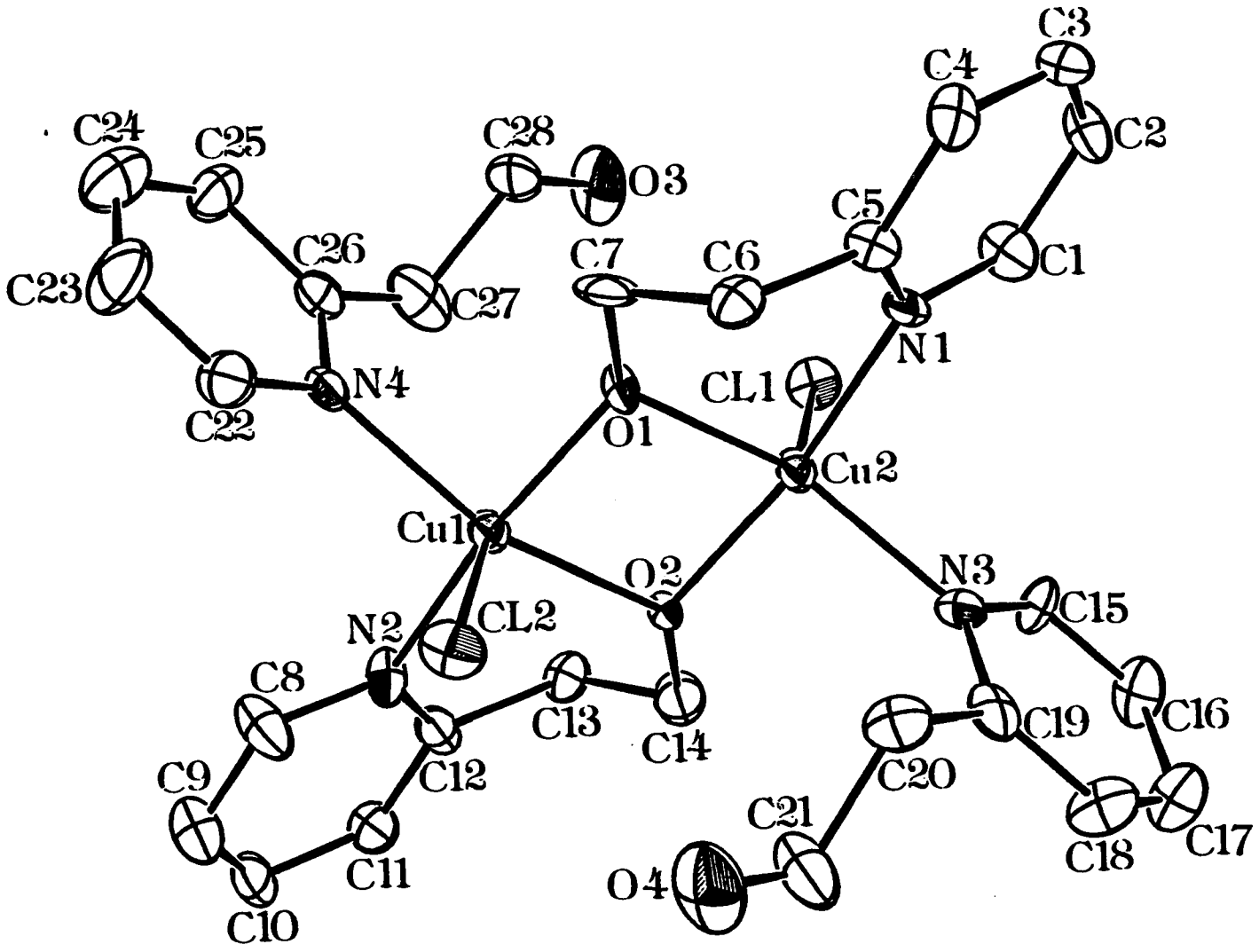

Fig. 4.3. ORTEP drawing(50 % thermal ellipsoids) of the molecular structure of $[CuCl(hep)(Hhep)]_2$.

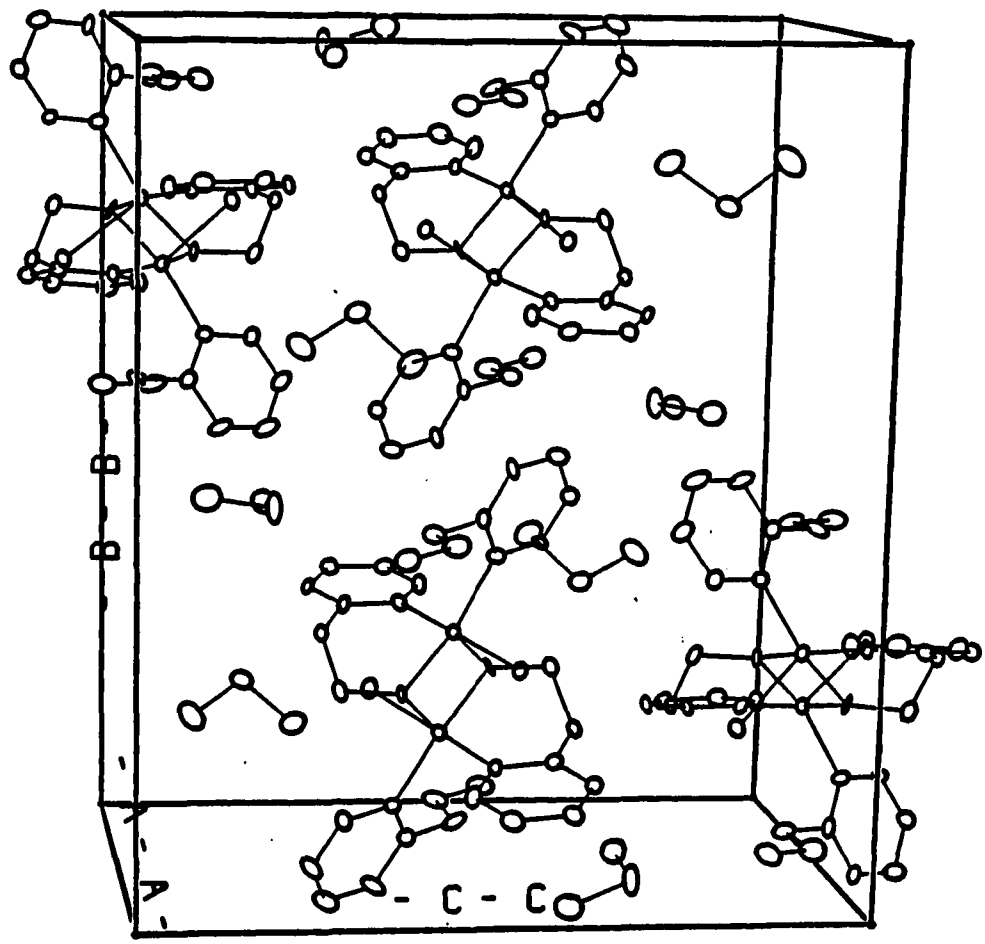

Fig. 4.4. ORTEP drawing (50 % thermal ellipsoids) of the unit cell of $[CuCl(hep)(Hhep)]_2 \cdot 2CH_2Cl_2$.

H-bondings between chloride ions and the uncoordinated OH groups on Hhep ligands. One such H atom was found in the electron density map with distances of 1.03 Å to O(3) and 2.06 Å to Cl(1). The O(3)HCl(1) angle is 168° which leads to an O(3)•••Cl separation of 3.080 Å. Although a hydrogen atom between O(4) and Cl(2) could not be located directly, H-bonding is evidenced by the fact that the O(4)•••Cl(2) separation of 3.095 Å is less than their van der Waals distance.

Compound 3

The molecular structure and a view of the unit cell of 3 are provided in Figs. 4.5 and 4.6, respectively. Two centrosymmetric $[CuCl(Hep)(py)]_2$ dimers are centered at two different positions, namely (0, 0, 0) and (1/2, 1/2, 1/2). Two monomeric units of CuCl(hep)(py) in each dimer are held together in the same way as in 1, and 2. The structural features of each Cu(II) dimeric unit in 3 are exactly the same as those of 1, except that the apical positions of the square pyramids around Cu atoms in 3 are occupied by pyridine molecules which, in turn, eliminate the possibility of polymerization of dimers. Compared to 1, the copper coordination geometries in 3 are distorted more from planar toward tetrahedral. The dihedral angle, τ, in the dimer centered at (0, 0, 0) is 10.24° and is 11.05° in the dimer centered at (1/2, 1/2, 1/2). The copper(II) atoms are 0.233 Å (ave.) out of the basal planes, each constituted by two O, one N, and one Cl atoms.

The apical Cu-Cl bonds, 2.597 Å (ave.), in 2 are significantly longer than the basal Cu-Cl bonds in 1, 3, 5, and 6. This weak apical bond is expected because of the four short Cu-O and Cu-N bonds in the basal plane. Similar to 2, the apical Cu-N bonds,

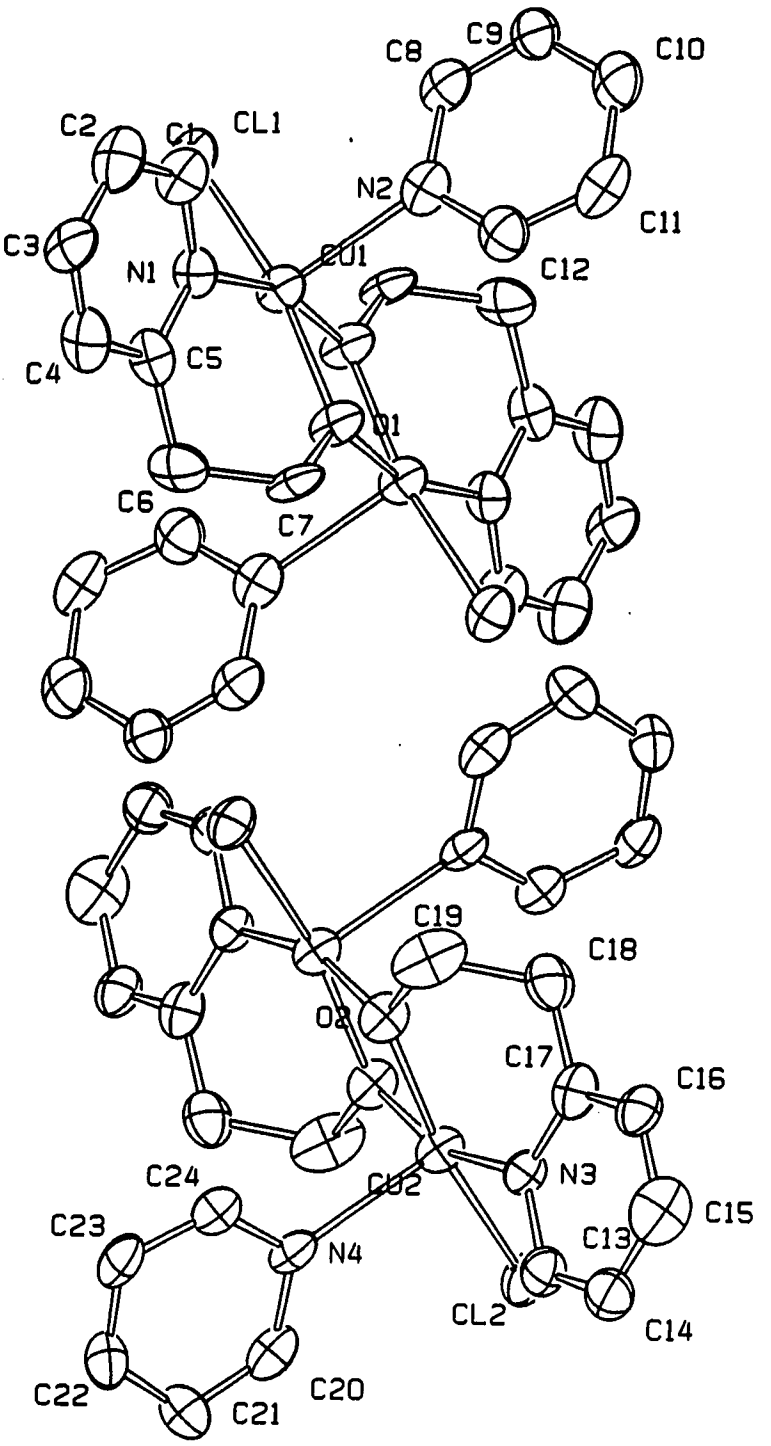

Fig. 4.5. ORTEP drawing (50 % thermal ellipsoids) of two $[CuCl(hep)(py)]_2$ dimers in 3. Dimer a is centered at (1/2, 1/2, 1/2) and dimer b at (0, 0, 0).

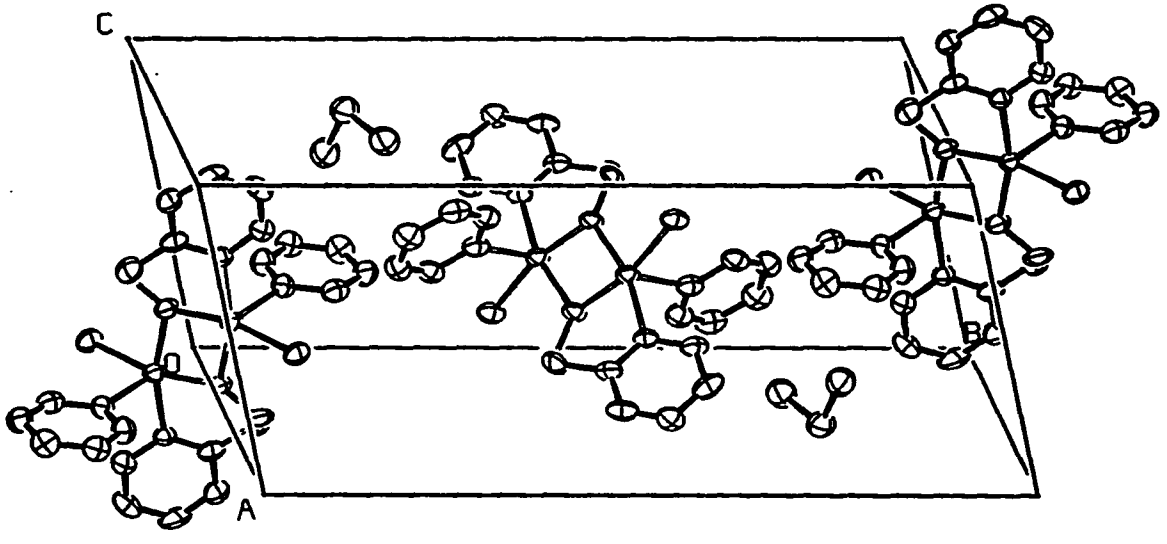

Fig. 4.6. ORTEP drawing (50 % thermal ellipsoids) of the unit cell of $[CuCl(hep)(py)]_2 \cdot CH_2Cl_2$.

2.31 Å (ave.), in 3 are significantly longer than the basal Cu-N bonds in 1, 2, and 3. This weakening of the apical bond around Cu(II) center has also been observed in analogous Cu(II) dimers with apical methoxide or ethoxide ligands.[19a,d] The Cu-O bond distances in 1, 2, and 3 each average to 1.940 Å and agree well with the corresponding values (1.90-1.96 Å) in compounds containing the Cu_2O_2 moiety.[13-21] The basal Cu-N distances of 2.028(4)Å in 1, 2.027 Å (ave.) in 2, and 2.060 Å (ave.) in 3 agree with values reported in the literature for similar Cu-N bond lengths.[13,22-24] In 2, possibly because of the chelating effect of the hep ligand, the Cu-N bond lengths (2.040(7), and 2.070(8) Å) for the unchelated Hhep are slightly longer than those for the chelated hep (1.993(7) and 2.006(7) Å). The bridging angle Cu-O-Cu, 105.2(1)°, and consequently the Cu•••Cu separation, 3.081(2) Å, in 1 differ little from the corresponding parameters in 2, 102.7° (ave.) and 3.026 Å, and in 3, 104.0° (ave.) and 3.057 Å (ave.), respectively. The O•••O distance of the Cu_2O_2 moiety is 2.359(6)Å in 1, 2.419 Å in 2, and 2.39 Å (ave.) in 3.

Infrared and UV/visible Spectra

Infrared spectra were obtained for samples of 1 using nujol mulls. The band assignments were aided by a comparison of spectra between the copper(II) complexes and the ligands. The vibration frequencies of 573(m) cm^{-1} and 510(w) cm^{-1} of 1 most likely arise from the Cu-O stretching modes of the Cu_2O_2 moiety. In compound 1 the intradimer (basal) Cu-Cl vibrations are probably those located at 357(m) and 323(w)

cm^{-1}. Also the bands at 440(sh) and 432(m) cm^{-1} likely originate from the Cu-N stretching modes. These band assignments are consistent with previously reported results for Cu-O,[1b,25] Cu-N,[26] and Cu-Cl[27] stretching vibrations. UV/visible spectra of 1 were taken in dilute CH_2Cl_2 solutions and gave three absorption bands (λ_{max}, nm: 260, 380, and 600-700 (broad)). The strong absorption band at λ_{max} = 260 nm most likely arises from the $\pi \longrightarrow \pi^*$ transition in 2-(2-oxoethyl)pyridine ligand and the absorption band at λ_{max} = 380 nm probably from the L $\longrightarrow$ M charge transfer from Cl to Cu. The broad band from 600 to 700 nm presumably originate from the d $\longrightarrow$ d transition of Cu(II) which has a roughly square planar coordination geometry.

Magnetic Properties

Magnetic susceptibility data for 1 were collected over the range 5 - 400 K, as shown in Fig. 4.7(a). In Fig. 4.7(b) are shown the data corrected for the usual diamagnetic core contributions, ferromagnetic impurity, a temperature independent paramagnetic term, Nα, and a paramagnetic impurity (μ_{eff} = 0.1 μ_B) evident in the raw data at T < 100 K. The small peak in the corrected data at ca. 50 K arises from an antiferromagnetic transition in crystalline O_2, traces of which condensed on the sample and could not be eliminated during the measurements. The constant susceptibility from 100-150 K reflects a singlet ground state for the dimer 1 and a relatively large singlet-triplet energy gap. The usual dipolar coupling approach of Van Vleck,[28] with a perturbing Hamiltonian -2J ($S_A \cdot S_B$) and $S_A = S_B = 1/2$, was used to fit the data in the range 150-400 K to eq. 1.

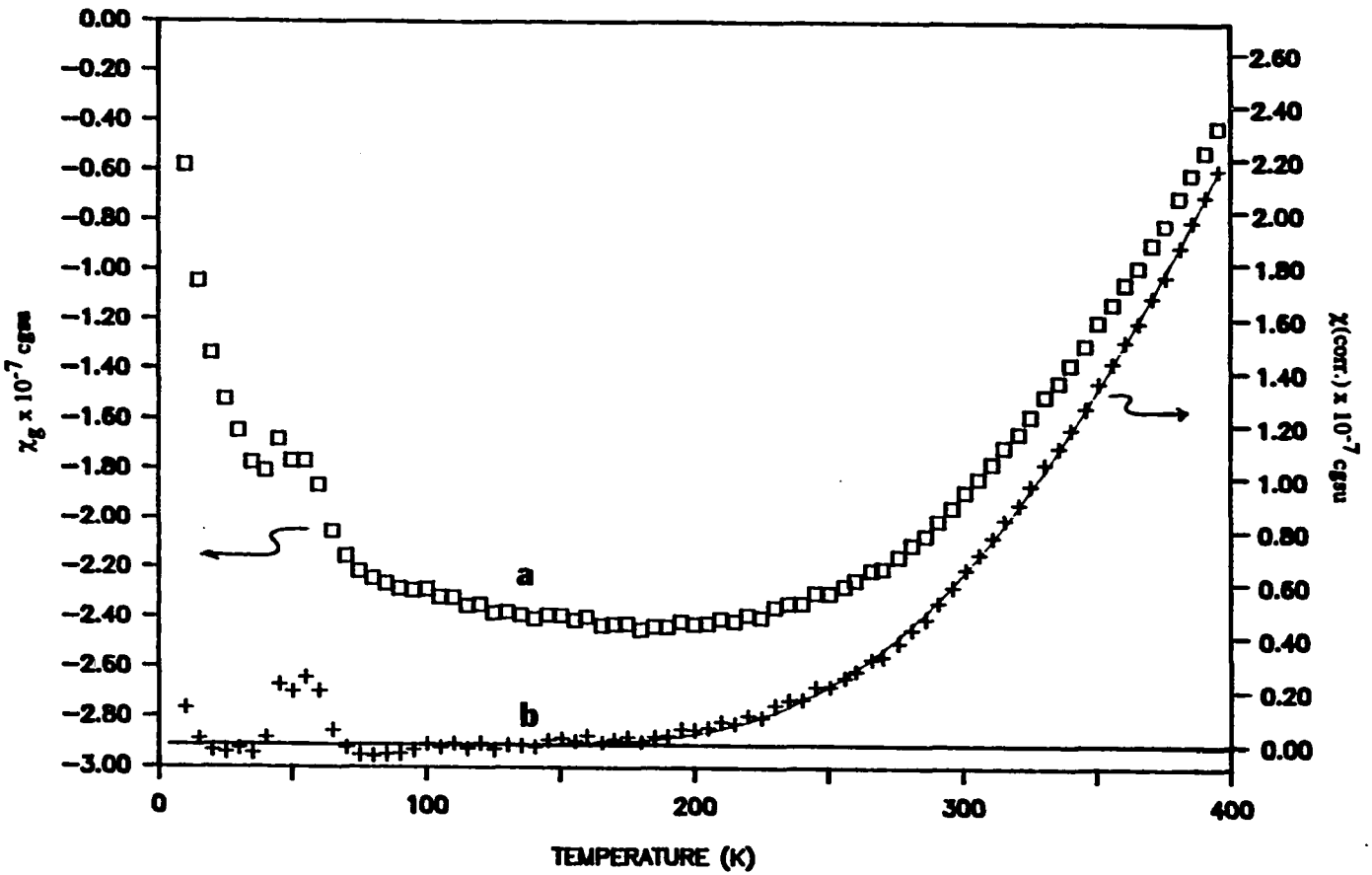

Fig. 4.7. Magnetic susceptibility data for 1. (a). Raw data. (b). Data corrected for diamagnetic atomic core contributions, temperature independent paramagnetism, and paramagnetic impurity susceptibility. Solid line drawn through the data points represents best least squares fit to eq. 1.

$$\chi_M^{corr.} = (Ng^2\mu_B^2/3kT)(1 + X^{2/3})^{-1} \quad (1)$$

where X = exp(-J/kT) and the other symbols have their usual meanings. From the nonlinear least squares program, the best fit to the data yield J = -649 ± 69 cm^{-1} and g = 2.43 ± 0.26. The singlet-triplet energy gap, 2J = -1298 ± 138 cm^{-1} was thus established. Because of this strong antiferromagnetic coupling within the dimer and the diamagnetic behavior at T < 150 K, the data would be relatively insensitive to a very weak magnetic interdimer coupling, and therefore the possible magnetic interaction between two dimers was not considered. This weak magnetic interaction between two dinuclear units containing the Cu_2O_2 moiety was recently observed by Sletten et al.[29]

The solution X-band ESR spectrum of 1 in CH_2Cl_2 at room temperature showed four lines with a hyperfine splitting of 90 G and an isotropic g value of 2.096. The spectrum of a frozen glass solution at T = 107 K also gave four lines, but with a larger hyperfine splitting of ca. 160 G. This spectrum is axial with $g_\perp$ = 2.221 and $g_{//}$ = 2.048. The spectra of powdered samples at both 107 and 297 K showed the same features as the glass sample. The spectral behavior observed is typical of magnetically dilute Cu(II) compounds and is attributable to the presence of monomeric impurities which are also revealed by the magnetic susceptibility data at T < 100 K in Fig. 4.7(a). The observed hyperfine splitting in the spectra indicate that the Cu(II) monomeric units (I = 3/2) are diluted in an essentially diamagnetic host lattice. It is then concluded that the pure dimeric complexes of 1 do not give any detectable ESR signal.

Hatfield et al.[30,31] have demonstrated that, in planar hydroxo-bridged dimers (type I), the singlet-triplet splitting resulting from exchange coupling, -2J, is a linear function of

the bridging CuOCu angle, ϕ, according to eq. 2. A quite different structural dependence of the magnetic properties has been observed by Sinn et al.[14b] for a series of diphenoxo-bridged dimers (type II), in which the ligand environment is considerably distorted from planar toward tetrahedral geometry. These compounds conform to eq. 3, where τ is the dihedral angle between the plane of the Cu_2O_2 bridging unit and the plane of the remaining ligands, as shown in III.

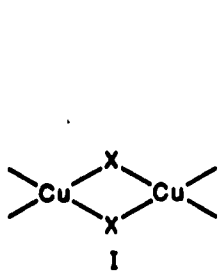

I

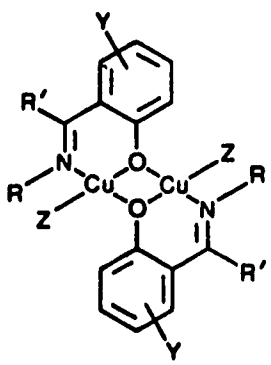

II

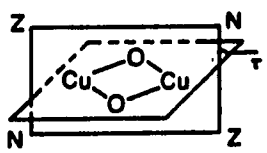

III

$$2J\ (cm^{-1}) = -74.53\ \phi + 7270 \qquad (2)$$

$$2J\ (cm^{-1}) = 29.7\ \tau - 1473 \qquad (3)$$

A typical example of a type II compound is 5. Compound 6 could be classified as type I in terms of the magnetic properties and the structural features.[13a] The molecular structure of 1 is closely related to that of type II except for the small τ angle of 5.56°, and the singlet-triplet splitting of -1298 ± 138 cm^{-1} agrees very well with that expected

from eq. 3. Notably, the value of $2J = -1298\ cm^{-1}$ is the largest known so far for dimeric copper compounds of type II.

As mentioned in the experimental section, compounds 2 and 3 are both interconvertible with 1. When under reduced pressure these interconversions are initiated by the loss of the apical ligands and then the $[CuCl(hep)]_2$ units polymerize through the interdimer Cu-Cl-Cu linkages to form compound 1. The shortest interdimer Cu to Cu distances are 8.213 Å (Cu(1)•••Cu(2)) in 2 and 8.17 Å (Cu(1)•••Cu(2)) in 3. Because of the difficulties encountered in the isolation process, the physical properties of 2 and 3 were not measured.

According to current orbital models for superexchange,[32-34] the extent of antiferromagnetic coupling in a bridged copper(II) dimer is mainly related to the superexchange overlap along the bridging bonds. The larger the overlap, the stronger the antiferromagnetic interaction. Since 1, 2, and 3 involve a planar Cu_2O_2 moiety, the superexchange overlap in these compounds depends on the orientation of the copper unpaired-electron orbital relative to the Cu_2O_2 bridging plane (the xy plane). In other words, the antiferromagnetic interaction is expected to become weaker as the copper unpaired electron density in this bridging plane diminishes.

Compounds 1, 2, and 3 belong to type II doubly bridged copper(II) dimers. Based on the argument of Chiari et al.,[19a] in type II system the site symmetry at copper is close to C_2 in which d_{xy} and d_{xz} belong to the same b irreducible representation and the d_{xy} orbital incorporates d_{xz} character to lie in the plane midway between the Cu_2O_2 plane (the xy plane) and the plane containing Cu and the remaining nonbridging donor atoms (eg. plane $Cu_2N_2Cl_2$ in 1). As the τ angle increases, the in-plane unpaired-

electron density decreases and thus weakens the antiferromagnetic interaction between copper centers, as qualitatively justified by eq. 3. The addition of a weak apical bond in 2 and 3 further reduces the site symmetry at copper from C_2 to C_1. In this latter symmetry, d_{xy} can mix with both d_{xz} and $d_{z}2$ owing to the common a symmetry. Consequently, the in-plane electron density at copper is reduced due to the increased interaction along the z axis and a much lower singlet-triplet energy gaps, as compared to that in 1, is expected in 2 and 3. Based on eq. 3 the larger τ angles in 2 and 3 will further weaken the antiferromagnetic coupling between Cu atoms. The important role that the apical bond plays in depressing the antiferromagnetic interaction between Cu atoms in Type II copper(II) dimers were also discussed elsewhere.[19a,d]

REFERENCES

1. (a) Mehrotra, R.C. Adv. Inorg. Chem. Radiochem., 1983, 26, 269; (b) Singh, J.V.; Baranwal, B.P.; Mehrotra, R.C. Z. Anorg. Allg. Chem., 1981, 477, 235.
2. Bradley, D.C.; Mehrotra, R.C.; Gaur, D.P. Metal Alkoxides; Academic Press, New York, 1978; pp 86-87.
3. (a) Goel, S.C.; Kramer, K.S.; Gibbons, P.C.; Buhro, W.E. Inorg. Chem., 1989, 28, 3620; (b) Horowitz, H.S.; McLain, S.J.; Sleight, A.W.; Druliner, J.D.; Gai, P.L.; Vankavelaar, M.J.; Wagner, J.L.; Biggs, B.D.; Poon, S.J. Science, 1989, 243, 66.
4. McMullen, A.K.; Tilley, T.D.; Rheingold, A.L.; Geib, S.J.; Inorg. Chem., 1989, 28, 3772.
5. Goel, S.C.; Kramer, K.S.; Chiang, M.Y.; Buhro, W.E. Polyhedron, 1990, 9, 611.
6. Skoog, D.A.; West, D.M. Fundamentals of Analytical Chemistry, Saunders, New York, 1976, p. 768-770.
7. Gilmore, G.J. J. Appl. Cryst., 1984, 17, p. 42-46.
8. TEXSAN - TEXRAY Structure Analysis Package, Molecular Structure Corporation (1985).
9. Stout, G.H.; Jensen, L.H. X-ray Structure Determination--A Practical Guide, New York, Macmillan, 1972, p. 246 and 311.
10. Walker, D.N.; Stuart, D. Acta Crystallogr., 1983, A39, 159.
11. Sheldrick, G.M. In: Crystallographic Computing 3, Eds., Sheldrick, G.M.; Kruger, C.; Goddard, R. Oxford University Press, 1985, p. 175-189.
12. B. A. Frenz & Associates, INC., College Station, Texas 77840, 1985.

13. (a) Hodgson, D.J. Prog. Inorg. Chem., 1975, 19, 173; (b) Countryman, R.M.; Robinson, W.T.; Sinn, E. Inorg. Chem., 1974, 13, 2013; (c) Chiari, B.; Piovesana,O.; Tarantelli, T.; Zanazzi, P.F. Inorg. Chem., 1987, 26, 952 and references therein; (d) Butcher, R.J.; Sinn, E. Inorg. Chem., 1976, 15, 1604.

14. (a) Harris, C.M.; Sinn, E. J. Inorg. Nucl. Chem., 1968, 30, 2723; (b) Sinn, E. Structures and Properties of Homo- and Hetero-Binuclear and Polynuclear Complexes Containing Copper. In Biological and Inorganic Copper Chemistry; Karlin, K.D.; Zubieta, J., Eds.; Adenine Press: Guilderland, NY, 1986; (c) Hein, F.; Beerstecher, W. Z. Anorg. Allg. Chem., 1955, 93, 282; (d) Hein, F.; Ludwig, W. Z. Anorg. Allg. Chem., 1965, 63, 338.

15. (a) Mergehenn, R.; Merz, L.; Haase, W. Z. Naturforsch., 1975, 30b, 14; (b) Mergehenn, R.; Haase, W. Z. Naturforsch., 1975, 30b, 155.

16. Sager, R.S.; Williams, R.J.; Watson, W.H. Inorg. Chem., 1967, 6, 951.

17. Schafer, H.L.; Morrow, J.C.; Smith, H.M. J. Chem. Phys., 1965, 42, 504.

18. Sager, R.S.; Williams, R.J.; Watson, W.H. Inorg. Chem., 1969, 8, 694.

19. (a) Chiari, B.; Piovesana,O.; Tarantelli, T.: Zanazzi, P.F. Inorg. Chem., 1988, 27, 4149 and references therein; (b) Oberhammer, H.; Seppelt, K. Angew. Chem., 1978, 90, 66; (c) Sinn, E. Inorg. Chem., 1976, 15, 366; (d) Matsumoto, N.; Kida, S.; Ueda, I. J. Coord. Chem., 1979, 9, 133.

20. (a) Gluvchinsky, P.; Mockler, G.M.; Healy, P.C.; Sinn, E. J. Chem. Soc., Dalton. Trans., 1974, 1156; (b) Miners, J.O.; Sinn, E.; Coles, R.B.; Harris, C.M. J. Chem. Soc., Dalton. Trans., 1972, 1149.

21. Melnic, M. Coord. Chem. Rev., 1982, 42, 259.

22. Omae, I. Coord. Chem. Rev., 1983, 52, 87.

23. Calm, C.J.; Busch, D.H. Coord. Chem. Rev., 1986, 69, 1.

24. Dunaj-Jurco, M.; Ondrejovic, G.; Melnik, M.; Garaj, J. Coord. Chem. Rev., 1988, 83, 1.

25. Nakamoto, K. Infrared Spectra of Inorganic and Coordination Compounds, John Wiley & Sons, NY, 1963, p. 210-227.

26. Nakamoto, K. Infrared Spectra of Inorganic and Coordination Compounds, John Wiley & Sons, NY, 1963, p. 146-151.

27. Whyman, R.; Hatfield, W.E. Inorg. Chem., 1967, 6, 1859.

28. Van Vleck, J.H. The Theory of Electric and Magnetic Susceptibilities; Oxford University Press: London, 1932; Chapter 9.

29. Sletten, J.; Sorensen, A.; Julve, M.; Journaux, Y. Inorg. Chem., 1990, 29, 5054.

30. (a) Hatfield, W.E. Comments Inorg. Chem., 1981, 1, 105; (b) Crawford, W.H.; Richardson, H.W.; Wason, J.R.; Hodgson, D.J.; Hatfield, W.E. Inorg. Chem., 1976, 15, 2107.

31. Hatfield, W.E. In Magneto-Structural Correlations in Exchange Coupled Systems; Reidel: Dordrecht, 1985, p. 555.

32. (a) Kahn, O. Angew. Chem. Int. Ed. Engl., 1985, 24, 834; (b) Kahn, O.; Charlot, M.F. Nouv. J. Chim., 1980, 4, 567; (c) Kahn, O.;Briat, B. J. Chem. Soc., Faraday Trans. 2, 1976, 72, 268.

33. Hay, P.J.; Thibeault, J.C.; Hoffmann, R.J. J. Am. Chem. Soc., 1975, 97, 4884.

34. Bencini, A; Gatteschi, D. Inorg. Chim. Acta, 1978, 31, 11.

SECTION 5. SYNTHESIS AND STRUCTURE OF A SOLUBLE COPPER(II) ALKOXIDE. A DOUBLE SALT FORMED BY BIS[2-(2-OXOETHYL)PYRIDINE]COPPER(II) AND LITHIUM TRIFLUOROMETHYLSULFONATE, $[Cu(C_5H_4NC_2H_4O)_2 \cdot LiO_3SCF_3]_2 \cdot 4CH_2Cl_2$.

ABSTRACT

The novel compound, $[Cu(hep)_2 \cdot LiO_3SCF_3]_2 \cdot 4CH_2Cl_2$ (1), where, hep = 2-(2-oxoethyl)pyridine, was prepared by reaction between $Cu(O_3SCF_3)_2$ and Lihep in THF. Blue crystals of 1, recovered upon recrystallization of the material from CH_2Cl_2, crystallized in the triclinic system, space group $P\bar{1}$. The unit cell dimensions are a = 8.890(3) Å, b = 10.863(5) Å, c = 14.214(7) Å, $\alpha = 111.35(2)^o$, $\beta = 91.52(3)^o$, $\gamma = 99.63(2)^o$, V = 1255(2) $Å_3$, and Z = 1. The structure was refined to R = 0.038, R_w = 0.055. Two $Cu(hep)_2$ monomers are held together through two bridging Li^+ ions of lithium trifluoromethylsulfonate, where each Li^+ is bound to two O atoms from one $Cu(hep)_2$ monomer, one O atom from the other monomer, and one O atom from the $CF_3SO_3^-$ anion. A cis configuration of hep ligands about the copper atom is observed. The local copper coordination geometry is slightly distorted square planar with an O(1)-Cu-O(2) angle of $84.77(9)^o$, an N(1)-Cu-N(2) angle of $91.9(1)^o$, and a bond angle sum around Cu of 360.8^o. The bond distances of Cu-O(1) and Cu-O(2) are 1.901(2) Å and 1.933(2) Å, respectively, and the average Cu-N bond distance is 2.009(3) Å.

INTRODUCTION

Syntheses of oxides based on hydrolysis of alkoxide precursors can have advantages over conventional methods.[1] Processing temperatures may be lowered and the gels thus formed may be drawn or cast into various forms, such as fibers or films.[1] Alkoxides of copper(II) are of interest as molecular precursors to solid state materials such as the high-Tc superconducting copper oxide complexes. Unfortunately, owing to the extensive alkoxide bridging between copper atoms, most of these compounds have proven to be insoluble and polymeric, with essentially unknown structures.[2] Because of this, efforts in the preparation of high-Tc superconductors from solutions of alkoxide precursors have suffered from a lack of soluble copper(II) alkoxides.[3-6] Recently, Horowitz et al. reported the preparation of two soluble copper(II) alkoxides, $Cu(OCH_2CH_2NEt_2)_2$ (2) and $Cu(OCH_2CH_2OBu)_2$ (3) and their use in the solution route to high-Tc superconductor.[7] About the same times, Goel et al.[8] reported the preparation of a soluble copper(II) alkoxide, $[Cu(OCH_2CH_2OCH_2CH_2OMe)_2]_n$ (4) where $n \geq 5$, and its use in the hydrolytic synthesis of $YBa_2Cu_3O_{7-x}$. However the structures of 2, 3, and 4 were not determined.

In this laboratory, syntheses of several new copper(II) alkoxides have been developed as a result of the general effort to prepare precursors suitable for synthesis of high Tc superconductors by the sol-gel approach.[9] In addition to the compounds $[CuCl(hep)]_2$ (5), $[CuCl(hep)(Hhep)]_2 \cdot 2CH_2Cl_2$ (6), and $[CuCl(hep)(py)]_2 \cdot CH_2Cl_2$ (7) reported earlier,[10] The synthesis and structure of a novel soluble copper(II) alkoxide complex, $[Cu(hep)_2 \cdot LiO_3SCF_3]_2 \cdot 4CH_2Cl_2$ (1), is described in this section.

EXPERIMENTAL SECTION

Materials and Methods

All the reactions and manipulations were carried out under inert atmospheres with the use of standard dry-box, vacuum, and Schlenk techniques. Copper(II) triflate, $Cu(O_3SCF_3)_2$, and 2-(2-hydroxyethyl)pyridine, Hhep, were used as commerically obtained. Tetrahydrofuran was dried by addition of sodium metal and benzophenone followed by stirring overnight, degassing, vacuum distillation, and then stored over 4A molecular sieves before use. Diethyl ether was dried in the same manner. Dichloromethane was refluxed over P_2O_5 for 8 hrs., then distilled and stored in a similar manner.

Infrared Spectra

Fourier-transform infrared spectra were recorded on an IBM IR98FT spectrometer, whose sample chamber was flushed with purified nitrogen. Samples were prepared as Nujol mulls and mounted on CsI plates.

Synthesis

The lithium salt of 2-(2-hydroxyethyl)pyridine, Lihep, was prepared by a dropwise addition of n-BuLi/hexane solution into 2-(2-hydroxyethyl)pyridine, Hhep, in THF. After

stirring for several hours at room temperature, the resulting yellowish white solid was filtered out, vacuum dried overnight, and then stored in the dry box. Compound 1 was synthesized by vacuum transfer of THF (20 ml) onto the solid mixture of $Cu(O_3SCF_3)_2$ (1.282 g, 3.55 mmol) and Lihep (0.915 g, 7.09 mmol). The reaction mixture was vigorously stirred at room temperature for one day. Although no precipitate was observed, the blue solution was filtered and a blue solid was obtained after vacuum removal of THF and washing of the product with diethyl ether. A solution of the blue solid was then prepared in CH_2Cl_2 and stored at -20°C. After 3 days, blue crystals of 1 were obtained. Far IR(CsI): 574(m), 558(m), 517(m), 470(w), 446(m), 424(m), 362(w), 350(w), 275(w), and 215(w).

Crystallographic Study

Crystals of 1 are air sensitive and subject to loss of solvent under reduced pressure, whereupon they turn purple. Thus, after recrystallization from CH_2Cl_2, a single crystal with the size of 0.50 x 0.20 x 0.30 mm^3 was picked up directly from the solution contained in a Schlenk tube held at -78°C. This crystal was then protected from air by epoxy resin, attached to a glass fiber, and immediately mounted on the diffractometer in a low temperature nitrogen stream (-70°C). Data were collected with an Enraf-Nonius CAD4 diffractometer equipped with locally modified low-temperature devices. Graphite-monochromated MoKα radiation was employed to collect data with $4^o \leq 2\theta \leq 50^o$. The ω scan technique was used. Intensity data were corrected for Lorentz and polarization effects. An empirical correction for absorption was based on ψ

scans. No decay of the intensities of three standard reflections was observed. Data collected in the hemisphere (h, ±k, ±l) yielded a total of 4709 reflections of which 3743 reflections with $I > 3\sigma(I)$ were considered as observed and used in the subsequent structure solution and refinement.

Lattice parameters were determined by a least-squares refinement of 22 accurately centered reflections with $26^{o} \leq 2\theta \leq 36^{o}$. The space group P1 was chosen based on the statistical test of intensities. The structure was solved by direct methods (SHELXS-86)[11] and refined by full-matrix least-square techniques to R = 0.038, R_w = 0.055. The final electron density difference map was flat with the highest peak of 0.85 e/Å^3 located near the copper atom. The refinement also showed that the sites for the CH_2Cl_2 molecules were fully occupied. All the hydrogen atoms were introduced at calculated positions with C-H = 1.05 Å.

Details of the data collection and refinement are given in Table 5.1. Final positional parameters and selected bond distances and angles are listed in Tables 5.2 and 5.3, respectively. The anisotropic temperature factors of atoms are listed in Table 5.4. Information about the least squares planes of atoms and comparison of calculated and observed structure factors are available as supplementary materials.

Table 5.1. X-ray crystallographic data for $[Cu(C_5H_4NC_2H_4O)_2 \cdot LiO_3SCF_3]_2 \cdot 4CH_2Cl_2$

empirical formula	$Cu_2Cl_8S_2F_6O_{10}N_4C_{34}Li_2H_{40}$
formula weight	1267.42
crystal system	triclinic
space group	$P\bar{1}$
a, Å	8.890(3)
b, Å	10.863(5)
c, Å	14.214(7)
α, deg	111.35(2)
β, deg	91.52(3)
γ, deg	99.63(2)
V, $Å^3$	1255(2)
Z	1
Calcd density, g/cm^3	1.68
F000	638
crystal size, mm	0.50 x 0.20 x 0.30
μ(Mo Kα), cm^{-1}	14.63
diffractometer	Enraf-Nonius CAD4
λ^a,	0.71069
T, °C	-70
2θ, deg	4-50
No. reflections collected	4709
No. observations($I > 3\sigma(I)$)	3743
No. variables	317
goodness of fit indicator[b]	1.68
max. shift in final cycle	0.14
largest peak in final diff. map, $e/Å^3$	0.85
scan mode	ω
transmission coeff.	0.3542-1.000
R^c, Rw^d	0.038, 0.055

[a]Graphite-monochromated

[b]Quality-of-fit = $[\Sigma\omega(|Fo|-|Fc|)^2/(N_{obs}-N_{parameters})]^{1/2}$

[c]$R = \Sigma||Fo|-|Fc||/\Sigma|Fo|$

[d]$Rw = [\Sigma\omega(|Fo|-|Fc|)^2/\Sigma\omega|Fo|^2]^{1/2}$; $\omega = 1/\sigma^2(|Fo|)$

Table 5.2. Positional parameters and B_{eq} for $[Cu(C_5H_4NC_2H_4O)_2 \cdot LiO_3SCF_3]_2 \cdot 4CH_2Cl_2$

atom	x	y	z	B_{eq}[a], Å^2
Cu	-0.01893(4)	0.21921(3)	0.90827(3)	1.76(1)
Cl(1)	0.3734(1)	0.5274(1)	0.69953(9)	4.76(5)
Cl(2)	0.2484(1)	0.7521(1)	0.68446(9)	4.52(5)
Cl(3)	0.1809(1)	0.2743(1)	0.4313(1)	5.26(5)
Cl(4)	0.3761(1)	0.0758(1)	0.37444(8)	3.85(4)
S	0.21238(8)	0.62828(7)	1.24822(6)	2.03(2)
F(1)	0.3274(3)	0.7755(3)	1.4332(2)	5.6(1)
F(2)	0.2163(4)	0.5756(3)	1.4125(2)	7.2(1)
F(3)	0.0828(4)	0.7223(3)	1.4147(2)	6.0(1)
O(1)	-0.1443(2)	0.2903(2)	1.0136(2)	2.13(7)
O(2)	0.1013(2)	0.3997(2)	0.9589(2)	1.87(6)
O(3)	0.0751(2)	0.5252(2)	1.2094(2)	2.53(7)
O(4)	0.3527(3)	0.5795(3)	1.2275(2)	3.8(1)
O(5)	0.2054(3)	0.7507(2)	1.2323(2)	2.87(8)
N(1)	-0.1194(3)	0.0284(2)	0.8835(2)	1.88(8)
N(2)	0.1129(3)	0.1582(2)	0.7942(2)	1.96(8)
Li	-0.0216(6)	0.4616(5)	1.0722(4)	2.2(2)

[a] $B_{eq} = 8\pi^2/3 \Sigma U_{ij} a_i^* a_j^* a_i \cdot a_j$, where the temperature factors are defined as $\exp(-2\pi^2 \Sigma h_i h_j a_i^* a_j^* U_{ij})$

Table 5.2. (continued)

atom	x	y	z	B_{eq}[a], Å^2
C(1)	-0.0350(4)	-0.0686(3)	0.8632(2)	2.5(1)
C(2)	-0.0960(4)	-0.1999(3)	0.8463(3)	2.8(1)
C(3)	-0.2537(4)	-0.2362(3)	0.8477(3)	2.9(1)
C(4)	-0.3410(4)	-0.1369(3)	0.8702(2)	2.6(1)
C(5)	-0.2710(3)	-0.0038(3)	0.8898(2)	2.0(1)
C(6)	-0.3587(3)	0.1090(3)	0.9207(2)	2.2(1)
C(7)	-0.2867(4)	0.2199(3)	1.0212(2)	2.3(1)
C(8)	0.0493(4)	0.0738(3)	0.7016(3)	2.5(1)
C(9)	0.1331(4)	0.0303(3)	0.6201(2)	2.8(1)
C(10)	0.2902(4)	0.0783(4)	0.6336(3)	3.0(1)
C(11)	0.3555(4)	0.1656(3)	0.7286(3)	2.7(1)
C(12)	0.2657(3)	0.2043(3)	0.8083(2)	2.0(1)
C(13)	0.3293(3)	0.2993(3)	0.9135(2)	2.3(1)
C(14)	0.2599(3)	0.4252(3)	0.9484(2)	2.4(1)
C(15)	0.2066(5)	0.5828(4)	0.6719(4)	4.7(2)
C(16)	0.3699(5)	0.2477(4)	0.4296(4)	5.0(2)
C(17)	0.2096(5)	0.6782(4)	1.3845(3)	3.7(1).

Table 5.3. Selected bond distances(Å) and angles(deg.) for $[Cu(C_5H_4NC_2H_4O)_2 \cdot LiO_3SCF_3]_2 \cdot 4CH_2Cl_2$

	bond distances		
Cu-O(1)	1.901(2)	O(2)'-Li	1.948(6)
Cu-O(2)	1.933(2)	O(3)-Li	1.937(6)
Cu-N(1)	2.012(3)	Cl(1)-C(15)	1.777(5)
Cu-N(2)	2.006(3)	Cl(2)-C(15)	1.755(5)
S-O(3)	1.451(2)	Cl(3)-C(16)	1.752(5)
S-O(4)	1.432(3)	Cl(4)-C(16)	1.754(5)
S-O(5)	1.438(3)	S-C(17)	1.814(4)
O(1)-C(7)	1.394(4)	F(1)-C(17)	1.323(4)
O(2)-C(14)	1.414(4)	F(2)-C(17)	1.322(5)
O(1)-Li	1.868(5)	F(3)-C(17)	1.319(5)
O(2)-Li	1.946(6)		
	bond angles		
O(1)-Cu-O(2)	84.77(9)	O(1)-Cu-N(2)	175.1(1)
O(1)-Cu-N(1)	92.2(1)	O(2)-Cu-N(2)	91.9(1)
O(2)-Cu-N(1)	166.8(1)	N(2)-Cu-N(1)	91.9(1)
Li-O(1)-Cu	96.6(2)	Cu-O(2)-Li	93.0(2)
Cu-O(2)'-Li	118.4(2)	Li-O(2)-Li'	79.8(2)
S-O(3)-Li	124.4(2)	O(1)-Li-O(3)	120.7(3)
O(1)-Li-O(2)'	114.0(3)	O(3)-Li-O(2)	119.1(3)
O(3)-Li-O(2)'	113.0(3)	O(2)-Li-O(2)'	100.2(2)

Table 5.4. Anisotropic temperature parameters for $[Cu(C_5H_4NC_2H_4O)_2 \cdot LiO_3SCF_3]_2 \cdot 4CH_2Cl_2$ ($Å^2$)[a]

Atom	U11	U22	U33	U12	U13	U23
Cu	0.0202(2)	0.0160(2)	0.0277(2)	0.0001(1)	0.0030(1)	0.0062(2)
Cl(1)	0.0623(7)	0.0582(7)	0.0637(8)	0.0169(5)	0.0031(5)	0.0243(6)
Cl(2)	0.0649(8)	0.0553(7)	0.0601(7)	0.0151(5)	0.0162(5)	0.0295(6)
Cl(3)	0.0610(8)	0.0518(7)	0.080(1)	0.0185(5)	0.0050(6)	0.0131(6)
Cl(4)	0.0470(6)	0.0461(6)	0.0482(6)	0.0090(4)	0.0009(4)	0.0119(5)
S	0.0271(4)	0.0199(4)	0.0277(4)	0.0004(3)	-0.0002(3)	0.0082(3)
F(1)	0.091(2)	0.054(2)	0.044(1)	-0.021(1)	-0.031(1)	0.009(1)
F(2)	0.171(3)	0.056(2)	0.046(1)	-0.011(2)	-0.024(2)	0.035(1)
F(3)	0.086(2)	0.077(2)	0.045(1)	0.003(2)	0.030(1)	0.003(1)
O(1)	0.024(1)	0.020(1)	0.031(1)	-0.0029(8)	0.0049(9)	0.0055(9)
O(2)	0.021(1)	0.017(1)	0.029(1)	0.0001(8)	0.0028(8)	0.0062(8)
O(3)	0.033(1)	0.028(1)	0.029(1)	-0.006(1)	-0.002(1)	0.010(1)
O(4)	0.033(1)	0.035(1)	0.073(2)	0.009(1)	0.007(1)	0.016(1)
O(5)	0.043(1)	0.028(1)	0.042(1)	0.002(1)	0.003(1)	0.019(1)
N(1)	0.025(1)	0.019(1)	0.028(1)	0.002(1)	0.002(1)	0.009(1)
N(2)	0.023(1)	0.019(1)	0.030(1)	0.0001(1)	-0.001(1)	0.008(1)

[a]The form of the anisotropic displacement parameter is $\exp[-2\pi^2(h^2a^2\,U(1,1) + k^2b^2\,U(2,2) + l^2c^2\,U(3,3) + 2hkab\,U(1,2) + 2hlac\,U(1,3) + 2klbc\,U(2,3))]$, where a, b, and c are reciprocal lattice constants

Table 5.4. (continued)

Atom	U11	U22	U33	U12	U13	U23
C(1)	0.036(2)	0.026(2)	0.035(2)	0.008(1)	0.003(1)	0.011(1)
C(2)	0.051(2)	0.022(2)	0.039(2)	0.011(1)	0.011(2)	0.015(1)
C(3)	0.055(2)	0.022(2)	0.033(2)	0.002(1)	0.008(2)	0.012(1)
C(4)	0.038(2)	0.024(2)	0.032(2)	-0.004(1)	0.007(1)	0.010(1)
C(5)	0.030(2)	0.020(1)	0.023(1)	-0.002(1)	0.001(1)	0.009(1)
C(6)	0.023(1)	0.024(2)	0.034(2)	0.000(1)	0.003(1)	0.010(1)
C(7)	0.027(2)	0.024(2)	0.033(2)	0.001(1)	0.006(1)	0.010(1)
C(8)	0.029(2)	0.026(2)	0.034(2)	0.004(1)	0.000(1)	0.007(1)
C(9)	0.043(2)	0.034(2)	0.028(2)	0.011(2)	0.000(1)	0.009(1)
C(10)	0.044(2)	0.038(2)	0.033(2)	0.012(2)	0.010(1)	0.014(2)
C(11)	0.030(2)	0.035(2)	0.039(2)	0.004(1)	0.008(1)	0.016(2)
C(12)	0.026(2)	0.021(1)	0.030(2)	0.003(1)	0.004(1)	0.012(1)
C(13)	0.020(1)	0.030(2)	0.033(2)	0.002(1)	-0.001(1)	0.008(1)
C(14)	0.022(1)	0.026(2)	0.036(2)	-0.003(1)	0.004(1)	0.006(1)
C(15)	0.043(2)	0.054(3)	0.082(4)	0.006(2)	0.012(2)	0.028(2)
C(16)	0.048(3)	0.045(3)	0.084(4)	0.001(2)	0.009(2)	0.010(2)
C(17)	0.069(3)	0.035(2)	0.028(2)	-0.008(2)	-0.004(2)	0.009(2)
Li	0.030(3)	0.021(2)	0.029(3)	0.001(2)	-0.002(2)	0.009(2)

RESULTS AND DISCUSSION

Description of the Structure

The structure of 1 consists of two $Cu(hep)_2$ monomeric units held together through two bridging molecules of lithium trifluoromethylsulfonate located above and below the plane constituted by the two copper(II) monomers. Each Li^+ is bound to three O atoms of the hep ligands, two from one Cu atom and one from the other, and to one O atom of one $CF_3SO_3^-$ anion. A view of the structure of one of the monomer units is given in Fig. 5.1 and the structure of the entire dimer is shown in Fig. 5.2. The Cu(II) atoms are 4-coordinate and adopt a cis configuration of the ligated atoms, with the CuO_2N_2 skeleton in essentially planar geometry, as shown by a bond angle sum about Cu of 360.8^o. The O(1)-Cu-O(2) angle is slightly closed from 90^o to $84.77(9)^o$, while the N(2)-Cu-N(1), O(1)-Cu-N(1), and O(2)-Cu-N(2) angles are each opened to about 92^o.

The only Cu(II) alkoxide complexes previously structured having essentially monomeric 4-coordinate units are trans-bis(N-n-butyl-pyridoxylideneiminato)copper(II) (8),[12] trans-bis(N-isopropyl-5,6-benzosalicylideneaminato)copper(II)(9)[13] and the recently published siloxide-pyridine complex trans-$Cu[OSi(OCMe_3)_3]_2(py)_2$(10).[14] Complex 10 is most closely related to 1, although the former was described as having a severely distorted tetrahedral bond configuration about Cu(II). The cis configuration of ligand atoms about the copper atom in 1 is observed for the first time in such bidentate complexes; compounds 8, 9, and 10 all have a trans configuration around Cu(II). This unusual cis configuration of 1 presumably arises from the bonding of the cis O atoms to

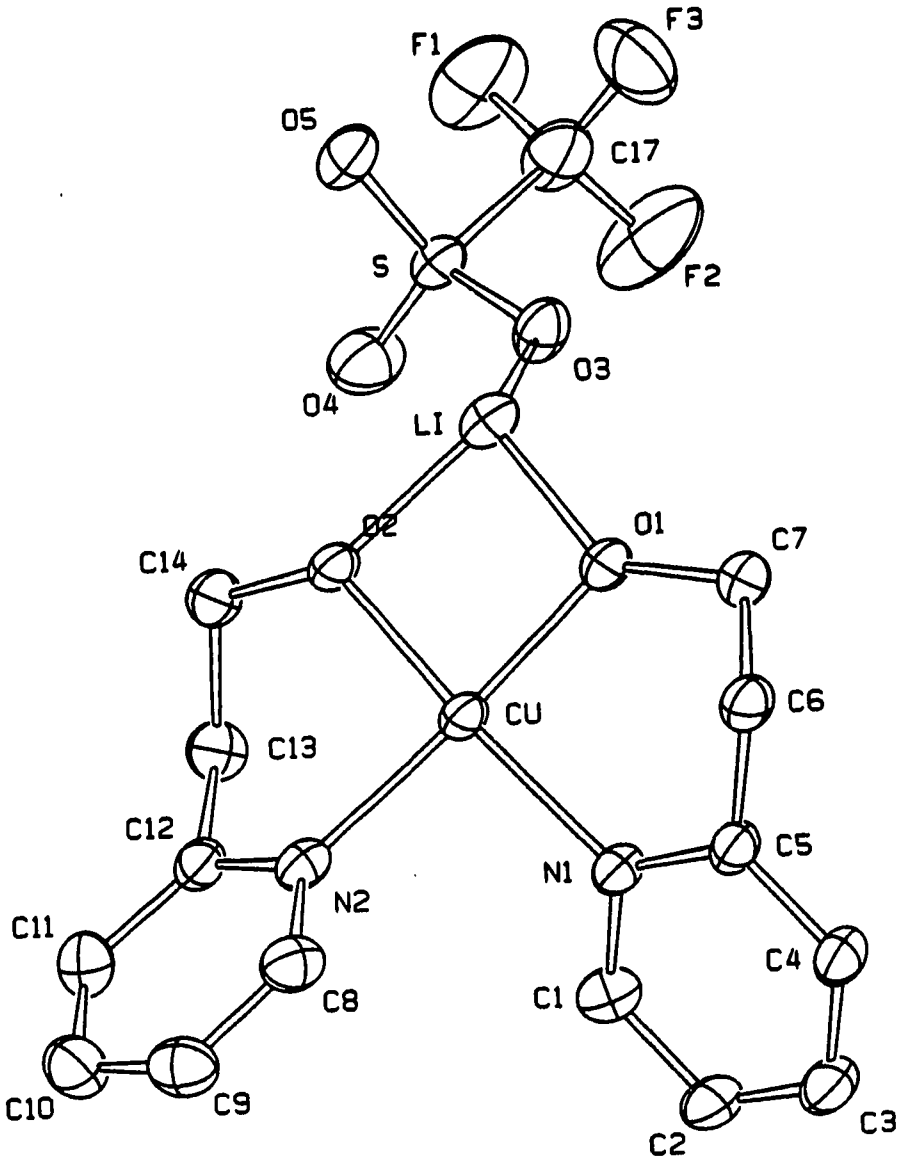

Fig. 5.1. Ortep drawing(50 % thermal ellipsoids) of the $Cu(hep)_2 \cdot LiO_3SCF_3$ monomer. Interdimer coupling by the lithium triflate is not shown.

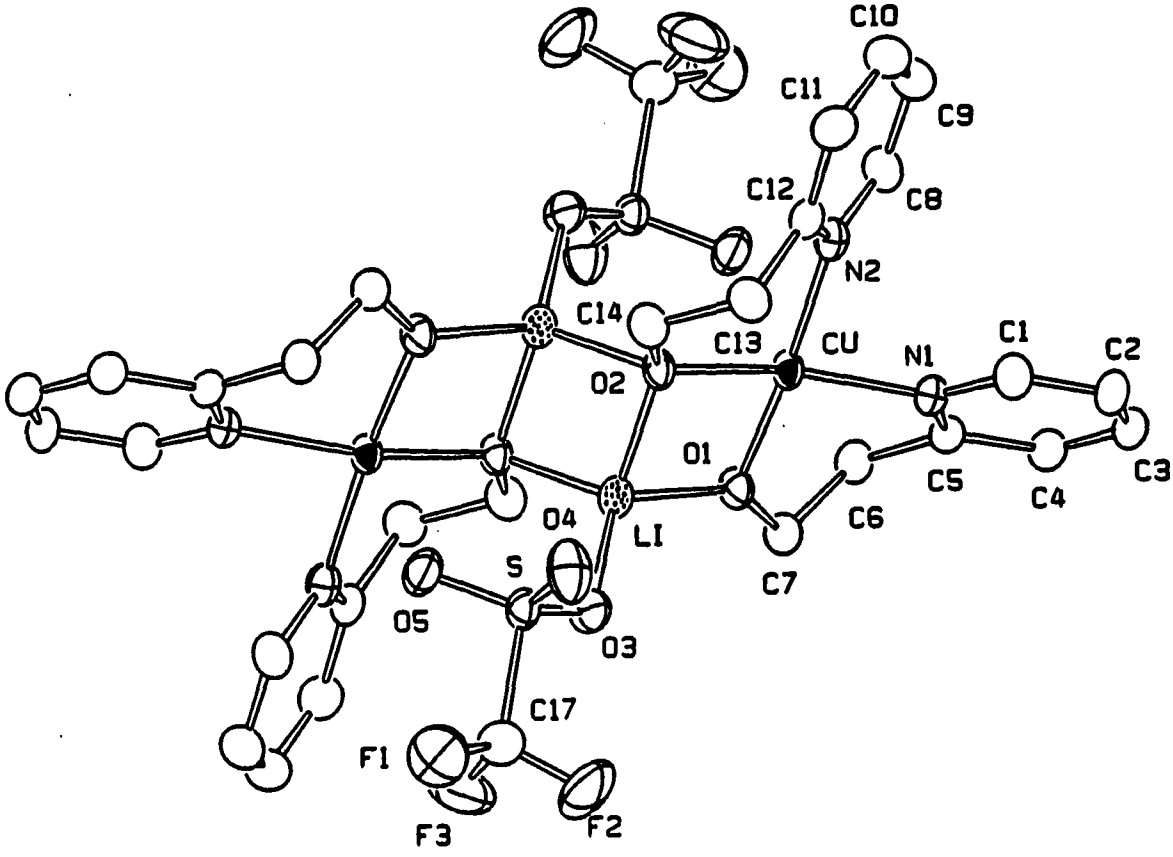

Fig. 5.2. Ortep drawing(50 % thermal ellipsoids) of $[Cu(hep)_2 \cdot LiO_3SCF_3]_2$ dimer showing the bridging of lithium triflate between two $Cu(hep)_2$ monomers.

one of the Li^+ ions in chelate fashion. It seems unlikely that the cis configuration would be obtained if the lithium triflate were not bonded in this way.

As illustrated in Fig. 5.2, 1 is the first compound whose structure involves two monomers held together through bridging-salts, as opposed to several other copper(II) alkoxide or phenoxide dimers[10,15,16] whose components are held together through organic ligands. The bridging-lithium ions have pseudo-tetrahedral coordination geometry. The LiO(2)Li'O(2)' plane is exactly planar owing to the crystallographic center of inversion. The Li-O(2)-Li' angle is $79.8(2)^o$, which leads to a value of $100.2(2)^o$ for the angle O(2)-Li-O(2)'. The Cu-O(2) bond distance of 1.933(2) Å is longer than that of Cu-O(1), 1.901(2) Å, most likely because of the higher coordination number of O(2) than of O(1). This coordination difference also explains the significant difference between the bond distances of Li-O(2), 1.947 (ave.), and Li-O(1), 1.868(5) Å. Interestingly, the Cu-O(1) distance in 1 is significantly shorter than the Cu-O distances (1.929 - 1.946 Å) in 5, 6, and 7. This shorter Cu-O(1) distance probably originates from the less electropositive Li^+ ion in 1 as compared to the divalent Cu^{+2} ions in 5, 6, and 7. The average Cu-N separation in 1, 2.009 Å, is consistent with previously reported values for Cu-N bond lengths (1.91 - 2.19 Å).[10,16-19] The presence of the bulky triflate ligands above and below the plane composed of the two copper(II) monomers and lithium ions in 1 may provide sufficient steric hindrance to prevent a 5-coordinate arrangement around the Cu(II) center.

Infrared Spectra

The infrared spectrum of 1 displays the characteristic absorption bands (cm^{-1}) of the trifluoromethane sulfonate ligand:[20-22] $\nu_{as}(CF_3)$ at 1285(m); $\nu_s(CF_3)$ at 1242(m); $\delta_s(CF_3)$ at 773(w); $\nu_{as}(SO_3)$ at 1165(m); $\nu_s(SO_3)$ at 1030(m); and $\delta_s(SO_3)$ at 558(m). The absorption bands at 574(m) and 517(m) cm^{-1} of 1 probably originate from the Cu-O stretching modes and those at 446(m) and 424(m) cm^{-1} most likely arise from the Cu-N stretching modes. These band assignments were aided by a comparison of spectra among 1, bis(trifluoromethylsulfonate)copper(II), and the hep ligand. The observed wave numbers agree with previously reported values for the $CF_3SO_3^-$ anion and for Cu-O[10,23,24] and Cu-N[10,25] stretching vibrations.

REFERENCES

1. Hubert-Pfalzgraf, L.G. New J. Chem., 1987, 11, 663.
2. (a) Mehrotra, R.C. Adv. Inorg. Chem. Radiochem., 1983, 26, 269; (b) Singh, J.V.; Baranwal, B.P.; Mehrotra, R.C. Z. Anorg. Allg. Chem., 1981, 477, 235.
3. Monde, T.; Kozuka, H.; Sakka, S. Chem. Lett., 1988, 287.
4. Nonaka, T.; Kaneko, K.; Hasegawa, T.; Kishio, K.; Takahashi, Y.; Kobayashi, K.; Kitazawa, K.; Fueki, K. Jpn. J. Appl. Phys., 1988, 27, L867.
5. Ravindranathan, P.; Komarneni, S.; Bhalla, A.; Roy, R.; Cross, L.E. J. Mater. Res., 1988, 3, 810.
6. Kramer, S.A.; Kordas, G.; McMillan, J.; Hilton, G.C.; Van Harligen, D.J. Appl. Phys. Lett., 1988, 53, 156.
7. Horowitz, H.S.; McLain, S.J.; Sleight, A.W.; Druliner, J.D.; Gai, P.L.; VanKavelaar, M.J.; Wagner, J.L.; Biggs, B.D.; Poon, S.J. Science, 1989, 243, 66.
8. Goel, S.C.; Kramer, K.S.; Gibbons, P.C.; Buhro, W.E. Inorg. Chem., 1989, 28, 3619.
9. Brinker, C.J. and Scherer, G.W. Sol-Gel Science, Academic Press, San Diago, CA, 1990.
10. Chen, S.C. and McCarley, R.E. Synthesis and Characterization of Three Copper(II) Alkoxide Chloride Dimers with the Anion of the Chelating Ligand 2-(2-Hydroxyethyl)pyridine, submitted to Inorg. Chem., July 1990.
11. Sheldrick, G.M. in Crystallographic Computing 3, Eds. Sheldrick, G.M.; Kruger, C.; Goddard, R. Oxford University Press, 1985, P. 175-189.

12. Bigoli, F.; Lanfranchi, M.; Leporati, E.; Pellinghelli, M.A. Inorg. Chim. Acta., 1982, 66, 213.

13. Tamara, H.; Ogawa, K.; Takeuchi, A.; Yamada, S. Cryst. Struct. Comm., 1982, 11, 707.

14. McMullen, A.K.; Tilley, T.D.; Rheingold, A.L.; Geib, S.J. Inorg. Chem., 1989, 28, 3772.

15. (a) Hodgson, D.J. Prog. Inorg. Chem., 1975, 19, 173; (b) Hatfield, W.E. In Magneto-Structural Correlations In Exchange Coupled Systems; Reidel: Dordrecht, 1985, 555; (c) Kato, M.; Muto, Y. Coord. Chem. Rev., 1988, 92, 45.

16. (a) Chiari, B.; Piovesana, O.; Tarantelli, T.; Zanazzi, P.F. Inorg. Chem., 1988, 27, 4149 and references therein; (b) Chiari, B.; Piovesana, O.; Tarantelli, T.; Zanazzi, P.F. Inorg. Chem., 1987, 26, 952 and references therein.

17. Omae, I. Coord. Chem. Rev., 1983, 52, 87.

18. Cairn, C.J.; Busch, D.H. Coord. Chem. Rev., 1986, 69, 1.

19. Dunaj-jurco, M.; Ondrejovic, G.; Melnik, M.; Garaj, J. Coord. Chem. Rev., 1988, 83, 1.

20. Lawrance, G.E. Chem. Rev., 1986, 86, P. 17-33 and references therein.

21. Miles, M.B.; Doyle, G.; Cooney, R.P.; Tobias, R.S. Spectrochim. Acta, Part A, 1969, 25, 1515.

22. Burger, H.; Burczyk, K.; Blaschette, A. Monatsh. Chem., 1970, 101, 102.

23. Singh, J.V.; Baranwal, B.P.; Mehrotra, R.C. Z. Anorg. Allg. Chem., 1981, 477, 235.

24. Nakamoto, K. Infrared Spectra of Inorganic and Coordination Compounds, John Wiley & sons, NY, 1963, P. 210-227.

25. Nakamoto, K. Infrared Spectra of Inorganic and Coordination Compounds, John Wiley & sons, NY, 1963, P. 146-151.

SECTION 6. THE PREPARATION AND PARTIAL CHARACTERIZATION OF SOME REDUCED TERNARY OR QUATERNARY OXIDES OF MOLYBDENUM AND ONE COPPER(II) ALKOXIDE COMPLEX

INTRODUCTION

The chemistry of ternary or quaternary molybdenum oxides containing discrete oligomeric cluster units just begin to be explored. Very few of these compounds are known to date. In the past five years compounds $BaMo_8O_{10}$,[1] $LaMo_5O_8$,[2] $PbMo_5O_8$,[3] $Tl_{0.8}Sn_{0.6}Mo_7O_{11}$,[3] and $In_{11}Mo_{40}O_{82}$[4] have been reported but none of their physical properties was discussed. In the course of this reduced molybdenum oxide research, besides compounds that have been structurally characterized and their physical properties have been discussed in Sections 1 and 2, several other compounds have also been synthesized and are tentatively formulated as $K_{0.5}M_{1.9}Mo_{14}O_{22}$ (M = Ca, Sr, Ba, Pb, and Sn), $Ca_{3-x}Mo_{14}O_{22}$, $PbMo_6O_{10}$ and $Sn_{3.6}Mo_{16}O_{24}$ (superstructure of $Sn_{0.9}Mo_4O_6$[5]). This section reports the preparation and partial characterization of these compounds.

In the course of research on the copper(II) alkoxide complex system with anion of 2-(2-hydroxyethyl)pyrindine as ligand, several interesting alkoxide complexes have been discovered (Sections 4 and 5). Reported here is another new compound discovered along this line.

EXPERIMENTAL

Materials

Potassium molybdate was prepared by the reaction of KOH (Fisher Certified A.C.S.) with a stoichiometric quantity of MoO_3 (Fisher Certified A.C.S.) in deionized water. The molybdate solution was filtered, its volume reduced by heating, and the precipitate collected on a glass frit. The product was finally dried at 120°C and stored in a dry box. Strontium molybdate was prepared by the reaction of $SrCO_3$ (Baker Analyzed, 99.6%) with a stoichiometric quantity of MoO_3 at 550°C in an open crucible. The resulting white powder was air cooled to room temperature and then stored in a desiccator. Calcium molybdate was prepared by mixing an aqueous solution of calcium chloride (Baker Analyzed Reagent) with an aqueous solution containing stoichiometric quantity of sodium molybdate (Fisher Certified A.C.S.). The white precipitate was filtered, washed with water, dried at 120 °C under vacuum, and then annealed at 800 °C. SnO was prepared by the method of Weiser and Milligan.[6] The prepared solid was dried and stored in a desiccator. Molybdenum tubing was obtained from Thermo-Electron Corp. (99.97%), molybdenum metal powder from Aldrich Chemical Co. (99.99%), molybdenum sheet from Rembar Co. (99.95%), and MoO_2 (99.0%) and PbO (99.9%) powder from Alfa Products.

Synthesis

$K_{0.5}M_{1.9}Mo_{14}O_{22}$ (M = Ca, Sr, Ba, Pb, and Sn)

In a typical reaction, a stoichiometric amount of MoO_3, K_2MoO_4, $MMoO_4$ (or M'O) (M = Ca, Sr, Ba, M' = Sn, Pb) and Mo were ground together in a mortar, pressed into a pellet, and sealed in an evacuated quartz tube which, in turn, was sealed in another evacuated quartz tube. In some reactions pellets were wrapped with Mo-foil before being sealed in the quartz tube and in some cases a 2-fold excess of K_2MoO_4 was used. The reaction conditions employed were at 1250 ^oC to 1280 ^oC for 8 days. The products of these reactions usually contained minor phases of Mo and/or MoO_2 and a major phase of the unknown compounds. X-ray powder diffraction data of these unknown compounds were the same and corresponded well to that of $K_3Mo_{14}O_{22}$ (Section 1) except with a higher symmetry. Quantitative elemental analysis without standards on four different crystals of the K-Ba-Mo-O phase were performed by SEM and resulted in an average mole ratio K : Ba : Mo = 0.23 : 0.94 :7. The formula $K_{0.5}M_{1.9}Mo_{14}O_{22}$ was thus tentatively assigned for these compounds. Notably also, compounds $K_{0.5}M_{1.9}Mo_{14}O_{22}$ were always observed as the major phase in products of reactions made up for the preparation of $K_2M_2Mo_{18}O_{28}$ (n = 4) compounds. Other minor phases in these latter products were phases corresponding to $M_xMo_4O_6$, MoO_2, and Mo.

$Ca_{3-x}Mo_{14}O_{22}$

The reactant mixture contains $CaMoO_4$, MoO_2, and Mo in mole ratio 3 : 5 : 6. The work-up procedure was the same as that of $K_2MMo_{14}O_{22}$, and the reaction condition was 1100°C for 6 1/2 days. No single crystals were observed in the product. The x-ray powder diffraction data of the bulk sample indicated a single phase corresponding to the compound tentatively formulated as $CaMo_5O_8$ (Anal. Found: Ca, 6.25; Mo, 72.0; Mo (+2.80)) by Toraradi.[7] In an attempt to grow single crystals suitable for x-ray data collection, the bulk sample was reground, left as powdered sample, sealed in double quartz tubes as usual, and then fired at 1150 °C for 16 days. The resulting product contained crystals that were too small to do any single crystal work.

$Sn_{3.6}Mo_{16}O_{24}$ (superstructure of $Sn_{0.9}Mo_4O_6$)

Cylindrical crystals of the title compound were discovered in a mixture resulting from the reaction of K_2MoO_4, SnO, MoO_3, and Mo in mole ratio 3 : 6 : 22 : 29 (aiming at $K_2Sn_2Mo_{18}O_{28}$ (n = 4)). The reactants were pelletized, sealed in a Mo tube which, in turn was sealed in a quartz tube, and then held at 1280°C for 8 days. The other phases in the product mixture were $K_{0.5}M_{1.9}Mo_{14}O_{22}$ (major) and crystals of Mo (cubic) and MoO_2 (needle). Single crystal data collection on the Rigaku diffractometer indicated that the unit cell belonged to the tetragonal system (space group I4/mmm) with cell dimensions a = b = 13.561(1) Å ($\sqrt{2}$ a'), c = 5.659(1) ($\sqrt{2}$c'), and V = 1040.7(3) $Å^3$, where a' and c' are the unit cell dimensions of $Sn_{0.9}Mo_4O_6$ subcell. The supercell thus has a volume four times the size of the subcell. Single crystal elemental analyses without

standards were done with SEM and the average mole ratio of Sn : Mo = 0.9 : 3.9 (no K was found) was observed. Therefore the formula of $Sn_{3.6}Mo_{16}O_{24}$ was tentativeiy assigned.

$\underline{PbMo_6O_{10}}$

Small plate crystals of the title compound were found in a mixture resulting from a stoichiometric reaction of PbO, MoO_3, and Mo. The reactants were sealed in a double quartz tube and fired at 1200°C for 7 days, slowly cooled down to 500°C, and then furnace cooled. A Guinier powder pattern of the bulk product indicated that it contained an unknown phase and a small amount of MoO_2. The standard quantitative element analysis on polycrystalline sample was done on a Cambridge S-200 microscope (SEM) with Mo, MoO_3 and PbO as standards. The analysis revealed a mole ratio of Pb : Mo : O = 1 : 5.97 : 10.8. The formula of $PbMo_6O_{10}$ was thus tentatively assigned.

<u>A new copper alkoxide complex</u>

The title compound was synthesized by the reaction of $Cu(O_3SCF_3)_2$ (0.48 g, 1.33 m mol) and a slightly excess of 2-(2-hydroxyethyl)pyridine (Hhep) [0.40 ml (d = 1.093 g/ml), 3.5 mmol] with an excess amount of KOH in THF at room temperature for 30 minutes. The resulting green mixture was then filtered to give a brown solid and a dark green filtrate. The dark green oily compound obtained after vacuum removal of THF was dissolved in a minimum amount of CH_2Cl_2 solvent. Blue crystals were obtained from this saturated CH_2Cl_2 solution after 1 month in freezer (-20 °C).

Powder Diffraction Data

An Enraf Nonius Delft triple focusing Guinier x-ray powder diffraction camera was used with Cu $K\alpha_1$ radiation (λ = 1.54056 Å) to obtain d-spacings. National Bureau of Standards silicon powder was mixed with all samples as an internal standard. The lines and their relative intensities for the compounds $K_{0.5}Ba_{1.9}Mo_{14}O_{22}$, $Ca_{3-x}Mo_{14}O_{22}$, and $PbMo_6O_{10}$ are listed in Tables 6.1 through 6.3, respectively.

Table 6.1. Observed d-spacings for $K_{0.5}Ba_{1.9}Mo_{14}O_{22}$

d-Spacing	Intensity[a]	d-Spacing	Intensity[a]
6.700	s	2.038	w
6.062	vw	1.943	s
3.111	w	1.911	vw
2.961	m	1.829	w
2.694	w	1.703	m
2.496	m	1.494	w
2.403	m-s	1.442	w
2.333	w	1.437	w
2.268	w	1.335	vw
2.198	w	1.223	vw

[a]Intensities: s = strong, m-s = medium to strong, m = medium, w = weak, vw = very weak

Table 6.2. Observed d-spacings for $Ca_{3-x}Mo_{14}O_{22}$

d-Spacing	Intensity[a]	d-Spacing	Intensity[a]
6.480	s	2.160	w
5.493	m	2.055	m
4.316	w	1.977	w
3.797	m	1.943	w
3.111	m	1.906	m
2.967	m	1.850	m
2.878	s	1.823	m
2.848	w	1.782	m
2.771	w	1.679	m
2.674	s	1.666	w
2.498	s	1.567	w
2.483	w	1.460	m
2.455	w	1.427	m
2.409	m	1.420	m
2.393	s	1.375	w
2.367	m	1.351	w
2.269	s	1.294	w
2.233	m	1.231	w
2.194	s	1.204	w

[a]Intensities: s = strong, m = medium, and w = weak

Table 6.3. Observed d-spacings for $PbMo_6O_{10}$

d-Spacing	Intensity[a]	d-Spacing	Intensity[a]
6.602	w	2.225	w
4.712	m	2.197	w
4.622	m	2.180	m
3.555	w	2.099	w
3.488	w	2.053	w
3.299	m	1.994	w
3.112	m	1.949	w
3.022	m	1.939	m
2.929	s	1.928	s
2.863	m	1.881	w
2.815	w	1.867	w
2.760	w	1.827	w
2.689	m	1.814	m
2.523	w	1.688	m
2.474	w	1.487	w
2.404	w	1.481	w
2.388	s	1.436	m
2.360	vw	1.422	w
2.310	vw		

[a]Intensities: s = strong, m = medium, w = weak, and vw = very weak

Single Crystal X-Ray Crystallographic Study

$Sn_{3.6}Mo_{16}O_{24}$ (supercell of $Sn_{0.9}Mo_4O_6$)

A black cylindrical crystal of $Sn_{3.6}Mo_{16}O_{24}$ having approximate dimensions of 0.20 x 0.06 x 0.08 mm^3 was mounted on a glass fiber. Data were collected with a Rigaku AFC6R diffractometer at room temperature up to $2\theta = 50^o$ by using graphite monochromated Mo Kα radiation and a 12 KW rotating anode generator. A scan mode of ω-2θ was used. Lattice parameters and the orientation matrix for data collection were measured from 25 carefully centered reflections with $13^o < 2\theta < 17^o$. The lattice was found to belong to the tetragonal (I-centered) system with cell dimensions: a = b = 13.561(1) Å, c = 5.659(1) Å, and V = 1040.7(3) $Å^3$. Three standard reflections which were measured after every 150 reflections showed no apparent variation in intensity during the data collection. An empirical absorption correction was applied, based upon azimuthal scans of several reflections with transmission factors in the range from 0.7491 to 1.000. Of the 554 reflections which were collected in the octant (h, k, 1), 536 were unique (R_{int} = 0.003) and 517 were considered as observed ($1 > 3\sigma(1)$). The Laue symmetry was determined as 4/mmm. and space group I4/mmm (#139) was then chosen based on the systematic absence of hkl: $h + k + l \neq 2n$, hk0: $h + k \neq 2n$, 0kl: $k + l \neq 2n$, and hhl: $l \neq 2n$.

$PbMo_6O_{10}$

The oscillation and zero-level Weissenberg photographs of two plate crystals of the title compound, each of which was twinned, resulted in unit cell dimensions : a = 9.98 Å, b = 9.4 Å, c = 7.44 Å, and $\alpha = 90^o$. Three zone axis ([100], [110], and [111]) electron diffraction patterns on powdered sample were measured on Jeol 100cx S/TEM microscope and the unit cell thus estimated was orthorhombic primitive with cell dimensions: a = 10.28 Å, b = 9.49 Å, c = 7.39 Å.

A new copper alkoxide complex

Like most of the copper(II) alkoxide complexes found in the course of this work, crystals of the title compound were subject to loss of solvent under reduced pressure. A crystal picked up from the solution contained in a Schlenk tube was thus mounted on the diffractometer in the low temperature nitrogen stream (-80°C). Data were collected with a Rigaku AFC6R diffractometer up to $2\theta = 50^o$ by using graphite-monochromated Mo Kα radiation and a 12 Kω rotating anode generator. A scan mode of ω-2θ was used. Cell constants and an orientation matrix for data collection obtained from a least-squares refinement of 25 carefully centered reflections with $13^o < 2\theta < 15^o$, corresponded to an orthorhombic cell with dimensions: a = 17.795(4) Å, b = 21.452 (6) Å, c = 9.403 (6) Å, and V = 3589(3) $Å^3$. Three standard reflections which were measured after every 150 reflections showed no apparent variation in intensity during the data collection. During the course of data collection the crystal was recentered almost every 150 reflections, and the need to do this probably arose from the presence

of two single crystals growing on top of each other in the specimen used for data collection. An empirical absorption correction was applied, based upon azimuthal scans of several reflections with transmission factors in the range from 0.8710-1.000.

In the octant (h, k, l), 3613 reflections were collected and 2677 of them were considered as observed ($I > 3\,\sigma(I)$). The Laue symmetry was determined as *mmm* and the statistical intensity test indicated an acentric space group. The space group $P2_1ab$ (#29 nonstandard setting) was chosen based on the systematic absence of h0l: $h \neq 2n$, hk0: $k \neq 2n$, (0k0: $k \neq 2n$), and (h00: $h \neq 2n$). This nonstandard cell was then transformed to the standard cell $Pca2_1$ by the matrix

$$\begin{bmatrix} 0 & 1 & 0 \\ 0 & 0 & 1 \\ 1 & 0 & 0 \end{bmatrix}.$$

RESULTS AND DISCUSSION

Several crystals of $K_{0.5}M_{1.9}Mo_{14}O_{22}$ examined by preliminary film work were twinned. Based on the crystal's appearance, crystals having better quality were observed in the product of reaction at 1280 ^{o}C and on $K_{0.5}Ba_{1.9}Mo_{14}O_{22}$. However, two crystals, one a K-Sn-Mo oxide and another a K-Ba-Mo oxide, appeared to have quality suitable for data collection based on the Weissenberg photographs, but these were subsequently found to be twinned. The continuous observation of $K_{0.5}M_{1.9}Mo_{14}O_{22}$ in the preparations aiming at $K_2M_2Mo_{18}O_{28}$ gave a strong sign about the existence of $K_{0.5}M_{1.9}Mo_{14}O_{22}$ and the necessity of further studies. Crystals of $Ca_{3-x}Mo_{14}O_{22}$ obtained from a longer reaction time (16 days) at 1150 ^{o}C were too small to do single crystal x-ray work. A higher reaction temperature and an even longer reaction time might be necessary for growing crystals suitable for x-ray diffraction work. Besides the conventional solid state preparation, other preparation options, such as chemical transport reaction and molten salt mixture, should be tested. The transport agent $BaCl_2$ and molten salt medium such as, $CaMoO_4$ and $CsMoO_4$, may be worth testing.

Axial photographs of $Sn_{3.6}Mo_{16}O_{24}$ agreed well with the indexed unit cell dimensions, but attempts to solve the structure based on the subcell structure refinement of $Sn_{0.9}Mo_4O_6$ were unsuccessful. Application of transmission electron microscope (TEM) technique may indeed be necessary for finding the real supercell of the $Sn_{0.9}Mo_4O_6$ subcell.

The unit cell dimensions (a = 10.28 Å, b = 9.49 Å, c = 9.39 Å orthorhombic) derived from TEM electron diffraction on powdered sample of $PbMo_6O_{10}$ agree well with those (a = 9.98 Å, b = 9.4 Å, c = 7.44 Å, and $\alpha = 90^o$) derived from the preliminary film work on twinned crystals. The point/space group of this compound may be determined by the Convergent Beam Electron Diffraction (CBED) technique. For a complete structural characterization, preparation of crystals suitable for single crystal x-ray data collection is necessary.

Both Patterson (SHELXS)[8] and direct methods (MITHRIL[9] and SHELXS[8]) were tested for the structure solution of the new copper alkoxide complex reported, but neither one of them gave a workable structure solution. A good x-ray diffraction data set collected on a single crystal is thus vital for the structure solution of this new copper alkoxide complex.

REFERENCES

1. Lil, K.H.; Wang, C.C. Inorg. Chem., 1988, 77, 407.
2. Hibble, S.J.; Cheetham, A.K.; Bogle, A.R.L.; Wakerley, H.R.; Cox, D.E. J. Am. Chem. Soc., 1988, 110, 3295.
3. Dronskowski, R; Simon, A. Angew. Chem. Int. Ed. Engl., 1989, 28, 758.
4. Mattausch, Hj; Simon, A.; Peters, E.-M. Inorg. Chem., 1986, 25, 3428.
5. Aufdembrink, B.A., Ph.D. Dissertation, Section 3, Iowa State University, Ames, Iowa, 1985.
6. Weiser, H.; Milligan, O. "Inorganic Colloid Chemistry: The Hydrous Oxides and Hydroxides"; J. Wiley and Sons, Inc.: London, 1933; Vol. III, p. 3039.
7. Torardi, C.C., Ph.D. Dissertation, Section V, Iowa State University, Ames, Iowa, 1981.
8. A menu driven interface to the SHELXS/PATSEE system is distributed with TEXSAN, which will create a reflection file in a proper SHELXS format as well as different input files that are necessary to run the program. But the SHELXS/PATSEE structure solution package is not distributed as part of the TEXSAN package.
9. Gilmore, C.J. J. Appl. Cryst., 1984, 17, p.42-46.

SUMMARY

Structures determined for the highly reduced ternary molybdenum oxides have been dominated by the Mo_4O_6 repeat unit derived by condensation of Mo_6O_{12} clusters, even though chains based on M_6X_8-type clusters have been previously observed in molybdenum chalcogenides and halides of early transition and rare earth metals. From the structural point of view, the reason for the formation of the Mo_6O_{12}-type cluster rather than the Mo_6O_8-type, is that the latter normally requires higher electon counts and much shorter Mo-Mo bonds which are then incompatible with the required Mo-Mo and O•••O spacings along the edge-shared chains.

In the chemistry of highly reduced molybdenum oxides, the preparation of compounds containing infinite chains of trans-edge-shared octahedra is well established in this laboratory. Six different crystallographic structure types have been discovered in this class of compounds. But very few compounds containing discrete oligomeric cluster units are known to date. A common structural feature of the oligomeric cluster units is the strong-weak bond alternation between apical Mo atoms. The stabilities of structural distortions (pairing of apical Mo atoms vs. tilting of Mo_6 octahedra) of these units were also studied by Extended Hückel calculations.[25] For example, in the structure of $K_3Mo_{14}O_{22}$, in which finite chains of three edge-fused octahedral cluster units (n = 3) are observed, the evident preference for an alternating pairing of the apical Mo atoms over a tilting of the Mo_6 octahedra is also suggested by Extended Hückel calculations. The study of magnetic properties suggested that $K_3Mo_{14}O_{22}$ might undergo charge disproportionation, such that clusters with 42 and 44 valence electrons, rather than 43, are formed. The compound $BaMo_5O_8$ with Mo_{10} cluster units has a short intercluster Mo-Mo bond distance of 2.778(3) Å, and therefore the cluster units can be thought of as

strong together in one dimensional infinite chains. And yet, the pressed pellet resistivity measurements suggests that the material is a low band gap semiconductor.

Exploration of the possible existence of the compounds $M_x^{I}M_{3-x}^{II}Mo_{14}O_{22}$ and $Ca_{3-x}Mo_{14}O_{22}$ suggests that research on the ternary or quaternary molybdenum oxides containing oligomeric cluster units of $n \geq 3$ should still be a fertile area. But the preparation of these compounds may require a higher reaction temperature ($T > 1300\ ^{o}C$) or different synthetic methods, such as use of chemical transport reactions, molten salt mixtures, and hydrothermal reactions. It also appears that K is probably too big for the formation of $K_4Mo_{18}O_{28}$, and that possibly, a rich chemistry of $K_xM_{4-x}Mo_{18}O_{28}$ (M = divalent metals) compounds is waiting to be discovered.

Considerable progress has been made in the research area of soluble copper(II) alkoxide complexes. The system of copper(II) alkoxides with anion of 2-(2-hydroxyethyl)pyridine (hep) as ligand has been explored in the course of this work. As a result, four soluble copper(II) alkoxides, $[CuCl(hep)]_2$(7), $[CuCl(hep)(Hhep)]_2 \bullet 2CH_2Cl_2$ (8), $[CuCl(hep)(py)]_2 \bullet CH_2Cl_2$(9), and $[Cu(hep)_2 \bullet LiO_3SCF_3]_2 \bullet 4CH_2Cl_2$(10), have been discovered.

Compound 7 has a strong antiferromagnetic coupling ($2J = -1298 \pm 138\ cm^{-1}$) within the dimeric unit and its structure is described more accurately as a polymer of dimers. Interestingly, when under reduced pressure, compounds 8 and 9 each lose the apical ligand and CH_2Cl_2 solvent molecules and converts to 7, a polymer of dimers. In compound 10, a cis configuration of hep ligands about Cu atoms is observed for the first time in such bidentate copper(II) alkoxide complexes. Compound 10 is a heterometallic alkoxide in which two $Cu(hep)_2$ monomers are held together through two bridging Li^+ ions of lithium trifluoromethylsulfonate to form a dimer.

Although compounds containing oligomers of $Cu(hep)_2$ units are still unknown and remain to be discovered, compounds **7**, **8**, **9**, and **10** are important in the general effort to prepare precursors suitable for the synthesis of high-Tc superconducting copper oxides by sol-gel approach. According to Caulton and Hubert-Pfalzgraf's discussion,[26] the remaining chlorines in the copper(II) alkoxide chloride compounds of **7**, **8**, and **9**, may act as functional groups and be subsequently replaced by OR groups (eq. 1).

$$[CuCl(hep)(L)]_2 + 2\,KOR \xrightarrow{THF} [Cu(OR)(hep)(L)]_2 + 2\,KCl \qquad (1)$$

In efforts to prepare copper(II) alkoxide complexes containing oligomers of $Cu(hep)_2$ units, the preparation of $[Cu(hep)_2{\bullet}LiO_3SCF_3]_2{\bullet}4CH_2Cl_2$ (**10**) could be modified as follows:

$$Cu(O_3SCF_3)_2 + 2\,Hhep + 2(\text{or excess})\,KOMe \xrightarrow{CH_2Cl_2} \text{(2)}$$

$$2/n\,[Cu(hep)_2]_n + 2\,MeOH + 2\,KO_3SCF_3 \qquad K_2[Cu(hep)_2OMe]_2 + HO_3SCF_3$$

$$K_2[Cu(hep)_2OMe]_2 \xrightarrow[\textbf{7, 8, or 9}]{CH_2Cl_2} [Cu_2(hep)_3(OMe)(L)]_2 + 2\,KCl \qquad (3)$$

The chloride and lithium-free copper(II) complexes thus prepared would be the potential precursors to the preparation of high-Tc superconductors through the sol-gel approach. It may be also possible to prepare heterometallic alkoxides containing Y, Ba and Cu in a stoichiometry corresponding to $YBa_2Cu_3O_7$ by reactions of these chloride- and lithium-free copper(II) complexes with alkoxides or oxoalkoxides of Ba and Y. Although Y-Ba-Cu heterometallic alkoxide complexes are not known to date, the heterobimetallic alkoxides $Ba_2Cu_2(OR)_4(acac)_4 \cdot 2HOR$ ($R = CH_2CH_2OCH_3$) has been recently prepared by Sauer et al.[27] (eq. 4).

$$[Cu(acac)(\mu\text{-}OR)]_2 + Ba(OR)_2 \xrightarrow{ROH} Ba_2Cu_2(OR)_4(acac)_4(ROH)_2 + [Cu(OR)_2]_m \qquad (4)$$

Hubert-Pfalzgraf and coworkers also claimed that a heterometallic oxoalkoxide containing both Y and Ba could be prepared by the reaction of $Y_5O(OPr^i)_{13}$ with $Ba(OPr^i)_2$ at room temperature.[28] In closing, the chemistry of homometallic or heterometallic copper(II) alkoxide complexes suitable for the preparation of high-Tc superconductors via either sol-gel or MOCVD (metal-organic chemical vapor-phase deposition) technology deserves further study through synthesis, characterization, and reactions.

REFERENCES

1. Torardi, C.C.; McCarley, R.E. J. Am. Chem. Soc., 1979, 101, 3963.
2. (a). Torardi, C.C.; McCarley, R.E. J. Less-Common Meals, 1986, 116, 169; (b). Lii, K.H.; Aufdembrink, B.A.; McCarley, R.E. unpublished research.
3. (a). McCarley, R.E. Philos. Trans. R. Soc. London A, 1982, 308, 141; (b). McCarley, R.E. Am. Chem. Soc. Symp. Ser., 1983, 211, 273; (c). Lii, K.H.; McCarley, R.E. unpublished research.
4. Calson, C.D.; Brough, L.F.; Edwards, P.A.; McCarley, R.E. J. Less-Common Meals, 1989, 156, 325.
5. McCarley, R.E.; Lii, K.H.; Edwards, P.A.; Brough, L.F. J. Solid State Chem., 1985, 57, 17.
6. Lii, K.H.; McCarley, R.E.; Kim, S.; Jacobson, R.A. J. Solid State Chem., 1986, 64, 347.
7. (a). Gougeon, P.; Gall, P.; McCarley, R.E. Acta Crystallogr. C, in press; (b). Gougeon, P.; Lee, K.H.; Schimek, G.; McCarley, R.E. unpublished results.
8. Mattausch, Hj; Simon, A.; Peters, E.-M. Inorg. Chem., 1986, 25, 3428.
9. Lii, K.H.; Wang, C.C. Inorg. Chem., 1988, 77, 407.
10. Dronskowski, R.; Simon, A. Angew. Chem. Int. Ed. Engl., 1989, 28, 758.
11. Hibble, S.J.; Cheetham, A.K.; Bogle, A.R.L.; WAkerley, H.R.; Cox, D.E. J. Am. Chem. Soc., 1988, 110, 3295.
12. Torardi, C.C.; Calabress, J.C. Inorg. Chem., 1984, 23, 3281.

13. (a) Mehrotra, R.C. Adv. Inorg. Chem. Radiochem., 1983, 26, 269; (b) Singh, J.V.; Baranwal, B.P.; Mehrotra, R.C. Z. Anorg. Allg. Chem., 1981, 477, 235.

14. Monde, T.; Kozuka, H.; Sakka, S. Chem. Lett., 1988, 287.

15. Nonaka, T.; Kaneko, K.; Hasegawa, T.; Kishio, K.; Takahashi, Y.; Kobayashi, K.; Kitazawa, K.; Fueki, K. Jpn. J. Appl. Phys., 1988, 27, L867.

16. Ravindranathan, P.; Komarneni, S.; Bhalla, A.; Roy, R.; Cross, L.E. J. Mater. Res., 1988, 3, 810.

17. Kramer, S.A.; Kordas, G.; McMillan, J.; Hilton, G.C.; Van Harligen, D.J. Appl. Phys. Lett., 1988, 53, 156.

18. Brinker, C.J. and Scherer, G.W. Sol-Gel Science, Academic Press, San Diago, CA, 1990.

19. McMullen, A.K.; Tilley, T.D.; Rheingold, A.L.; Gelb, S.J.; Inorg. Chem., 1989, 28, 3772.

20. Horowitz, H.S.; McLain, S.J.; Sleight, A.W.; Druliner, J.D.; Gal, P.L.; VanKavelaar, M.J.; Wagner, J.L.; Biggs, B.D.; Poon, S.J. Science, 1989, 243, 66.

21. Goel, S.C.; Kramer, K.S.; Gibbons, P.C.; Buhro, W.E. Inorg. Chem., 1989, 28, 3619.

22. Goel, S.C.; Kramer, K.S.; Chiang, M.Y.; Buhro, W.E. Polyhedron, 1990, 9, 611.

23. Bradley, D.C.; Mehrotra, R.C.; Gaur, D.P. Metal Alkoxides; Academic Press, New York, 1978; pp 86-87.

24. (a) Goel, S.C.; Kramer, K.S.; Gibbons, P.C.; Buhro, W.E. Inorg. Chem., 1989, 28, 3620; (b) Horowitz, H.S.; McLain, S.J.; Sleight, A.W.; Druliner, J.D.; Gal, P.L.; Vankavelaar, M.J.; Wagner, J.L.; Biggs, B.D.; Poon, S.J. Science, 1989, 243, 66.

25. Wheeler, R.A.; Hoffmann, R. J. Am. Chem. Soc., 1988, 110, 7315.

26. Caulton, K.G.; Hubert-Pfalzgraf, L.G. Chem. Rev., 1990, 90, 969.

27. Sauer, N.N.; Garcia, E.; Salazar, K.V.; Ryan, R.R.; Martin, J.A. J. Am. Chem. Soc., 1990, 112, 1524.

28. Reference #58 in reference #26. Poncelet, O.; Hubert-Pfalzgraf, L.G. unpublished results.

ACKNOWLEDGEMENTS

I wish to thank Professor Robert E. McCarley for his guidance, patience, support, and encouragement during the course of this work. His suggestions during our many discussions proved insightful and helpful. The discussions, suggestions, support, and companionship provided by other members of this research group were also much appreciated, especially Dr. Clark D. Carlson and Dr. Lorraine E. Aleandri whose wonderful friendship and support have helped me through some difficult times.

I am also grateful to the scientific community here at Iowa State University for their aid throughout my research, especially Professor Robert A. Jacobson and Dr. Thomas Hendrixson, as well as Dr. Lee M. Daniels for their valuable assistances in the x-ray single crystal structure determinations on Rigaku and CAD4 diffractometers, respectively. Special thanks are due to Professor David C. Johnston and members of his group and to Professor Douglas K. Finnemore and Mr. Jerome E. Ostenson for their assistances in obtaining d.c. resistivity and magnetic susceptibility measurements, respectively. The electron paramagnetic resonance spectra could not have been obtained without the help of Dr. Vinko Rutar, for which I am grateful.

My deepest appreciation goes to my fiancee, Ching-Chi (Wendy) Chang for her love, support, and encouragement. Finally, I would like to dedicate this thesis to my mother whose love and support has been limitless.